

**TR diss**  
**2795 S**

# Stellingen

behorende bij het proefschrift

*Characterisation, Testing and Deactivation of Sulfided Catalysts in  
the Hydrodemetallisation of Vanadyl-tetraphenylporphyrin*

van

Jean-Paul Janssens

1. Een goed proefschrift leest als een doctorsroman.
2. Het bestuderen van wetenschappelijke literatuur kan tot verwarring leiden. Het regelmatig publiceren van zogenaamde 'critical reviews' is onontbeerlijk.
3. Milieu-problemen kunnen zowel bij de bron als 'end-of-pipe' worden opgelost. Een economische- en exergie-analyse zal bepalen welke oplossing gekozen dient te worden.
4. De disciplines scheikundig technologie, materiaalkunde, mijnbouwkunde en petroleumwinning vertonen meer overeenkomsten dan de beoefenaars ervan zelf denken. Samensmelting van deze disciplines kan de nodeloze overlap doen verminderen.
5. De organisatie-structuur van faculteiten is verouderd en leidt vaak tot 'random walk' besluitvorming. Snelle, consistente besluitvorming, die vereist wordt in de huidige maatschappij, maakt een verandering in deze organisatie-structuur noodzakelijk.

6. De huidige en toekomstige generaties onderzoekers en assistenten in opleiding zullen in versterkte mate zowel wetenschappelijke als management en marketing kwaliteiten dienen te bezitten.
7. De betrouwbaarheid en validiteit van de uitkomsten van de huidige assessment centres voor specialistisch opgeleid personeel is op z'n minst twijfelachtig.
8. De formulering 'Op dit moment moeten we ons tevreden stellen met een gevoel van verwondering en ontzag, want we kennen het antwoord niet. En wie weet is dat gevoel van verwondering en ontzag wel bevredigender dan het kennen van een antwoord — voorlopig tenminste <sup>1</sup> ' geeft de bescheiden en geduldige opstelling van wetenschappers ten aanzien van de oorsprong van het leven weer.  
(<sup>1</sup> uit *Gödel, Escher, Bach* van D.R. Hofstadter)
9. Om het deactiveringsgedrag van katalysatoren te kunnen beschrijven, is naast kennis van reactie kinetiek en diffusief transport, ook inzicht in de dynamiek van de katalysator poreuze textuur en de morfologie van de deactiveringscomponent noodzakelijk.  
(dit proefschrift)
10. 'Molecular modelling' is een uitstekend hulpmiddel om tot het reactie mechanisme te komen <sup>1</sup>. Kinetische analyse alleen is hiervoor niet voldoende <sup>2</sup>.  
(<sup>1</sup> dit proefschrift, <sup>2</sup> G.F. Froment, *Chem. Eng. Sci.*, **42** (1987) 1073)
11. Modelverbindingen kunnen uitstekend gebruikt worden om inzicht te krijgen in de fundamentele processen die spelen in reële aardolie voedingen.  
(dit proefschrift)

**Characterisation, Testing and Deactivation of Sulfided  
Catalysts in the Hydrodemetallisation  
of Vanadyl-tetraphenylporphyrin**

**Jean-Paul Janssens**

# Characterisation, Testing and Deactivation of Sulfided Catalysts in the Hydrodemetallisation of Vanadyl-tetraphenylporphyrin

PROEFSCHRIFT

ter verkrijging van de graad van doctor  
aan de Technische Universiteit Delft,  
op gezag van de Rector Magnificus Prof. ir. K.F. Wakker,  
in het openbaar te verdedigen ten overstaan van een commissie,  
door het College van Dekanen aangewezen,

op dinsdag 17 september 1996 te 10.30 uur

door

**Jean-Paul JANSSENS**

ingenieur in de scheikundige technologie

geboren te Haarlem



Dit proefschrift is goedgekeurd door de promotoren:

Prof. dr. J.A. Moulijn

Prof. dr. ir. S.T. Sie

Toegevoegd promotor: Dr. A.D. van Langeveld

Samenstelling promotiecommissie:

Rector Magnificus (of diens plaatsvervanger), Technische Universiteit Delft, voorzitter

Prof. dr. J.A. Moulijn, Technische Universiteit Delft, promotor

Prof. dr. ir. S.T. Sie, Technische Universiteit Delft, promotor

Dr. A.D. van Langeveld, Technische Universiteit Delft, toegevoegd promotor

Prof. dr. R. Prins, ETH Zürich, Zwitserland

Prof. dr. ir. G.F. Froment, Rijksuniversiteit Gent, België

Dr. B. Scheffer, Shell Research and Technology Centre, Amsterdam

Dr. C.M. Lok, Unilever Research Port Sunlight, Engeland

Prof. dr. J.A.R. van Veen, Technische Universiteit Eindhoven

The research reported in this thesis has been carried out at Delft University of Technology, Faculty of Chemical Technology and Materials Science (*Julianalaan 136, 2628 BL Delft, The Netherlands*). The research was financially supported by the European Community under contract number JOUF 0049 and the Shell Research and Technology Centre, Amsterdam (SRTCA).

Janssens, Jean-Paul

Characterisation, testing and deactivation of sulfided catalysts  
in the hydrodemetallisation of vanadyl-tetraphenylporphyrin / Jean-Paul Janssens

Proefschrift Technische Universiteit Delft

- met samenvatting in het Nederlands

Drukwerk: Ponsen & Looijen B.V., Wageningen

Copyright © by Jean-Paul Janssens

All rights reserved

Cover by Litho Nieuwe Stijl B.V., Vijfhuizen

# Preface

## *Introduction*

In 1986 research on hydrodemetallisation of porphyrinic model compounds was started at the University of Amsterdam by Raimond L.C. Bonn  under supervision of Prof. Dr. Jacob A. Moulijn. This research was part of an European Community project entitled '*Development of Tailor-made Catalysts for Application in Hydroconversion*', (contract number JOUF 0049). Co-operating institutes in this project were Imperial College (London, United Kingdom), Eindhoven University of Technology (The Netherlands), University of Karlsruhe (Germany) and Escuela de Ingenieros Bilbao (Spain). The results are described in the Ph.D thesis '*Hydrodemetallisation of Ni-TPP and VO-TPP over Sulfided Molybdenum and Vanadium Catalysts*' by Raimond L.C. Bonn  and formed the starting-point for the research finalised in the present Ph.D thesis. The Shell Research and Technology Centre, Amsterdam (SRTCA) and the European Community (continuation of JOUF 0049) financially supported parts of the research presented, which is highly appreciated.

## *Objectives*

At the start of the hydrodemetallisation project at Delft University of Technology (early 1992) the objectives were formulated as follows:

- i)* Development of dedicated equipment for Temperature Programmed Sulfiding experiments and hydrotreating catalyst testing, *i.e.* batch autoclave- and microflow reactors;
- ii)* Preparation of vanadium catalysts on alumina and silica to identify the type of surface species;
- iii)* Catalyst characterisation by textural analysis and Temperature Programmed Reactions;
- iv)* Hydrotreating catalyst testing:
  - for the hydrodemetallisation of porphyrinic model compounds
  - detailed reaction kinetics analysis
  - identification of intermediate products in the hydrodemetallisation of metallo-tetraphenyl porphyrins
  - establishment of the structure-activity correlation for vanadium catalysts
  - assessment of the influence of sulfur and nitrogen containing compounds on hydrodemetallisation
  - elucidation of catalytic active sites during metal deposition
- v)* Development of a catalyst deactivation model for hydrodemetallisation

## *Outline of this Thesis*

The research presented in this thesis deals with the characterisation, testing and deactivation of sulfided catalysts in the hydrodemetallisation of vanadyl-tetraphenylporphyrin (VO-TPP). An attempt is made to cover several broad and interesting topics, which are of importance in the hydrodemetallisation and hydrotreating process. Testing and deactivation of sulfided catalysts has been carried out under industrial reaction conditions.

The thesis is divided in eight chapters which are arranged as follows. Chapter 1 is the *general introduction* on hydrotreating and hydrodemetallisation. Chapter 2 is the *experimental part*. Equipment used for catalyst testing, an autoclave reactor and a micro-flow reactor, will be discussed. Details of reaction kinetics data evaluation will be presented because this forms the back-bone this thesis.

In Chapter 3 the influence of different support materials on the *hydrodemetallisation and hydrodesulfurisation activity of vanadium catalysts* is assessed.

The *influence of hetero-atom containing compounds*, such as quinoline, ammonia, benzofuran, water, dibenzothiophene and an aromatic solvent like anthracene on the rate of metal removal is reported in Chapter 4. Effects of competitive adsorption of hetero-atom containing compounds, which could be present in model compounds and real feeds hydrodemetallisation, are studied.

The *development of a catalyst deactivation model during hydrodemetallisation*, in order to predict catalyst life-times and metal deposition profiles in catalyst pellets, is described in Chapter 5. Chapter 6 reports a *study on the metal deposition process under industrial conditions*. Vanadium deposition profiles in wide pore silica pellets are determined experimentally. The effect of quinoline and H<sub>2</sub>S on the vanadium deposition profiles is assessed and model predictions are made to evaluate the proposed catalyst deactivation model.

Chapter 7 is an *investigation on the hydrodemetallisation reaction mechanism of metallo-tetraphenylporphyrin*. The reaction mechanism is extended and validated in order to determine the elementary steps on a molecular level. Based on molecular modelling calculations and GC-MS new reaction intermediates are identified and an extended reaction mechanism is proposed. Chapter 8 summarizes the *general conclusions* and gives the *evaluation and implications* of the thesis.

## *Final Remarks*

The writing of this thesis took place in chronological order of the performed research. Each chapter in this thesis is written as a separate publication so the chapters can be read independently from each other. Consequently, some repetitions are unavoidable !

I wish everyone who is interested in the subjects described in this thesis much pleasure reading it, I have certainly enjoyed writing the present work !



ter nagedachtenis aan mijn vader  
(overleden 17 april 1995)

voor mijn moeder

# Contents

Chapter 1	<b>Introduction</b>	1
	1. Upgrading of heavy oil	
	1.1. Composition of petroleum	
	1.2. Upgrading technologies	
	2. Hydrotreating	
	2.1. Removal of hetero-atoms by hydrotreatment	
	2.2. Metal compounds in petroleum	
	2.3. HDM/HDS hydroprocessing technology	
	2.4. Catalyst regeneration	
	3. Catalyst deactivation	
Chapter 2	<b>Equipment for Catalyst Testing and Deactivation</b>	19
	1. Batch autoclave reactor	
	1.1. Experimental set-up	
	1.1.1. Gas supply system	
	1.1.2. Autoclave reactor	
	1.1.3. Control section	
	1.2. Experimental procedures	
	1.2.1. Catalyst introduction	
	1.2.2. Catalyst sulfiding	
	1.2.3. Run procedure	
	1.2.4. Sample analysis	
	1.3. Reaction mechanism and kinetics	
	1.3.1. Reaction mechanism	
	1.3.2. Reaction kinetics	
	1.3.3. Thermodynamics	
	1.3.4. Reaction kinetics parameter estimation and software	
	2. Microflow reactor	
	2.1. Process flow scheme	
	2.2. Process control equipment	
	2.3. HDM catalyst deactivation tests	
	2.3.1. Filling of the reactor	
	2.3.2. Catalyst sulfiding	
	2.3.3. Reaction conditions	
	2.3.4. In-situ production of hydrogensulfide	
	2.3.5. UV-VIS liquid sample analysis	

1. Introduction
2. Experimental
  - 2.1. Catalyst preparation
  - 2.2. Catalyst characterisation
  - 2.3. Thiophene hydrodesulfurisation activity
  - 2.4. Vanadyl-tetraphenylporphyrin hydrodemetallisation
3. Results
  - 3.1. Temperature programmed reduction and sulfiding
  - 3.2. Catalyst activity
    - 3.2.1. Thiophene HDS activity
    - 3.2.2. VO-TPP HDM activity
4. Discussion
  - 4.1. Catalyst characterisation
  - 4.2. Catalyst activity
    - 4.2.1. Thiophene HDS activity
    - 4.2.2. VO-TPP HDM activity
5. Conclusions

1. Introduction
2. Experimental
  - 2.1. Catalyst preparation
  - 2.2. Hydrodemetallisation of VO-TPP
3. Results
  - 3.1. Blank test of VO-TPP hydrodemetallisation
  - 3.2. Influence of the nitrogen containing compounds quinoline and ammonia
  - 3.3. Influence of the sulfur containing compound dibenzothiophene
  - 3.4. Influence of the oxygen containing compounds benzofuran and water
  - 3.5. Influence of anthracene
4. Discussion
5. Conclusions

Chapter 5      **Catalyst Deactivation in the Hydrodemetallisation of Vanadyl-tetraphenylporphyrin under Industrial Conditions**      73

1. Introduction
2. Approach for modelling HDM catalyst deactivation
  - 2.1. HDM reaction kinetics and diffusion
  - 2.2. Catalyst porous texture
  - 2.3. Mass balances and model equations
3. Experimental
  - 3.1. HDM reaction kinetics
  - 3.2. Catalyst deactivation
4. Results and discussion
  - 4.1. HDM reaction kinetics
  - 4.2. Catalyst deactivation: experimental and modelling
5. Conclusions

Chapter 6      **On the Metal Deposition Process during the Hydrodemetallisation of Vanadyl-tetraphenylporphyrin**      95

1. Introduction
2. Experimental and computational techniques
  - 2.1. Preparation and characterisation of fresh catalyst
  - 2.2. HDM reaction kinetics in autoclave reactor
  - 2.3. Vanadium deposition experiments
    - 2.3.1. Microflow equipment
    - 2.3.2. Sulfiding of the catalyst
    - 2.3.3. Reaction conditions
    - 2.3.4. EPMA analysis
    - 2.3.5. High Resolution Electron Microscopy
  - 2.4. Computer simulations on vanadium deposition in catalyst pellets
3. Results
  - 3.1. Estimation of reaction kinetic parameters for VO-TPP hydrodemetallisation
  - 3.2. Vanadium deposition experiments
  - 3.3. Localisation of vanadium deposits on Mo/SiO<sub>2</sub> catalyst
4. Discussion
5. Conclusions

## Development of a Mechanistic Picture of the Hydrode- metallisation Reaction of Metallo-Tetraphenylporphyrin on a Molecular Level

1. Introduction
2. Experimental and computational techniques
  - 2.1. Catalyst
  - 2.2. Batch autoclave experiments
  - 2.3. Gas chromatography-mass spectrometry
  - 2.4. Molecular modelling
3. Results
  - 3.1. Analyses of the ring fragments with GC-MS
  - 3.2. Molecular modelling of reactant and intermediates
4. Discussion
  - 4.1. Molecular modelling of reactants and intermediates in HDM reaction mechanism of metallo-tetraphenylporphyrin
    - 4.1.1. First hydrogenation step: formation of M-TPC out of M-TPP
    - 4.1.2. Second hydrogenation step: formation of M-TPB and M-TPiB out of M-TPC
    - 4.1.3. Third hydrogenation step: formation of M-TPHP and M-A out of M-TPiB or M-TPB
    - 4.1.4. Fourth hydrogenation step: formation of M-TPOP and M-B out of M-TPHP
    - 4.1.5. Formation of a corrin-type of porphyrin M-Corr out of M-A
    - 4.1.6. Formation of a bilane-type of porphyrin M-Bil out of M-B
    - 4.1.7. Ring cleavage: formation of ring fragments
  - 4.2. Proposal for an extended reaction mechanism
5. Conclusions

## Summary and Evaluation

Characterisation, Testing and Deactivation of Sulfided Catalysts  
in the Hydrodemetallisation of Vanadyl-tetraphenylporphyrin

<b>Samenvatting</b>	151
<b>List of Symbols</b>	155
<b>List of Publications and Orals</b>	159
<b>Dankwoord</b>	161
<b>Curriculum Vitae</b>	163

# Chapter 1

## Introduction

---

The oil demand of the Western World has undergone major changes in the last decades due to overcapacity of primary crude, fluctuating crude prices, oil crises and the development of other energy sources, like coal and nuclear fission. In general, the oil market shows an increasing demand for light and middle distillates, such as naphtha, gasoline, jet fuels and diesel and a decreasing demand for heavy products, such as heavy fuel oil and coke (*I*). To cope with this change in the oil market, the refining industry has to convert heavy feedstocks such as residual oils into lighter and more employable products, the so-called '*whitening of the barrel*'.

These heavy feedstocks can be defined in terms of a high carbon to hydrogen (C/H) ratio, high viscosity, large amounts of asphaltenes and high contents of hetero-atoms, such as sulfur, nitrogen, oxygen, nickel and vanadium. Therefore, the main objectives of upgrading and conversion of these heavy feedstocks are lowering of the C/H ratio, the viscosity and the hetero-atom content for further downstream conversion.

Governments put an additional constraint on refineries by more stringent environmental demands on the products and processes. The presence of sulfur and nitrogen in crudes poses serious environmental hazards in the form of SO<sub>x</sub> and NO<sub>x</sub> emissions in combustion processes. Since these emissions contribute to the greenhouse effect, acid rain and destruction of the ozone layer, the society will put more and more stringent regulations on these emissions.

---

## 1. UPGRADING OF HEAVY OIL

### 1.1. Composition of petroleum

Petroleum is a complex mixture of hydrocarbons and non-hydrocarbon organic compounds with a wide boiling range. It extends from the simplest alkanes to highly complex structures with molecular mass up to many thousands. In general, the complexity of the mixture increases with increasing boiling point range.

Residual oil is the heaviest fraction, it can be divided into atmospheric residue, which is the fraction boiling above 618 K and vacuum residue, which is the fraction boiling above 813 K. Many crude oils contain 10 to 30 % residue (2), and in the future even lower quality crude oil (with residue fractions > 40 %) has to be processed.

The complexity and hetero-atom content of crude oil increases with increasing boiling point. The oil residua are characterized by sulfur contents of 0.2 to 6.5 wt.%, nitrogen of 0.1 to 1.1 wt.%, oxygen of 0.5 to 1.5 wt.% and high concentrations of polyaromatic asphaltenic structures. Of the metals, vanadium and nickel are the most abundant and troublesome. Figure 1 depicts the typical range of values for the hetero-atom content in residua (3).

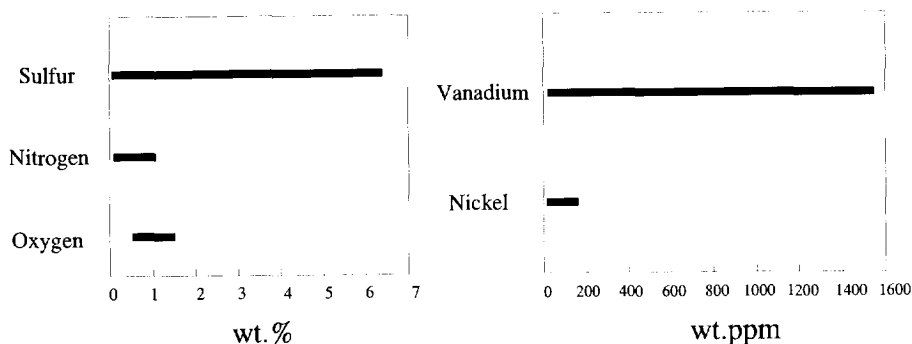


**Figure 1.** Typical values for the hetero-atom content in oil residua.  
(the dimension wt.ppm corresponds with mg/kg)

Lowering of the C/H ratio of oil residua can be achieved by either rejection of carbon or addition of hydrogen. Upgrading technologies can be divided into thermal and catalytic processes. The next paragraph discusses the various available upgrading technologies.

### 1.2. Upgrading technologies

Heavy oil requires upgrading to improve the properties, especially the C/H ratio and the hetero-atom content should be lowered. Lowering of the C/H ratio is accomplished by either addition of hydrogen to or rejecting of carbon from the feedstock.

The available catalytic and thermal upgrading processes can be divided into the following classes:

- i) hydrogen addition: - catalytic hydroprocesses (hydrotreating, hydrocracking)  
- non-catalytic hydroprocesses (hydrovisbreaking, donor-solvent-processes, hydrolysis)
- ii) carbon rejection: - catalytic cracking (Fluid Catalytic Cracking)  
- thermal processes (visbreaking, coking)
- iii) other processes: - partial oxidation, steam reforming, production of syngas

Thermal processes are, in general, less selective for the desired product and require higher temperatures than catalytic processes, therefore, catalytic processes are the most promising for the future.

Catalytic hydrotreating is a well established process for the removal of hetero-atoms, such as sulfur (HydroDeSulfurisation, HDS), nitrogen (HydroDeNitrogenation, HDN), oxygen (HydroDeOxygenation, HDO) and metals (HydroDeMetallisation, HDM).

## 2. HYDROTREATING

### 2.1. Removal of hetero-atoms by hydrotreatment

Hetero-atoms present in heavy oil have to be removed for environmental reasons and for downstream conversion benefits, for example, protection of expensive downstream catalysts (FCC and reforming catalysts).

Hydrotreatment removes the hetero-atoms sulfur, nitrogen and oxygen as gaseous hydrogen sulfide, ammonia and water, respectively. The metals, vanadium and nickel, are deposited as metal sulfides on the internal catalyst surface. These metal deposits cause, together with the



inevitable coke deposits, deactivation of the hydrotreating catalyst by the interaction of the deposited metals with the original active sites ('*active site poisoning*') or the loss of pore volume due to the deposition within catalyst pores ('*pore plugging*') (4). Both deactivation phenomena are depicted in Figure 2.

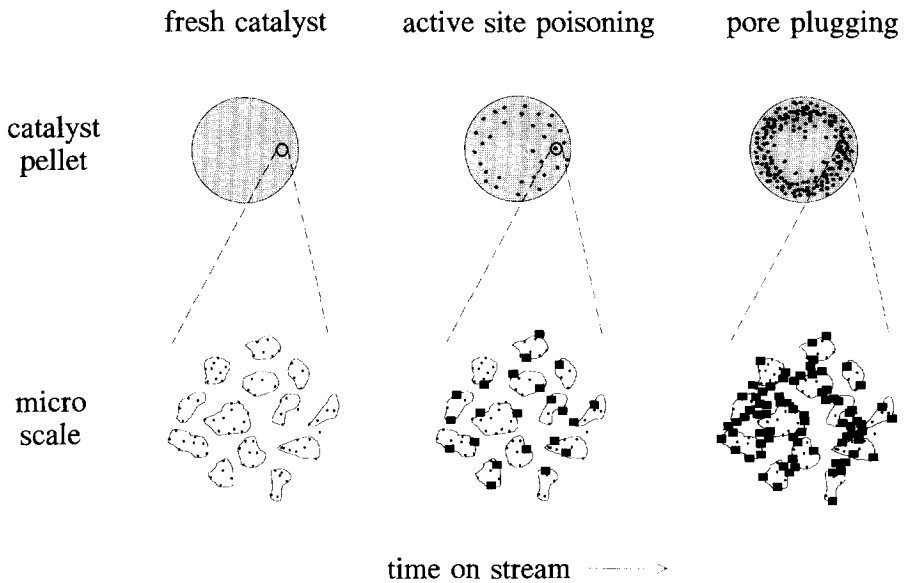


**Figure 2.** Metal deposition process in hydrotreating catalysts.

## 2.2. Metal compounds in petroleum

Vanadium and nickel are present in heavy oil as soluble organo-metallic complexes and fall into two categories; metallo-porphyrins and non-porphyrin complexes.

Metallo-porphyrins are well defined structures. The basic skeleton of porphyrin is a closed ring of four pyrrole groups which are linked together by methine bridges, as depicted in Figure 3. Porphyrins may have various substituents replacing the hydrogens at the eight  $\beta$ -pyrrolic carbon positions and at the four methine bridge carbon positions. Metallo-porphyrins are formed by chelation of a metal ion into the centre of the porphyrin. Nickel is always present as  $\text{Ni}^{2+}$  and vanadium is present as  $\text{V}^{4+}$  in vanadyl  $\text{VO}^{2+}$ . The prevalence of nickel and vanadium in comparison with other metals is a consequence of the stronger chelation strength of Ni and V in the porphyrin nucleus (5).

## Introduction

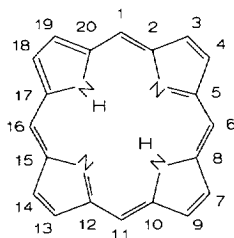


**Figure 3.** Structure of porphyrin with IUPAC numbering.

The majority of the metallo-porphyrins in crude oil can be classified into the groups DPEP, Etio, Di-DPEP, Rhodo-Etio and Rhodo-DPEP porphyrins, as depicted in Figure 4 (6-13). Metallo-porphyrins are reported to account for as much as 5-70 % of the metal compounds in crude oils. Of the total vanadium and nickel content, 6-34 wt.% is complexed in porphyrin (3).

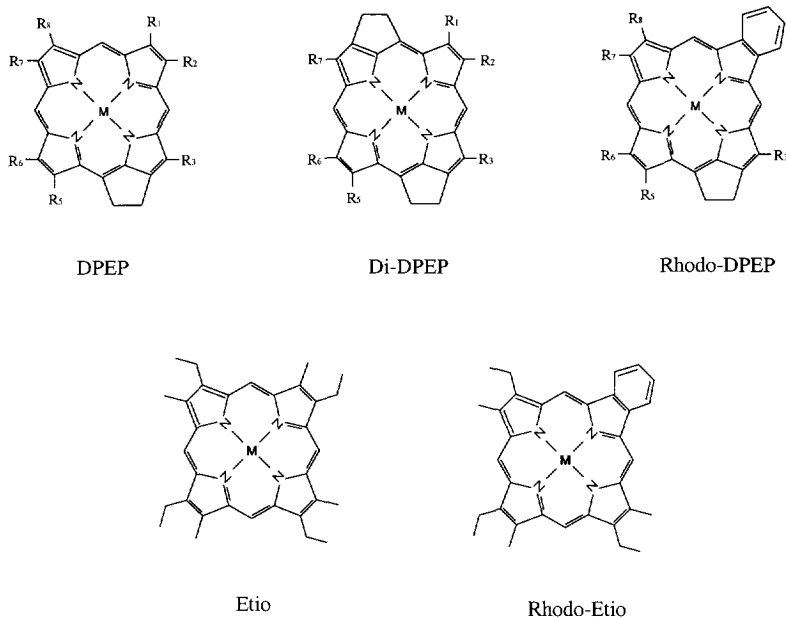


**Figure 4.** Metallo-porphyrins occurring in crude oil (DPEP: deoxophylloerythroetioporphyrin; Etio: etioporphyrin).

A characteristic property of porphyrins is their intense colour in the ultra-violet and visible range. Each type of porphyrin has a specific spectrum that allows unique identification and quantitative analysis. This property makes porphyrins extremely suitable as model compounds for fundamental research on hydrodemetallisation.

Non-porphyrin metal complexes are all other metal compounds in crude oil. In general, these complexes are poorly characterized with respect to their structure and properties and they are more polar than metallo-porphyrins. The non-porphyrin compounds comprise a wide variety of coordinated complexes resulting at least partly from the reaction of inorganic metals forms with polar organic molecules (11).

### 2.3. HDM/HDS hydroprocessing technology

Typical process conditions for catalytic HDM/HDS hydroprocessing are temperatures between 573 and 673 K and hydrogen pressures between 5 and 15 MPa. Some of the available catalytic hydrotreatment processes with their properties are summarized in Table 1.

**TABLE 1**  
Catalytic residue hydrotreating processes.

Name	Company	Type of reactor	Catalyst
H-Oil	HRI/Texaco	Ebullated bed	*
LC Fining	Lummus	Ebullated bed	CoMo or NiMo
HYVAHL F	IFP, Elf, Total	Fixed bed	NiMo
HYVAHL M	IFP, Elf, Total	Moving bed	NiMo
RDS or VRDS	Chevron	Fixed bed	*
RESIDfining	EXXON	Fixed bed	CoMo, NiMo
Gulf HDS	Gulf	Fixed bed	*
Unicracking RDS	Union Oil	Fixed bed	*
RCD Unibon	UOP	Fixed bed	CoMo
HYCON	Shell	Bunker flow + fixed bed	NiV/SiO <sub>2</sub> for HDM CoMo or NiMo for HDS
R.HYC	Idemitsu Kosan	Fixed bed	*
ABC	Chiyoda	Fixed bed	*

\* not published in open literature

## Introduction

A typical flowsheet of a fixed bed catalytic process is given in Figure 5. The reactor operates in downflow mode with the liquid feed trickling downward over the solid catalyst cocurrent with hydrogen gas. The catalyst consists of cylinders, lobed cylinders or rings. The main limitation of this type of reactor is the gradual accumulation of metals and the forthcoming catalyst deactivation. At the end of a run cycle the reactor must be shut down to replace the catalyst.

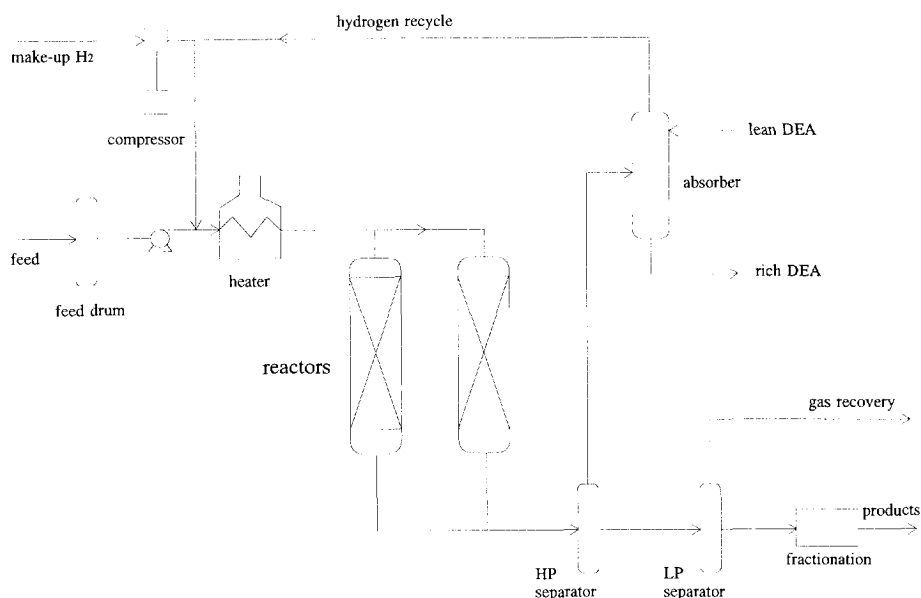


**Figure 5.** Schematic representation of a fixed bed catalytic process.

A flowsheet of a catalytic ebullated bed process is given in Figure 6 (LC Fining process). Ebullated bed reactors can be used to process feeds which contain solid material such as minerals. Liquid and hydrogen are introduced in the bottom of the reactor and the product is taken from the top. The upward flow of liquid, achieved by internal recycle pumps and recycle gas, is used to expand the catalyst bed and maintain the entire reactor backmixed, including the catalyst pellets. The catalysts used for ebullated bed reactors are equivalent in composition to the catalysts for fixed bed processes, however, the pellet diameter is usually smaller than 1 mm to facilitate complete suspension of the catalyst in the liquid phase and to avoid mass transfer limitations.

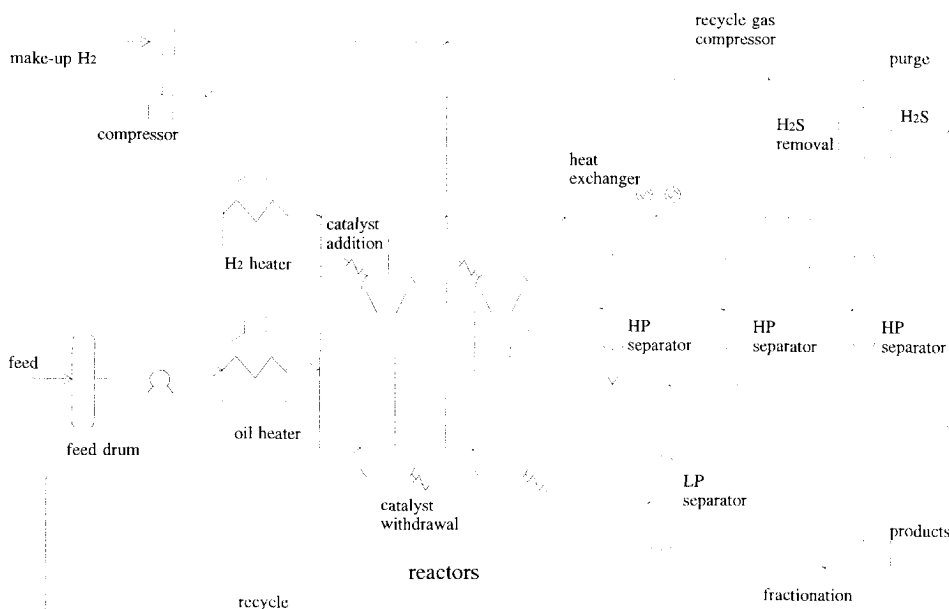


**Figure 6.** Schematic representation of an ebullated bed process.

An example of a process using a moving-bed reactor is Shell HYCON process, which is depicted in Figure 7. This is an example of a technology for hydroprocessing of heavy oil in a two-stage process (14, 15). In the first stage bunker flow reactors are used for HDM. The catalyst is fed to the top of these reactors and removed at the bottom, so that catalyst pellets gradually progress downward through the reactor as a part of a moving packed bed. In the second stage, trickle bed reactors are used for HDS and HCON. Typical performance of this process is (for Arabian Heavy residue): desulfurisation: 92%, demetallisation: 95 %, conversion to distillables < 798 K: 55 %.

Selection of reactor and catalyst type for HDM/HDS hydroprocessing depends on the type of feedstock and the metal content in the feedstock and is a compromise between activity and stability. Application of a highly active catalyst results in a low stability, that is a short catalyst life-time and vice versa. Table 2 summarizes the reactor and catalyst types for HDM/HDS hydroprocessing dependent on the metal content in the feedstock (16). A process cycle of 0.5 to 1 year is assumed.

Introduction

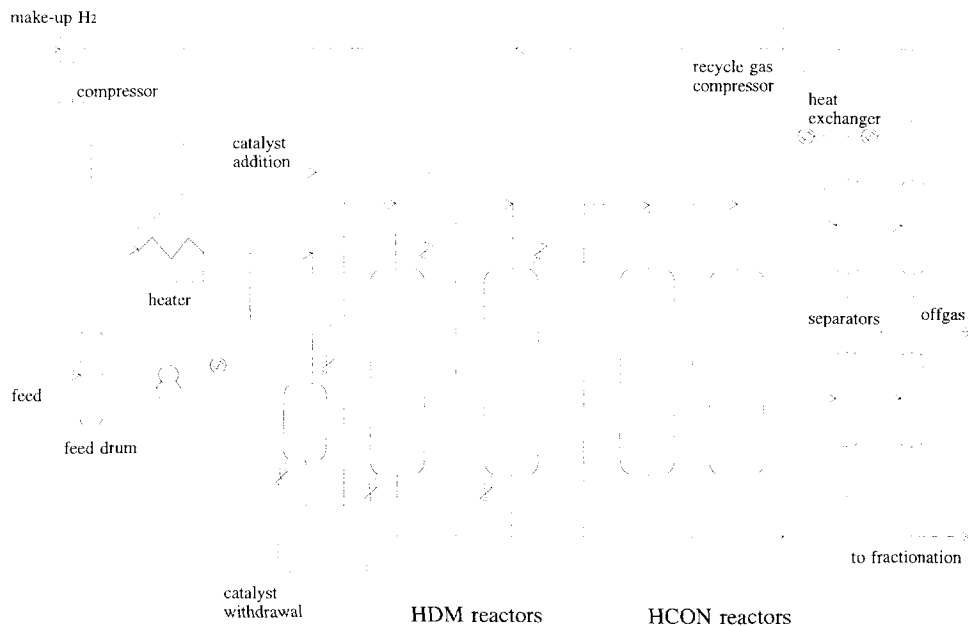
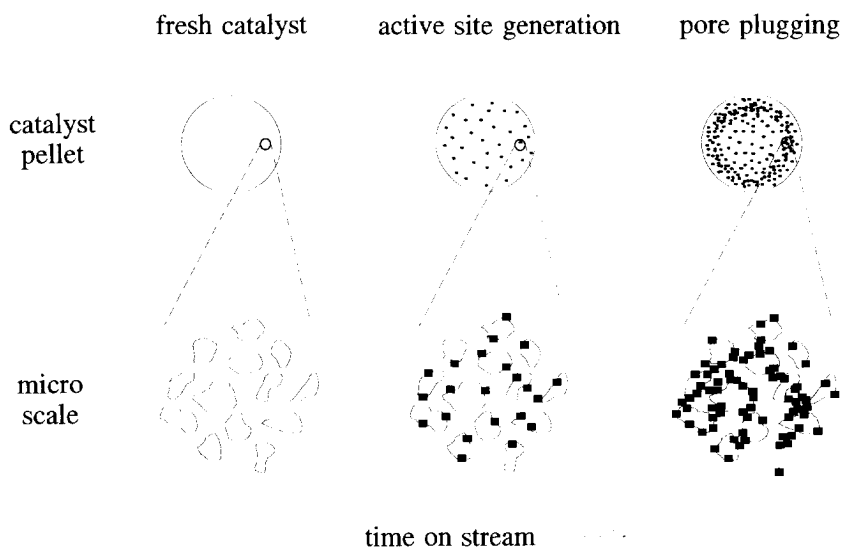


Figure 7. Schematic representation of a moving bed process.

**TABLE 2**  
Selection of the catalyst system and reactor type.

Feedstock metal content	Catalyst system	Reactor type
< 25 wt.ppm	narrow pore HDS catalyst	Fixed bed
25 - 50 wt.ppm	dual catalyst system top: wide pore HDS catalyst bottom: narrow pore HDS catalyst	Fixed bed
50 - 100 wt.ppm	triple catalyst system HDM catalyst preceding the dual catalyst system	Fixed bed
> 75 wt.ppm	triple catalyst system	Moving-bed (bunker flow)
above a few hundred wt.ppm	triple catalyst system + catalyst regeneration	Moving bed

The catalyst type for HDM/HDS hydroprocessing determines the catalyst deactivation phenomena. As previously mentioned, a CoMo or NiMo HDS catalyst deactivates due to active site poisoning and pore plugging. Metal deposition on a silica based wide pore catalyst can cause an increased activity for HDM due to the auto-catalytic effect of the deposited nickel and vanadium ('*active site generation*'). Eventually, at high metal loadings *pore plugging* becomes the dominant deactivation phenomenon (see Figure 8).



**Figure 8.** Metal deposition process in wide-pore HDM catalysts, starting from bare support.

#### 2.4. Catalyst regeneration

Spent residue hydrotreating catalysts are difficult to regenerate due to the presence of nickel and vanadium sulfide deposits. Coke deposits can be removed easily by calcination. Leaching of the catalysts in a weak acid, e.g. oxalic acid, can give significant recovery in activity, provided that the leaching is controlled to avoid excessive leaching of the original active phase (CoMo or NiMo) (17).

Shell developed a Demetallisation Catalyst Rejuvenation (DCR) process for deactivated HYCON catalysts (18). This process, which is depicted in Figure 9, is based on acid extraction of vanadium and nickel and consists of five steps.

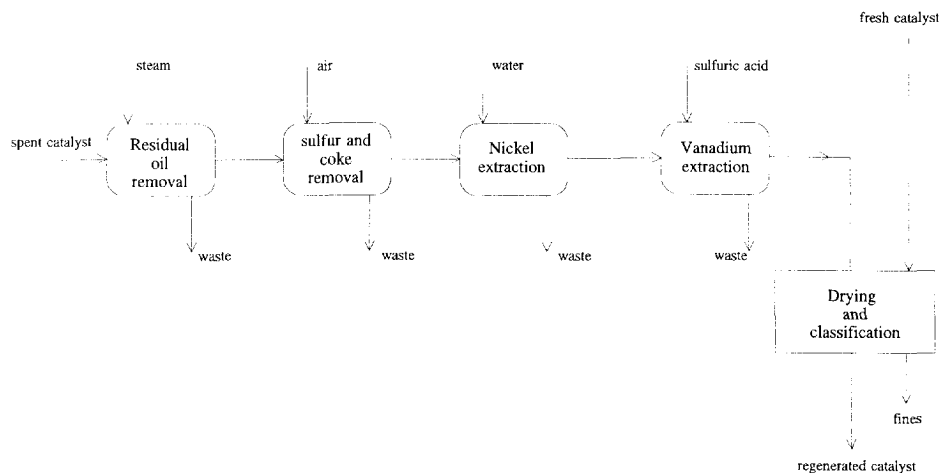


**Figure 9.** Shell's Demetallisation Catalyst Rejuvenation (DCR) process.

Residual oil is removed from the catalyst pellets by contact with steam at temperatures below 1073 K. Simultaneously some sulfur and coke deposits are also removed. The remaining sulfur and coke are removed by oxidation with air at temperatures between 623 and 873 K, sulfur and coke form sulfur dioxide and carbon dioxide respectively. Nickel is removed by water extraction at temperatures between 323 and 423 K. Vanadium is removed by sulfuric acid extraction at pH between 1 and 2 (19). After the extraction the catalyst pellets are dried at 620 K, classified to remove disintegrated pellets and returned into the process.

### 3. CATALYST DEACTIVATION

Figure 10 shows the typical three stage activity decline of a hydrotreating catalyst while processing an oil residue (20). A rapid initial decline in the activity is observed, which is due to coke and initial metal sulfides deposits on the catalyst. After this initial deactivation, a steady and slow decline in activity is observed which is caused by the build-up of metals. Next, a fast and complete deactivation is observed which is due to pore plugging.



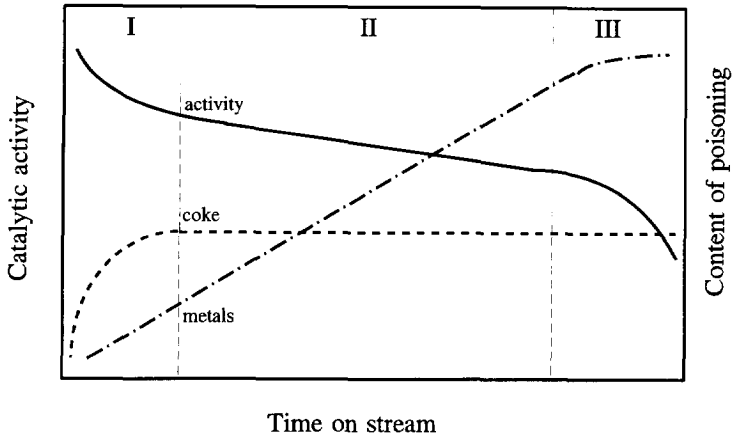


**Figure 10.** Typical three stage activity decline of a residue hydrotreating catalyst.

It is generally accepted that during hydrodemetallisation the catalyst equilibrates rapidly in a few hours with a coke level between 2-10 wt.%, depending on its initial "acidity", feedstock characteristics, temperature and hydrogen partial pressure (21). Therefore, catalyst deactivation by coke deposits will be assumed to be in steady state and is not considered further in the present work.

The phenomena relevant to catalyst deactivation due to metal deposition are schematically organised in Figure 11.

HDM reaction kinetics and mechanistic studies are limited to porphyrinic metal containing model compounds (22-38). It is well-known that HDM studies with model compounds provide insight into fundamental rate processes. The reason is that the use of porphyrinic model compounds eliminates many of the complicated and competing reactions encountered with petroleum residua, thus enabling a clearer picture of the reactions to be ascertained.

Figure 12 shows the various porphyrins employed in the HDM studies. Etio- and octaethyl-type porphyrin have been identified in crude oil and comprise up to 50% of the metal in free porphyrin fraction. Tetraphenyl-type porphyrins as such are not identified in crude oil, but can be representative of bound porphyrins of higher aromaticity existing in petroleum asphaltenes (39).

Introduction

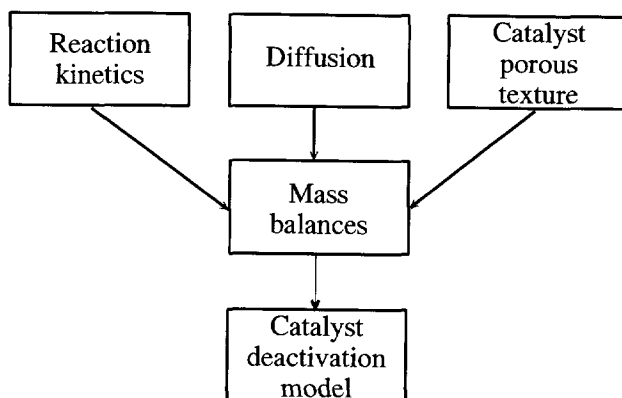


Figure 11. Phenomena relevant to catalyst deactivation model.

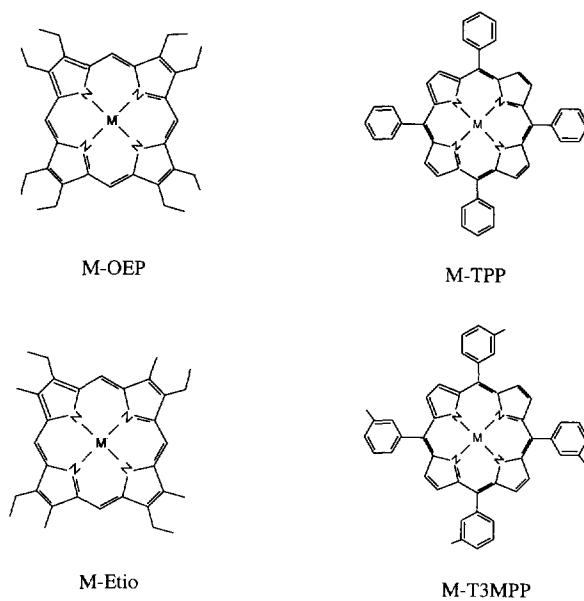
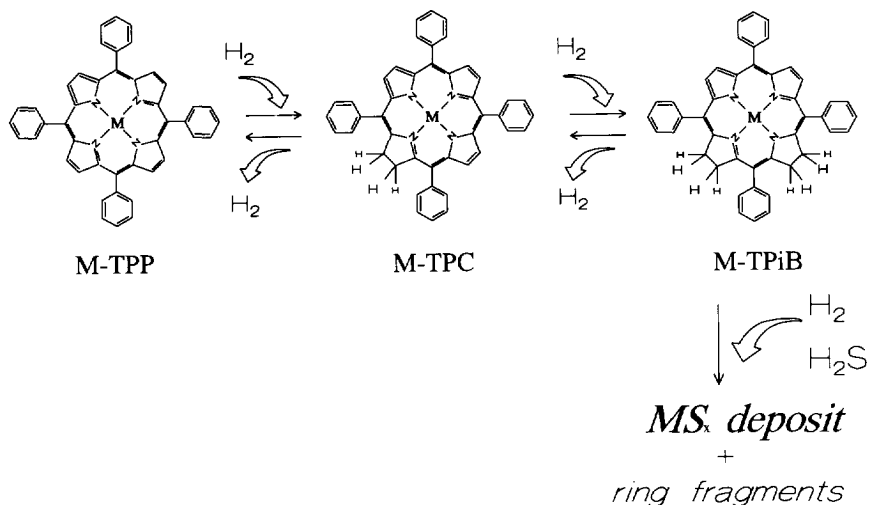


Figure 12. Porphyrins employed in reaction kinetics studies (M-OEP: metallo-octaethylporphyrin; M-TPP: metallo-tetraphenylporphyrin; M-Etio: metallo-etiochlorophyllin; M-T3MPP: metallo-tetra(3-methylphenyl) porphyrin).

The reaction mechanism for the hydrodemetallisation of metallo-tetraphenylporphyrin is depicted in Figure 13. M-TPP is reversibly hydrogenated to metallo-tetraphenylchlorin (M-TPC), which is also reversibly hydrogenated to metallo-tetraphenylisobacteriochlorin (M-TPiB). In the last ring cleavage reaction M-TPiB is demetallized and forms metal sulfide deposits on the internal catalyst surface and ring fragments (37, 38).

Hydrodemetallisation reactions require the diffusion of polyaromatic molecules into the pore structure of the catalyst pellet prior to the reaction. When the pore diameter approaches the effective molecular diameter of the diffusing species, the diffusion rate drops dramatically. This results from geometric exclusion at the pore wall and increased viscous drag in the pore and is termed restrictive or configurational diffusion.



**Figure 13.** Hydrodemetallisation reaction mechanism of metallo-tetraphenylporphyrin (M-TPP). (M-TPC: metallo-tetraphenylchlorin, M-TPiB: metallo-tetraphenylisobacteriochlorin)

Restrictive diffusion was first observed in mass transfer through membranes (40). In general, if the solute molecular size is significant with respect to the pore size, a restrictive factor is introduced to account for the reduction in diffusivity within the pore. This restrictive factor, which is the ratio between the effective and bulk diffusion coefficient, is a function of the ratio of the solute and the pore diameter (see Figure 14) and has been determined by various researchers (41-55). This picture may be an oversimplification for situations where

adsorption is important. Adsorption can lead to strongly increased mass transfer (56) which could cause a maximum in the curve for the restrictive factor.

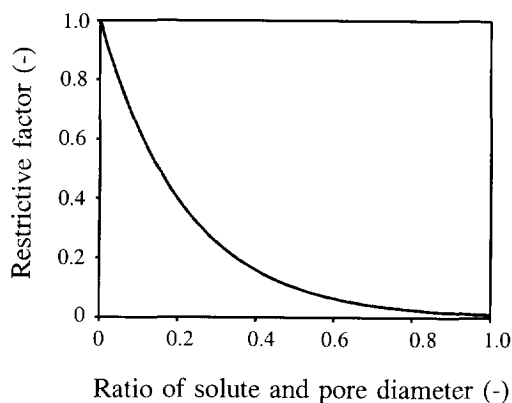


**Figure 14.** Example of the restrictive factor as a function of the ratio of the solute and pore diameter (41).

Reaction kinetics and diffusion are the important phenomena determining the rate of metal deposition and, therefore, the rate of catalyst deactivation. However, an other important phenomenon is the description of the catalyst porous texture. Variables characterising the catalyst porous texture, such as the porosity, tortuosity and interconnectivity of pores, are changing during the metal deposition process and have to be described.

Reaction kinetics, diffusion and catalyst porous texture are integrated in the mass balances and determine the catalyst deactivation model.

## REFERENCES

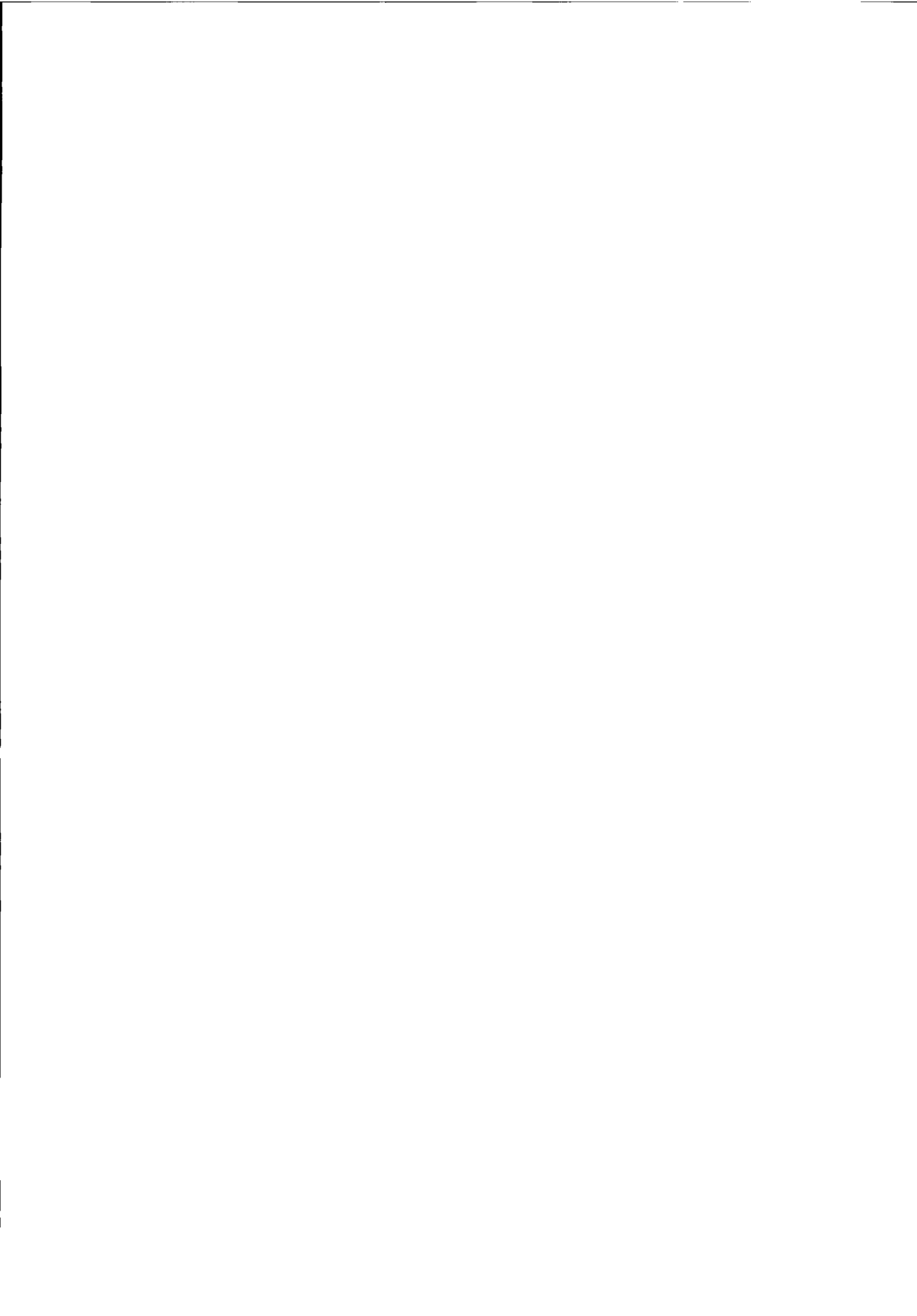
1. Valais, M., 'Natural Gas and crude oil, parallel outlooks or complementary destinies', 17th International Energy Conference, IRCEED, University of Colorado, Boulder, April 2 - May 2, 1990.
2. Aalund, L., *Oil Gas J.*, **81**(15) 93-95, **81**(18) 204-215 (1983).
3. Quann, R.J., Ware, R.A., Hung, C.W., and Wei, J., *Adv. Chem. Eng.*, **14** (1988) 159.
4. Sie, S.T., in 'Catalyst deactivation', Delmon, B. and Froment G.F. (Eds.), Elsevier Scientific Publishing Company, Amsterdam (1980) 545.

## Chapter 1

5. Buchler, J.W., in 'Porphyrins and Metalloporphyrins' (Smith, K.M., Ed.), Chapt. 5, Elsevier, Amsterdam (1975).
6. Baker, E.W., *J. Am. Chem. Soc.*, **88** (1966) 2311.
7. Baker, E.W., and Palmer, S.E., in 'The Porphyrins' (Dolphin, D., Ed), Vol. 1, Chapt. 11, Academic Press New York (1978)
8. Baker, E.W., Yen, T.F., Dickie, J.P., Rhodes, R.E., and Clark, L.F., *J. Am. Chem. Soc.*, **89** (1967) 3631.
9. Yen, T.F., and Silverman, S.R., *ACS Prepr. Div. Petrol. Chem.*, **14** (1969) E32-E39.
10. Fisher, L.R., and Dunning, H.N., *Bur. Mines Rep. Invest.*, (1961) 5844.
11. Sugihara, J.M., Branthaver, G.Y., Wu, G.Y., and Weatherbee, C., *ACS Prepr. Div. Petrol. Chem.*, **15** (1970) C5.
12. Yen, T.F., 'The Role of Trace Metals in Petroleum', Ann Arbor Science Publ., Ann Arbor, Michigan (1975).
13. Barwise, A.J.G., and Whitehead, E.V., *ACS Prepr. Div. Petrol. Chem.*, **25** (1980) 268.
14. van Zijll Langhout, W.C., Ouwerkerk, C., and Pronk, K.M.A., *Oil Gas J.*, **78**(48) (1980) 120.
15. Röbschlager, K.W., Deelen, W.J., and Naber, J.E., 'The Shell residue hydrocarbon conversion process: Development and future applications', Proc. Int. Symp. on Heavy Oil and Residue Upgrading and Utilization (Han, C., and Hsi, C, Eds.). International Academic, Beijing, (1992) 249.
16. Stork, W.H.J., 'Catalysts for residue conversion', Paper presented at First Shell Workshop, Santa Domingo, March 10-11 (1983).
17. Stanislaus, A., Marafi, M., Absi-Halabi, M., *ACS Prepr. Div. Petrol. Chem.*, **38**(1) (1993) 62.
18. Kwant, P.B., and van Zijll Langhout, W.C., *I<sup>2</sup>-Procestechnologie*, **10** (1986) 11.
19. European Patent, Application no. 81200151.9 (1981).
20. Thakur, D.S., and Thomas, M.G., *Appl. Catal.*, **15** (1985) 197.
21. Toulhoat, H., Szymanski, R., and Plumail, J.C., *Cat. Today*, **7** (1990) 531.
22. Hung, C-W, and Wei, J., *Ind. Eng. Chem. Process Des. Dev.* **19** (1980) 250.
23. Hung, C-W, and Wei, J., *Ind. Eng. Chem. Process Des. Dev.* **19** (1980) 257.
24. Kameyama, H., Sugishima, M., Yamada, M., and Amano, A., *J. Jpn. Petrol. Inst.*, **24** (1981) 317.
25. Kameyama, H., and Amano, A., *J. Jpn. Petrol. Inst.*, **25** (1982) 118.
26. Rankel, L.A., and Rollmann, L.D., *Fuel*, **62** (1983) 44.
27. Weitkamp, J., Gerhardt, W., Rigoni, R., and Dauns, H., *Erdöl und Kohle - Erdgas - Petrochemie*, **36** (12) December (1983) 569.
28. Agrawal, R., and Wei, J., *Ind. Eng. Chem. Process Des. Dev.*, **23** (1984) 505.
29. Agrawal, R., and Wei, J., *Ind. Eng. Chem. Process Des. Dev.*, **23** (1984) 515.
30. Morales, A., Garcia, J.J., and Prada, R., *8th Proc. Int. Congr. Catal.*, Berlin, July 2-6, **2** (1984) 341.
31. Kameyama, H., Shibuya, M., Teshigahara, I., and Amano, A., *J. Jpn. Petrol. Inst.*, **28** (1985) 83.

## Introduction

32. Ware, R.A., and Wei, J., *Prepr. ACS, Div. Petr. Chem.*, **30** (1985) 62.
33. Ware, R.A., and Wei, J., *J. Catal.*, **93** (1985) 100.
34. Ware, R.A., and Wei, J., *J. Catal.*, **93** (1985) 135.
35. Webster, I.A., and Wei, J., *Prepr. ACS, Div. Petr. Chem.*, **30** (1985) 37.
36. Smith, B.J., and Wei, J., *J. Catal.*, **132** (1991) 1.
37. Vaughan, G.B., Tynan, E.C., and Yen, T.F., *Chem. Geol.*, **6** (1970) 203.
38. Bonné, R.L.C., Steenderen, P. van, and Moulijn, J.A., *Bull. Soc. Chim. Belg.*, **100** (11-12) (1991) 877.
39. Bonné, R.L.C., Ph.D thesis, University of Amsterdam (1992).
40. Renkin, E.M., *J. Gen. Physiol.*, **38** (1954) 225.
41. Satterfield, C.N., Colton, C.K., and Pitcher, W.H., *AIChE J.*, **19** (3) (1973) 628.
42. Spry, J.C. and Sawyer, W.H., *68th Ann. AIChE Meeting*, Los Angeles (1975).
43. Prasher, B.D., G.A. Gabriel, and Ma, Y.H... *Ind. Eng. Chem. Process Des. Dev.*, **17** (1978) 266.
44. Tsai, M.C. and Ruckenstein, E., *AIChE J.*, **27** (1981) 697.
45. Chantong A., and Massoth, F.E., *AIChE J.*, **29** (1982) 725.
46. Galiasso, R., R. Blanco, C. Gonzalez, and Quinteros, N., *Fuel*, **62** (1983) 817.
47. Galiasso, R., and Morales, A., *Appl. Catal.*, **7** (1983) 57.
48. Seo, G., and Massoth, F.E., *AIChE J.*, **31** (3) (1985) 494.
49. Lee, S.Y., Seader, J.D., Tsai, C-H., and Massoth, F.E., *Ind. Eng. Chem. Res.*, **30**, (1991) 22.
50. Lee, S.Y., Seader, J.D., Tsai, C-H., and Massoth, F.E., *Ind. Eng. Chem. Res.*, **30** (1991) 29.
51. Lee, S.Y., Seader, J.D., Tsai, C-H., and Massoth, F.E., *Ind. Eng. Chem. Res.*, **30** (1991) 607.
52. Lee, S.Y., Seader, J.D., Tsai, C-H., and Massoth, F.E., *Ind. Eng. Chem. Res.*, **30** (1991) 1683.
53. Tsai, C-H., Seader, J.D., Lee, S.Y., and Massoth, F.E., *Ind. Eng. Chem. Res.*, **30**, 22-28. 1991.
54. Tsai, C-H., Seader, J.D., Lee, S.Y., and Massoth, F.E., *Fuel Proc. Tech.*, **29** (1991) 153.
55. Tsai, M-C, Chen, Y-W, and Li, C., *Ind. Eng. Chem. Res.*, **32** (1993) 1603.
56. Bakker, W.J.W., Kapteijn, F., Poppe, J., and Moulijn, J.A., 'Permeation characteristics of a Metal-Supported Silicalite-1 Zeolite Membrane', *J. Membr. Sci.*, in press.



# Chapter 2

## Equipment for Catalyst Testing and Deactivation

---

Testing has always been an important issue in catalytic research and development. Catalyst testing is necessary to determine and understand the performance of the catalyst, to check new ideas and developments.

An important aspect in catalyst testing is the relation between laboratory scale and industrial, commercial scale. Since small performance differences often are of great economic importance on industrial scale, laboratory tests must give accurate results which can discriminate between even small performance differences (1). Therefore, the 'scaling- rules' between laboratory scale catalyst testing and industrial scale should be very well understood.

Scaling-down of catalyst testing equipment has some major advantages, such as lower construction and installation costs, less consumption of materials and less waste, reduced demands on laboratory infrastructure, an increased intrinsic safety and reduced manpower needs (1, 2).

Catalyst testing is necessary to understand the theory, *i.e.* important aspects are complexity of the feedstock, unknown detailed reaction networks and the lack of basic kinetic data. Knowledge of all this makes computer modelling possible which is an efficient tool in process development and design.

In this chapter, two types of catalyst testing equipment are discussed. The batch autoclave reactor and the microflow reactor. The batch reactor has proven to be very (time) efficient in generating basic kinetic data and catalyst screening (3). The microflow reactor has proven to give comparable results with large scale reactors (1) and is suitable for catalyst stability or deactivation tests.

---



## 1. BATCH AUTOCLAVE REACTOR

### 1.1. Experimental set-up

Hydrodemetallisation reaction kinetic experiments were performed in a batch autoclave reactor equipped with a swinging capillary stirrer. The batch autoclave experimental set-up, as depicted in Figure 1, comprises three parts, (1) gas supply system, (2) autoclave reactor, and (3) analysis and control section.

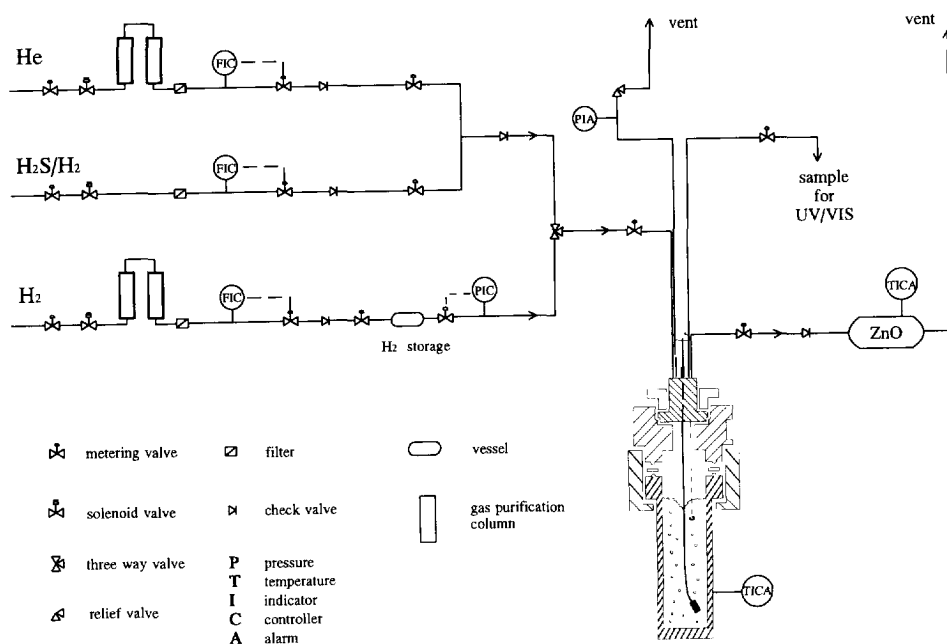


**Figure 1.** Experimental set-up of the autoclave reactor.

#### 1.1.1. Gas supply system

Three gases are available, He at 0.6 MPa (Air Products, purity 99.996 %) - for purging of the total set up, 15 mol% H<sub>2</sub>S/H<sub>2</sub> at 0.6 MPa (Scott Specialty Gases, purity 99.99 %) - for sulfiding and the hydrodemetallisation reaction, and H<sub>2</sub> at 15 MPa (Air Products, purity 99.95%) - for the hydrodemetallisation reaction. The tubing in the gas supply system is

## *Equipment for Catalyst Testing*

equipped with dust filters, stop cocks, solenoid valves, mass flow controllers (Bronkhorst HI-TEC, model F-033C), pressure controllers (Bronkhorst HI-TEC, model P-522C) and check valves, in order to control both flow to and pressure in the autoclave.

The H<sub>2</sub> and He gas streams are purified in gas purification columns, filled with Pd/Al<sub>2</sub>O<sub>3</sub> (BASF, R 0-21) and Cu/SiO<sub>2</sub> (BASF, R 3-11) extrudates respectively, to convert any oxygen present in the gas feed into water. Water is captured subsequently in columns filled with mol sieve 5A (Pleuger, Uetikon 5 Å).

### *1.1.2. Autoclave reactor*

The 250 ml autoclave reactor is made of stainless steel SS-316Ti (design and construction: Delft University of Technology) and is equipped with a thermocouple for internal temperature measurements and a pressure transducer (Kulite, XTME-190M), both connected to an alarm. The oven for heating the autoclave (Wilmod, bandheater 2000 W) is equipped with both a control and alarm thermocouple.

For safety purposes, a safety valve is mounted on the reactor. This valve is of the spring type and opens at 175 bar to the regular fume disposal channel.

The reactor is equipped with a type of stirring device, which is based on a flexible capillary tube. The capillary tube is closed on one side, and a slightly arched rod is inserted on the other side, so the capillary tube forms an arch. By fixing one end of the capillary to the autoclave cover, and by rotating the rod, the free end acts as a rotating stirrer (4).

Effluent gases can be released via a ZnO (BASF, R 5-10) vessel to purify the gas from H<sub>2</sub>S.

### *1.1.3. Control section*

Analogue signals from thermocouples are fed to a multi-loop control rack (West Gardsman). This rack can control up to eight temperature loops, of which two are in use by the HDM autoclave; one for controlling the temperature of the autoclave oven and one for the temperature of the ZnO vessel. Temperature programmes can be set up for the autoclave oven for employment in different sulfiding procedures.

The flow rates (Bronkhorst HI-TEC, model E-5612-E40-AD) and pressure (Kulite, model DDM80A) within the system are monitored and controlled on a control panel.

## 1.2. Experimental procedures

### 1.2.1. Catalyst introduction

Approximately 80 to 100 mg of catalyst is introduced in the autoclave (which was removed from the set-up to enable careful cleaning). The autoclave is mounted into the set-up with eight nuts. The nuts are treated with Never Seez, a high temperature lubricant, to facilitate loosening of the nuts afterwards. Leak tests were performed with 0.6 MPa He and with H<sub>2</sub> up to 5 MPa. The system was considered free of leaks when the pressure drop after 1 hour was less than 1%.

### 1.2.2. Catalyst sulfiding

An excess of liquid dimethyldisulfide (DMDS, 2 g per batch) is dissolved in 50 ml of *o*-xylene and introduced into the autoclave. DMDS is readily hydrogenated to form methane and H<sub>2</sub>S. A hydrogen pressure of 2 MPa is applied, after purging the autoclave. The decision to take 50 ml of solvent was based on the requirement that the stirrer should be (partially) immersed in the liquid. This leaves 75 ml of solvent for the dissolution and introduction of the porphyrins, which proved to be sufficient.

The setpoint of the autoclave oven is set immediately to 623 K, and the stirrer is set to 2000 rpm. Sulfiding takes place at 623 K during three hours, including the time required for heating up.

### 1.2.3. Run procedure

After sulfiding and cooling down the autoclave, the sulfiding gases are discarded through the ZnO vessel and He is led through the autoclave to remove all H<sub>2</sub>S. Approximately 80 to 100 mg VO-TPP is dissolved in 75 ml *o*-xylene. Complete dissolution of VO-TPP is accomplished only by placing the flask in an ultrasonic bath for 30 minutes. Table 1 summarizes the total amounts of reactant, solvent, catalyst and sulfiding agent added to the reactor system. The relatively low ratio between the amount of the reactant VO-TPP and the vanadium on the catalyst gives no problems in the reaction kinetics experiments since not all vanadium present on the catalyst acts as a catalytic active site.

TABLE 1

Amounts of reactant, solvent, catalyst and sulfiding agent added to the autoclave.

Reactant	Solvent	Catalyst	Sulfiding agent
VO-TPP	<i>o</i> -xylene	V(2.2 at./nm <sup>2</sup> )/Al <sub>2</sub> O <sub>3</sub>	DMDS
mol	mol	mol V	mol
(120 - 150)·10 <sup>-6</sup>	1.0	(30 - 40)·10 <sup>-6</sup>	31·10 <sup>-3</sup>

The reaction mixture is introduced into the autoclave via a filling tube by means of a syringe with a long needle. The H<sub>2</sub>S/H<sub>2</sub> gas mixture is passed through at 50 ml/min for 10 minutes. Then the autoclave gas outlet is closed, and 0.3 or 0.4 MPa of H<sub>2</sub>S/H<sub>2</sub> is fed into the autoclave. With H<sub>2</sub>, the final autoclave pressure is set to 5.0 MPa. The autoclave is then heated to the reaction temperature as fast as possible. Only a few degrees K before the reaction temperature is reached, the stirrer is set to the appropriate revolution speed to avoid premature conversion of VO-TPP. At 578 K, the autoclave pressure should be about 10.0 MPa. At chosen time intervals liquid samples of 0.5 ml are taken via the sampling tube and are analysed *ex-situ* with UV-VIS spectroscopy to determine the porphyrin concentrations.

What has to be born in mind is the possibility of mass transport limitations in the reaction mixture during a run. The catalyst particles may not be suspended evenly throughout the whole reaction mixture volume, and the homogenization or mixing time of the reaction mixture may not be sufficiently high as to eliminate reactant concentration gradients. These limitations can all be overcome by setting the stirring speed to a value high enough to approach ideal mixing and suspension. A lot of information about the behaviour of the slurry as a function of the stirring speed can be obtained when this behaviour is visualized; a glass beaker with approximately the same dimensions as the autoclave can be used instead of the autoclave itself to study the hydrodynamic behaviour. As the liquid dynamic viscosity and density can be expected to be very important parameters in catalyst particle suspension, a liquid must be chosen that, at ambient conditions, has a similar viscosity and density as *o*-xylene at process conditions. Acetone proved to be the most suitable liquid.

The observed hydrodynamic behaviour is depicted in Figure 2. From the drawings it can be seen that solid suspension becomes complete between 1500 and 1750 rpm, and that gas bubbles become abundant between 1750 and 2000 rpm. Also note that the sample filter acts as a baffle at higher speeds.

Another convenient way to determine the minimal stirring speed required for complete suspension and homogenization is to keep on increasing the stirring speed in subsequent runs until no further change in the reaction rate constants is observed. Runs were conducted at 1000, 2000 and 2200 rpm as stirring speed. The individual reactions rate constants at different stirring speeds were determined. This showed that at 1000 rpm poor solid suspension leads to low values for the reaction rate constants. It is concluded that at 2000 rpm and higher, the variations in reaction rate constants are barely significant and that the minimum stirring speed to avoid mass transfer limitations is attained at 2000 rpm.

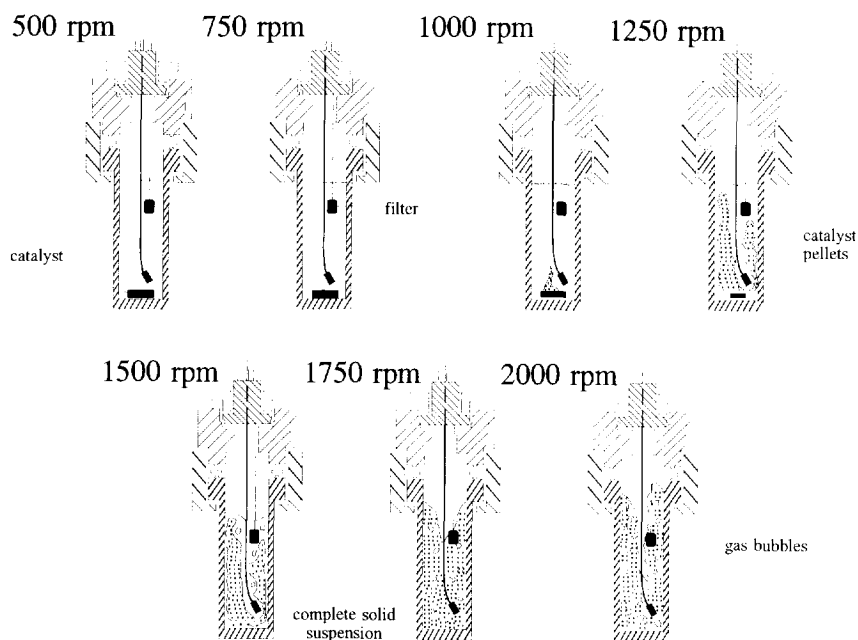


**Figure 2.** Hydrodynamics in the autoclave as a function of the stirring speed.

Table 2 summarizes published criteria for complete solid suspension and homogenization of the reaction mixture for a turbine agitator with flat blades. Application of these criteria and available empirical correlations (5) to the 'swinging capillary' stirring device shows that the reaction kinetic experiments, conducted at 2000 rpm, reach complete solid suspension and homogenization of the reaction mixture.

TABLE 2

Criteria for complete solid suspension and homogenization of the reaction mixture.

	'swinging capillary'	criterion (5)
stirring speed (rpm)	2000	> 1390 for complete solid suspension
mixing time (s)	74	20 - 100 for complete homogenization
Reynolds number (-)	$4.5 \cdot 10^4$	> $10^4$ for turbulent flow

#### 1.2.4. Sample analysis

One of the most striking properties of porphyrins is their intense colour, even when dissolved in a liquid, and the presence of intense absorption bands in the visible region of the electronic spectrum. In this region it is possible to discriminate between VO-TPP and its hydrogenated intermediates since they have very characteristic absorption bands that can be used for qualitative as well as for quantitative analysis. Figure 3 shows a typical evolution of the UV-VIS absorption spectrum of VO-TPP and its intermediates during reaction. In analogy with literature, the absorption bands in Figure 3 are assigned to (1) VO-TPP, (2) VO-TPC and (3) VO-TPiB, respectively.

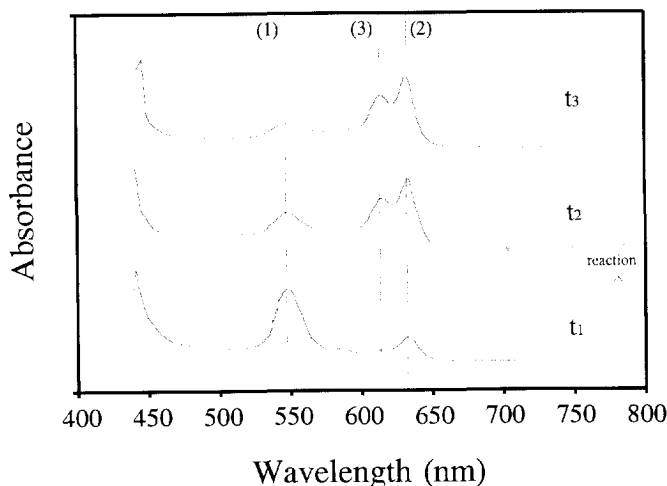


**Figure 3.** Typical evolution of UV-VIS absorption spectrum of product samples during VO-TPP hydrodemetallisation (reaction time:  $t_1 < t_2 < t_3$ ).

Concentrations of the various porphyrinic compounds can be calculated from their absorption maxima in conjunction with Lambert-Beer's law:

$$A_i = \epsilon_i L C_i \quad (1)$$

In order to estimate the concentrations of the various porphyrinic compounds, their specific wavelengths (at which maximum absorption occurs) and molar extinction coefficients at these wavelengths have to be known. These are presented in Table 3.

**TABLE 3**  
Characteristic wavelengths ( $\lambda$ ) and molar extinction coefficients ( $\epsilon$ ) of VO-TPP and its hydrogenated intermediates ( $\delta$ ).

Compound	$\lambda$ (nm)	$\epsilon$ (m <sup>2</sup> /mol)
VO-TPP	548.0	2300
VO-TPC	632.7	4400
VO-TPiB	615.1	6700

Since the concentrations in the cuvette are determined at room temperature and atmospheric pressure, corrections have to be applied to calculate the actual concentrations in the autoclave. These corrections are discussed in section 1.3.3.

The UV-VIS analysis was done with a Beckman model 35 spectrophotometer. About 0.2 ml of the liquid was introduced in a 1.00 mm quartz cuvette. Dilution of the sample was not necessary. The spectrophotometer was calibrated at 548 nm with pure *o*-xylene as reference.

### 1.3. Reaction mechanism and kinetics

#### 1.3.1. Reaction mechanism

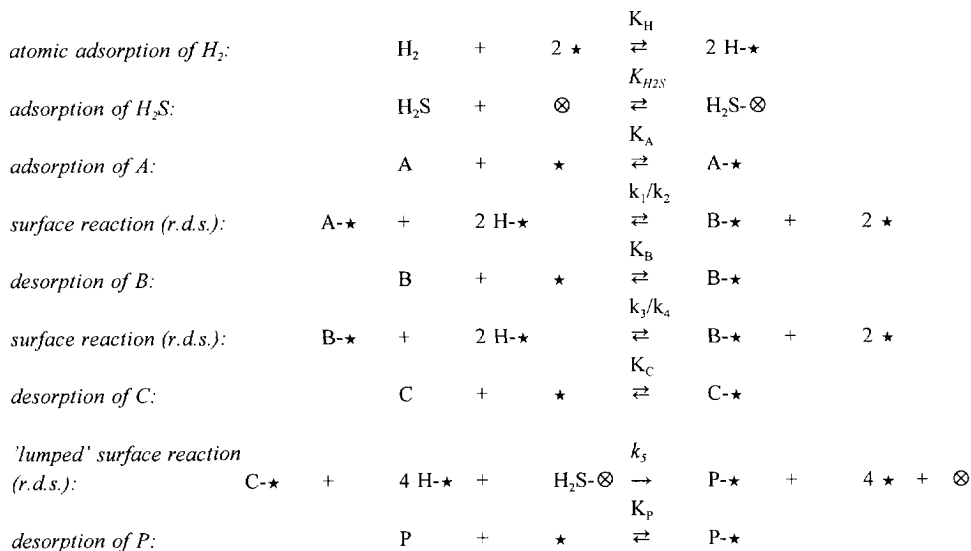
Although vanadyl-5,10,15,20-tetraphenylporphyrin (VO-TPP) is not a metallo-porphyrin occurring naturally in petroleum feedstocks, its difference with metallo-porphyrins that do occur in petroleum (*e.g.* porphyrins of the etio-type), is restricted to the groups substituted to the tetrapyrrole nucleus. But as the VO-TPP substituents are representative of porphyrins with a high degree of aromaticity (due to the substituted phenyl groups) and enhanced stability (due

to sterically hindered adsorption of central metal ion), insight in the VO-TPP HDM reaction mechanism may help to comprehend the complex HDM reactions that do occur in petroleum.

The vanadium metal atom in VO-TPP is removed in a series of reactions which involve two hydrogenation steps and a lumped ring cleavage step. In the presence of H<sub>2</sub>S, Bonn  (7) detected two hydrogenated intermediates in the reaction mixture, being vanadyl-5,10,15,20-tetraphenylchlorin (VO-TPC) and vanadyl-5,10,15,20-tetra-isobacteriochlorin (VO-TPiB), both of which are formed in reversible hydrogenation/dehydrogenation reactions. No other intermediates were observed, so it was assumed that the demetallisation reaction takes place after the formation of VO-TPiB. It will be shown later that this demetallisation reaction probably consists of a series of fast hydrogenation and hydrogenolysis reactions (8, 9).

### 1.3.2. Reaction kinetics

Metallo-tetraphenylporphyrin proved to be an excellent model compound for reaction kinetics experiments since it reacts on a time scale at which batch reactors can be used. Based on numerous experiments, Bonn  (10) proposed the following set of elementary reactions for the hydrodemetallisation of M-TPP (A = M-TPP, B = M-TPC, C = M-TPiB, P = products; ★ = hydrogenation site, ⊗ = hydrogenolysis site):



A Langmuir-Hinshelwood type of kinetics with competitive adsorption of hydrogen applies for the M-TPP hydrodemetallisation. Competitive adsorption of H<sub>2</sub>S and the reaction products



(ring fragments) are found to be negligible (10, 11). If competitive adsorption of H<sub>2</sub> is taken into account, the Langmuir-Hinshelwood rate equations for this sequential reaction mechanism lead to:

$$-r_A = \frac{k_1 K_H C_A C_{H_2} - k_2 C_B}{(1 + \sqrt{K_H C_{H_2}})^3} \quad (2)$$

$$-r_B = \frac{-k_1 K_H C_A C_{H_2} + k_2 C_B + k_3 K_H C_B C_{H_2} - k_4 C_C}{(1 + \sqrt{K_H C_{H_2}})^3} \quad (3)$$

$$-r_C = \frac{-k_3 K_H C_B C_{H_2} + k_4 C_C}{(1 + \sqrt{K_H C_{H_2}})^3} + \frac{k_5 K_H^2 C_C C_{H_2}^2 C_{H_2S}}{(1 + \sqrt{K_H C_{H_2}})^5} \quad (4)$$

Equilibrium constants  $K_{ij}$  of these rate equations are defined as:

$$K_{12} = \left( \frac{C_B}{C_A C_{H_2}} \right)_{eq} \cdot \frac{1}{K_H} = \left( \frac{k_1}{k_2} \right) \quad (5)$$

and

$$K_{34} = \left( \frac{C_C}{C_B C_{H_2}} \right)_{eq} \cdot \frac{1}{K_H} = \left( \frac{k_3}{k_4} \right) \quad (6)$$

Values for the H<sub>2</sub> adsorption constant were found to be small but statistically significant (12):

$$K_H = (7.5 \pm 6.2) \cdot 10^{-5} \text{ m}^3/\text{mol}.$$

For this combination, the values for  $K_{12}$  and  $K_{34}$ , as defined by equations 5 and 6, were found to be (for VO-TPP):

$$K_{12} = 42 \pm 16$$

$$K_{34} = 46 \pm 24$$

### 1.3.3. Thermodynamics

The conditions at which porphyrin concentrations are measured (with UV-VIS, at room temperature and atmospheric pressure) and at which porphyrins react in the autoclave differ significantly. A correction is necessary since these concentrations are not equal in both cases.

Liquid densities are of course a function of primarily the temperature (a slight influence of pressure is also observed). A significant fraction of the solvent introduced into the autoclave at room temperature may have moved to the gas phase at elevated temperatures. Hydrogen and hydrogen sulfide concentrations in the liquid phase are definite functions of both temperature and pressure. All these factors influence the porphyrin concentration, and when converting the measured concentrations to actual concentrations, they must be accounted for.

Relationships between the above properties and process conditions are determined with computer programme SUPRTRAP (National Bureau of Standards, Boulder, Colorado, USA). The polynomials are based on thermodynamic calculations conducted by van Steenderen (13) and Bonné (14) using the Peng-Robinson equation of state for mixture compositions and corresponding state relations for component properties (15).

Values for the hydrogen and hydrogensulfide liquid phase concentration at reaction conditions are (10 MPa, 578 K):

$$\begin{aligned} C_{H_2} &= 650 - 750 \text{ mol/m}^3 \\ C_{H_2S} &= 16 - 17 \text{ mol/m}^3 \end{aligned}$$

### 1.3.4. Reaction kinetics parameter estimation and software

The reaction kinetic parameter estimation is carried out by iteratively solving the set of coupled ordinary differential equations describing the conversion of the reactant and intermediates in time, and comparing the calculated concentrations with the measured values. Initial estimates for the reaction rate constants  $k_i$  are adjusted and the sequence is repeated until the differences between calculated and measured concentrations are considered sufficiently small.

Parameter estimation ('fitting') is done by minimizing the total of the squared differences between the measured and calculated concentration of component  $i$  at time  $t$  (the so-called Sum of Squares of Residuals, SSR). In formula:

$$SSR = \sum_{i=1}^3 \sum_{j=1}^n (C_{EXP,ij} - C_{CALC,ij})^2 \quad (7)$$

where  $C_{EXP,ij}$  and  $C_{CALC,ij}$  are the  $j^{\text{th}}$  measured and calculated concentrations of component  $i$ , respectively, and  $n$  is the number of samples taken.

With non-linear regression one is always concerned whether the found estimate vector  $\underline{k}$  leading to the minimal value for the  $SSR(\underline{k})$  is the correct one. Since it might just be a local minimum instead of the global minimum  $SSR_0(\underline{k})$  one is searching for. No rigorous procedures exist to tackle this problem and find the global minimum in all cases with 100 % certainty. An important test to check local minima, however, is to verify different initial estimates for the vector  $\underline{k}$  always lead to the same minimum  $SSR(\underline{k})$  value or not. If this is the case, it can be concluded that  $SSR(\underline{k})$  is equal to  $SSR_0(\underline{k})$ .

A Fortran programme using the NLS (Non-Linear Systems) libraries is developed to tackle the problem of parameter estimation in a set of coupled ordinary differential equations (ODE's) (16). The subroutines contain the coupled ODE's that are solved with the Bulirsch-Stoer method (17). This method is highly efficient and large steps can be taken in the direction of integration. The routine is not well suited for stiff problems, however, our system of ODE's is not stiff at all so this will not cause any problem.

In the subroutine the number of parameters is set, either as a fixed or as a variable parameter. In the kinetic analysis, the hydrogenation and dehydrogenation rate constants are not taken as independent variables, but the ratios  $k_1/k_2$  and  $k_3/k_4$ , which are the equilibrium constants  $K_{12}$  and  $K_{34}$ , are kept constant.

For the minimization of the SSR, the program provides different (combinations) of methods (Simplex, Simplex + Levenberg-Marquardt, Powell, Powell + Levenberg-Marquardt (17)), all of which finally lead to the same results. Since the Simplex + Levenberg-Marquardt algorithm has the most sophisticated convergence criteria to be met by minimization it is used in the present work.

## 2. MICROFLOW REACTOR

### 2.1. Process flow scheme

Figure 4 shows the simplified flow scheme of the microflow equipment.

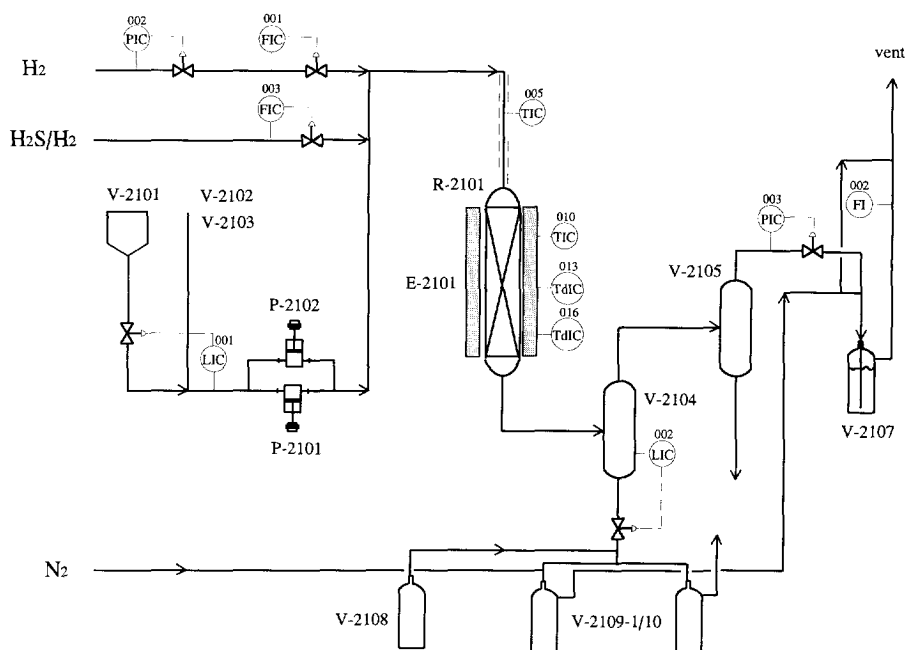


**Figure 4.** Experimental set-up of the microflow reactor.

The liquid feed is pumped from storage vessel (V-2101) by pump (P-2101/P-2102) towards the reactor (R-2101). Prior to entrance the feed is mixed with the hydrogen and preheated. The hydrogen pressure is first reduced to about 10 MPa (PIC002) and then the hydrogen is fed via the flow controller (FIC001) to the liquid line. After combining the hydrogen with the liquid feed, the gas-liquid mixture is preheated to about 50 K below the operating temperature of the reactor (TIC005). In the reactor the temperature of the reactants is brought to the desired temperature (TIC010, TdIC013, TdIC016) by an oven (E-2101).

The catalyst sample is located in the middle of the reactor while the rest of the reactor is filled with inert material (SiC) which ensures good heat equalization and flow distribution.

After leaving the reactor, the gas and liquid are phase separated (V-2104). The overhead vapours are further cooled and possible entrained liquid or condensate is trapped (V-2105).

The overhead gas from V-2105 is let down to atmospheric pressure by a pressure controller (PIC003). As this gas still contains  $H_2S$ , it has to be scrubbed in the caustic scrubber (V-2107) before its flow can be measured (FI002). After FI002 the hydrogen is disposed in the vent system. The liquid product flow is controlled by the level controller (LIC002) and finally collected in the sample collecting system containing vessels (V-2109/1-10).

During liquid sampling  $N_2$  is introduced in the sampling collecting system to strip off the  $H_2S$  and  $NH_3$  formed during hydrotreatment. As a result of the pressure reduction between V-2104 and V-2109 some dissolved gas is liberated which transports the liquid feed towards V-2109. This gas is combined with the effluent  $N_2$  gas.

The dosing pumps (P-2101/P-2102) are running at a fixed stroke and frequency and the flow is measured indirectly by determining the rate of fall of the level in the standpipe. This standpipe (V-2102/V-2103) is installed parallel to the feed line. The level controller (LIC001) ensures that this standpipe always contains liquid. The signal to LIC001 is also used for calculating the flow. The above situation is at normal (catalyst stability testing) operation. During presulfiding with  $H_2S/H_2$ , the liquid flow is stopped and the amount of  $H_2S/H_2$  needed is fed into the hydrogen feed line (FIC003).

All piping is made of 1/4" stainless steel pipe. This size is chosen mainly for mechanical reasons as it combines a reasonable rigidity with small inner diameter (hold up). Flow rates are sufficiently small to prevent pressure drops.

## 2.2. Process control equipment

YEWPACK MARK II is used as control system for the microflow reactor. An operating computer together with the field control unit monitors and controls the entire set-up. Process values are processed in sequence tables and are displayed on the computer monitor. Setpoints can be manipulated by the operator via the operating computer.

## 2.3. HDM catalyst deactivation tests

### 2.3.1. Filling of the reactor

In order to ensure good and constant operating conditions it is of importance to fill the reactor properly. The catalyst bed was separated in four small beds of 5 mm height each. This separation offers the possibility to determine an axial concentration profile in the reactor. The

reactor has a length of 35 cm and a diameter of 15 mm. Four round trays of 5 mm height and an internal diameter of 13 mm are placed in the reactor. The top sides of the trays are open and the bottom side is made from wire gauze. These trays enable the separation of the catalyst pellets during filling and emptying of the reactor. The reactor is closed on top and bottom by a nut.

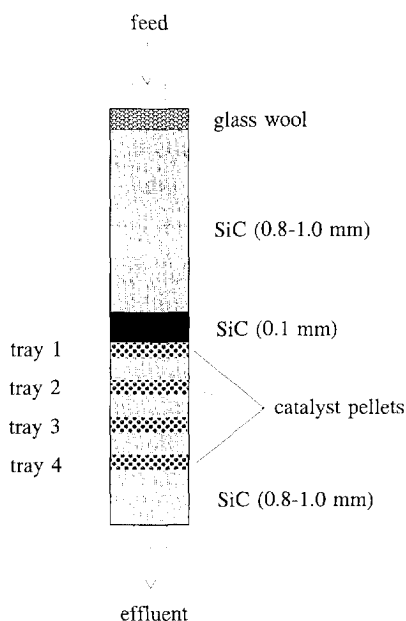


**Figure 5.** Detailed view of filling of the microflow reactor.

A schematic view of the filling of the reactor is shown in Figure 5. In the bottom of the reactor a layer of 5 cm silicon carbide (SiC) is placed. The diameter of the SiC particles is between 0.8 and 1 mm. On this first layer, the four trays with 20 catalyst pellets each are installed. The catalyst pellets with a diameter of 2 mm are too large for micro scale applications (18). To ensure proper liquid distribution, the catalyst beds are diluted with fine 0.1 mm SiC particles. Between the trays a small layer of SiC (0.8-1 mm) is placed. On the top of the trays a layer of 2 cm of fine SiC is placed. The remaining part of the reactor is filled with SiC (0.8-1 mm) and quartz wool. The quartz wool and the SiC on top of the catalyst are sufficient to provide a good radial distribution of the liquid in the reactor (18).

After the filling, the reactor is mounted in the microflow set-up. The nuts are greased with Never Seez, a high temperature lubricant, and fixed with a momentum of 100 Nm.

### 2.3.2. Catalyst sulfiding

Before starting the deactivation test, the catalyst has to be sulfided. The sulfiding is carried out with 3 l/h 15 mol% H<sub>2</sub>S/H<sub>2</sub> at 623 K for three hours at atmospheric pressure.

### 2.3.3. Reaction conditions

A crucial parameter in the HDM catalyst deactivation tests is ratio between the H<sub>2</sub> and liquid flow rate, which consists of a solution of VO-TPP in a mixture of xylene isomers. A high ratio causes crystallization of VO-TPP on SiC in the top of the reactor due to the fact that the VO-TPP/xylene solution reaches a supersaturated state. An other important parameter is the dimensionless wetting number *W*. The catalyst pellets are completely wetted and evenly irrigated when *W* is larger than 5 (18). The reaction conditions are set as shown in Table 4.

**TABLE 4**  
Reaction conditions of HDM deactivation experiments

Temperature (K)	H <sub>2</sub> pressure (MPa)	Xylene flow rate (ml/h)	H <sub>2</sub> flow rate (l/h)	VO-TPP concentration (mol/m <sup>3</sup> )	Wetting number, <i>W</i> (-)
553	9.0	12 - 28	2.5 - 5	0.04 - 0.4	150-300

### 2.3.4. In-situ production of hydrogensulfide

The ring cleavage step in the hydrodemetallisation reaction mechanism of VO-TPP requires hydrogen sulfide. For this reason the sulfur-containing compound dimethyldisulfide, which hydrodesulfurises very easily, is spiked in the liquid feed. The concentration of H<sub>2</sub>S is a parameter in the reaction kinetic model (see section 1.3.2.). It is therefore of importance to determine the exact concentration of DMDS added and the conversion of DMDS into H<sub>2</sub>S before it enters the catalyst bed. When the conversion is not complete at that point, the conversion will continue in the catalyst bed, which causes an unknown axial concentration profile of hydrogen sulfide over the catalyst bed.

Experiments were carried out to determine the conversion of DMDS. The feed and the

effluent of the reactor have been examined with Sievers SCD detector linked to a Hewlett Packard gas chromatograph. This showed that DMDS is readily converted into H<sub>2</sub>S and methane before entering the reactor and thus an axial H<sub>2</sub>S concentration profile is absent.

### 2.3.5. UV-VIS liquid sample analysis

The liquid feed and effluent are analysed with UV-VIS spectroscopy. This analysis is analogous to the procedure for the batch reactor samples (see section 1.2.4.). The concentrations of the reactant and intermediates are used to determine the conversion of VO-TPP.

## NOTATION

A	: absorption at its specific wavelength $\lambda$	-
C	: liquid phase concentration	mol/m <sup>3</sup>
$\epsilon$	: molar extinction coefficient	m <sup>2</sup> /mol
$k_1, k_3$	: hydrogenation reaction rate constants	s <sup>-1</sup>
$k_2, k_4$	: dehydrogenation reaction rate constants	s <sup>-1</sup>
$k_5$	: ring cleavage reaction rate constant	m <sup>3</sup> /mol·s
$K_{ij}$	: equilibrium constant of reaction i and j	-
$K_H$	: hydrogen adsorption coefficient	m <sup>3</sup> /mol
$K_{H_2S}$	: hydrogensulfide adsorption coefficient	m <sup>3</sup> /mol
$K_A, K_B, K_C, K_P$	: adsorption coefficient for component A, B, C, P	m <sup>3</sup> /mol
L	: radiation path-length in the liquid (or cuvette length)	m
$\lambda$	: wavelength	nm
n	: number	-
r	: rate of reaction	mol/m <sup>3</sup> ·s
SSR, SSR <sub>0</sub>	: sum of squares of residuals in local and global minimum	-
W	: wetting number	-

### Subscripts

-	: vector
CALC	: calculated
EXP	: experimental or measured
eq	: equilibrium
A,B,C,P	: M-TPP, M-TPC, M-TPiB, Products
H <sub>2</sub> , H <sub>2</sub> S	: hydrogen, hydrogensulfide
i	: compound, number
j	: number



## REFERENCES

1. Sie, S.T., *ACS Prepr. Div. Petrol. Chem.*, **40** (3) (1995) 463.
2. Sie, S.T., *I<sup>2</sup>-Procestchnologie*, **5** (1987) 115, in Dutch.
3. Bonné, R.L.C., 'Hydrodemetallisation of Ni-TPP and VO-TPP over Sulfided Molybdenum and Vanadium Catalysts', Ph.D thesis, University of Amsterdam (1992), Chapter 9.
4. Tajik, S., Berg, P.J. van den, and Moulijn, J.A., *Meas. Sci. Technol.*, **1** (1990) 815.
5. Trambouze, P., Landeghem, H. van, and Wauquier, J.P., 'Chemical Reactors, design/engineering/operation', Gulf Publishing Company (1988), Appendix A1 and references therein.
6. Kameyama, H., Shibuya, M., Teshigahara, I., and Amano, A., *Sekiyu Gakkaishi*, **28** (1985) 83.
7. Bonné, R.L.C., 'Hydrodemetallisation of Ni-TPP and VO-TPP over Sulfided Molybdenum and Vanadium Catalysts', Ph.D thesis, University of Amsterdam (1992), Chapter 3.
8. Chapter 7 of this thesis.
9. Janssens, J.P., Elst, G., Schrikkema, E.G., Langeveld, A.D. van, Sie, S.T., and Moulijn, J.A., submitted for publication in *Recueil des Travaux Chimiques des Pays-Bas*.
10. Bonné, R.L.C., 'Hydrodemetallisation of Ni-TPP and VO-TPP over Sulfided Molybdenum and Vanadium Catalysts', Ph.D thesis, University of Amsterdam (1992), Chapter 5.
11. Chapter 4 of this thesis.
12. Bonné, R.L.C., 'Hydrodemetallisation of Ni-TPP and VO-TPP over Sulfided Molybdenum and Vanadium Catalysts', Ph.D thesis, University of Amsterdam (1992), Chapter 8.
13. Steenderen, P. van, 'Gekatalyseerde en Niet-gekatalyseerde Hydrodemetallisering van Nikkel en Vanadium Porphyrines', AIO-2 report, University of Amsterdam (1992) in Dutch.
14. Bonné, R.L.C., 'Hydrodemetallisation of Ni-TPP and VO-TPP over Sulfided Molybdenum and Vanadium Catalysts', Ph.D thesis, University of Amsterdam (1992), Appendix 1.
15. Robinson, D.B., Peng, D.Y., and Chung, S.Y.K., *Fluid Phase Equilibria*, **24** (1985) 25.
16. Non-Linear Systems Fortran program developed by Dr. F. Kapteijn.
17. Press, W.H., Flannery, B.P., Teukolsky, S.A., and Vetterling, W.T., 'Numerical Recipes, The Art of Scientific Computing', Cambridge University Press (1989).
18. Sie, S.T., *Rev. Inst. Fr. Pétrol.*, **46** (4) (1991) 501.

# Chapter 3

## Influence of the Support Material on the Hydrotreating Activity and Selectivity of Vanadium Catalysts

### ABSTRACT

---

In hydrotreating processing of heavy oil residua vanadium is deposited on the catalyst surface. This deposition causes a loss of catalyst activity due to active site poisoning and pore plugging. In order to assess the structure and hydrotreating activity of vanadium, a series of alumina and silica supported catalysts has been prepared. The structure of vanadium was characterised using temperature programmed reduction and sulfiding. The catalytic activity of vanadium was determined by hydrodesulfurisation (HDS) of thiophene and hydrodemetallisation (HDM) of vanadyl-tetraphenylporphyrin (VO-TPP).

Alumina and silica supported vanadium catalysts show differences in dispersion. Vanadium is present in a more dispersed form on alumina than on silica. This dispersion effect is clearly noticeable in catalyst activities, the silica supported catalysts show a much lower activity for thiophene HDS and a lower hydrogenation rate in VO-TPP HDM than the alumina supported catalysts.

The two catalyst systems show large differences in the hydrogenation-ring cleavage selectivity for VO-TPP HDM. For alumina supported vanadium catalysts a much higher selectivity is found than the silica supported catalysts, which is due to the presence of at least two different types of reactive sites. Hydrogenation reactions in VO-TPP HDM take place on structure or dispersion sensitive sites, whereas ring cleavage is associated with large clusters of active phase or the type of support material.

An identical sulfiding mechanism for both catalyst systems is found. At 1273 K alumina and silica supported vanadium catalysts show complete sulfiding to  $V_2S_3$ , at 673 K the catalysts are partially sulfided and are in an oxy-sulfide state.

---

## 1. INTRODUCTION

In hydrotreating processing of heavy oils hetero-atoms such as sulphur, nitrogen, oxygen and metals, are catalytically removed. These metals, mainly vanadium and nickel, remain in the reactor as solid deposits accumulating on the catalyst surface after decomposition of the organo-metallic compounds. Metal deposition causes loss of catalyst activity, which can be attributed to the interaction of the deposited metals with the active sites of the catalyst ('*active site poisoning*') and the loss of pore volume due to the obstruction of catalyst pores ('*pore plugging*') (1). The removal of metals from heavy oil by catalytic hydrotreatment is called hydrodemetallisation (HDM).

A significant proportion of the metal compounds in heavy oil residua is complexed in porphyrins (2). The use of porphyrinic model compounds in reaction kinetics research eliminates many of the complicated competing reactions encountered with heavy oil residua, thus enabling a clearer picture of the reactions to be ascertained. The reaction mechanism of porphyrinic model compounds involves a sequence of hydrogenation steps and a final ring cleavage. Figure 1 depicts the HDM reaction mechanism for vanadyl-tetraphenylporphyrin (VO-TPP) (3). The reactant VO-TPP is reversibly hydrogenated to vanadyl-tetraphenylchlorin (VO-TPC), which can be reversibly hydrogenated to vanadyl-tetraphenylisobacteriochlorin (VO-TPiB). The last step in the reaction mechanism, the ring cleavage, is a lumped step. In this step the porphyrin is further hydrogenated and broken up into ring fragments. Vanadium is removed from the porphyrin and deposited on the catalyst surface. Therefore, the lumped ring cleavage step consists of both hydrogenation and hydrogenolysis reactions.

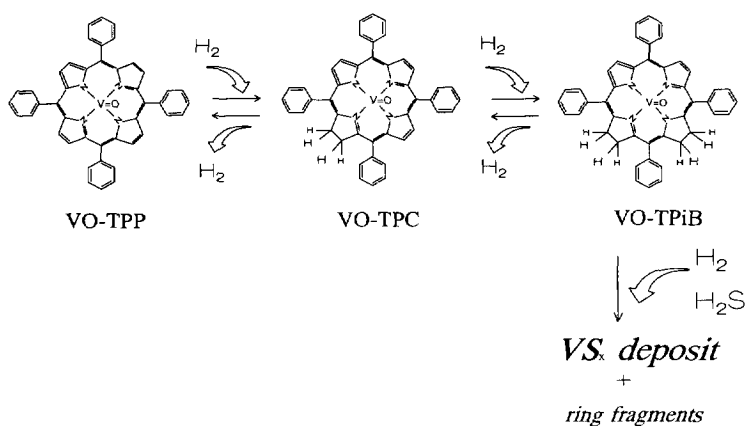


**Figure 1.** HDM reaction mechanism of vanadyl-tetraphenylporphyrin (VO-TPP).

(VO-TPC: vanadyl-tetraphenylporphyrin, VO-TPiB: vanadyl-tetraphenylisobacteriochlorin)

A Langmuir-Hinshelwood type of kinetics applies for the hydrodemetallisation of VO-TPP. It was concluded that a two-site model applies in which hydrogenation and ring cleavage occur on two different sites (3).

The vanadium deposits formed during hydrodemetallisation can act as catalysts for the HDM reaction. Therefore, it is of importance to determine the structure and catalytic activity of vanadium. Present work deals with the characterisation of vanadiumoxide and -sulfide on alumina and silica. Thiophene hydrodesulfurisation (HDS) activity and VO-TPP hydrodemetallisation activity tests are used to determine the catalytic activity of small amounts of vanadium deposits on alumina and silica support material.

## 2. EXPERIMENTAL

### 2.1. Catalyst preparation

Both support materials,  $\gamma$ -Al<sub>2</sub>O<sub>3</sub> and SiO<sub>2</sub> (supplied by Shell Research and Technology Centre, Amsterdam), were grounded and sieved after which the particle size fraction of 63-160  $\mu$ m was used for catalyst preparation. Before impregnation the support was dried at 393 K overnight.

The alumina supported vanadium catalysts were prepared by multiple-step wet impregnation. The alumina support was impregnated with a saturated solution of ammonium metavanadate (Aldrich, 99%) in water, using a vacuum rotary evaporator. After each impregnation step, which resulted in a vanadium loading of 0.1 atoms/nm<sup>2</sup>, the catalyst was dried in vacuum at 353 K. After the third impregnation and drying step the catalyst was dried overnight in an oven at 353 K. Subsequently, the catalyst was dried at 383 K with a heating rate of 0.033 K/s for 1 h. Next the temperature was increased to 753 K with a heating rate of 0.083 K/s for 2 h. This procedure was repeated until the desired vanadium loading was reached.

The silica supported vanadium catalysts were prepared by wet impregnation with a solution of vanadylacetylacetonate (Janssen Chimica, purity 99 %) in methanol (Aldrich, >99.9%) (4). In this case the solubility of the precursor is not limiting and the required loadings can be reached by a single impregnation step. The silica support was impregnated with the precursor solution, using a vacuum rotary evaporator. After the impregnation step the catalyst was dried overnight in an oven at 393 K. Subsequently, the catalyst was calcined at 823 K with a heating rate of 0.083 K/s for 12 h. Thermal gravimetric analysis of vanadium catalysts showed that vanadium sublimates above 1000 K.

The catalysts were stored in an oven at 353 K until short before use. The characteristics of the investigated catalysts are summarized in Table 1.

**TABLE 1.**  
Characteristics of Al<sub>2</sub>O<sub>3</sub> and SiO<sub>2</sub> supported vanadium catalysts.

Catalyst	loading		surface area m <sup>2</sup> /g	pore volume cm <sup>3</sup> /g	pore radius nm
	at. V/nm <sup>2</sup>	wt.% V			
Al <sub>2</sub> O <sub>3</sub>	-	-	190	0.90	9
V(1.2)/Al <sub>2</sub> O <sub>3</sub>	1.2	1.9	188	0.63	7
V(2.2)/Al <sub>2</sub> O <sub>3</sub>	2.2	3.4	180	0.61	7
V(3.1)/Al <sub>2</sub> O <sub>3</sub>	3.1	4.7	176	0.58	7
SiO <sub>2</sub>	-	-	59	1.51	51
V(1.3)/SiO <sub>2</sub>	1.3	0.6	55	1.42	51
V(2.5)/SiO <sub>2</sub>	2.5	1.0	48	1.44	60
V(4.6)/SiO <sub>2</sub>	4.6	1.3	35	1.20	69

The vanadium loadings are determined by Atomic Absorption Spectrometry, the surface area and pore volume of the alumina supported vanadium catalysts by N<sub>2</sub> adsorption and the surface area and pore volume of silica supported vanadium catalysts by Hg porosimetry. The pore radius is calculated by assuming cylindrical pores;  $r_p = 2 \cdot (\text{pore volume}) / (\text{surface area})$ .

## 2.2. Catalyst characterisation

The reduction and sulfiding behaviour of the oxidic vanadium catalysts were studied with Temperature Programmed Reduction (TPR) and Sulfiding (TPS). Experiments were performed in an atmospheric flow reactor. The heating rate was 0.167 K/s and the sample weight varied between 100 and 150 mg. For TPR a gas mixture consisting of 66 mol% H<sub>2</sub> in Ar (total flow rate: 33 μmol/s) was employed and for TPS a gas mixture consisting of 3 mol% H<sub>2</sub>S, 25 mol% H<sub>2</sub> and 72 mol% Ar (total flow rate: 28 μmol/s) was used.

The H<sub>2</sub> consumption of the catalyst samples was monitored with a Thermal Conductivity Detector (TCD) and the H<sub>2</sub>S consumption or production is monitored with an UV-spectrophotometer tuned at 205 nm. A detailed description of the TPR and TPS apparatus is given in (5) and (6), respectively.

### *2.3. Thiophene hydrodesulfurisation activity*

Thiophene HDS activity tests have been carried out with a gas mixture consisting of 6 mol% thiophene (Merck, >99%) in H<sub>2</sub> (total flow rate: 37 μmol/s) in an atmospheric flow reactor at 623 K. The catalysts were sulfided *in situ* using a mixture of 10 mol% H<sub>2</sub>S in H<sub>2</sub>, the applied heating rate was 0.10 K/s from 293 to 673 K. The sample weight used was approximately 200 mg.

The reaction products were analysed with an on-line gas chromatograph after 3 hours time on stream. From the analysis results the first order reaction rate constants for the hydrodesulfurisation of thiophene are determined.

### *2.4. Vanadyl-tetraphenylporphyrin hydrodemetallisation*

The HDM reaction mechanism of tetraphenylporphyrin is independent of the type of catalyst employed (3), which makes this reaction suitable for screening and testing of different catalyst systems.

The HDM experiments were carried out with VO-TPP (Rhône Poulenc) in *o*-xylene (Janssen Chimica, p.a. grade) as solvent in a 250 ml batch autoclave. An amount of approximately 100 mg of catalyst was weighed and introduced in the reactor. The catalyst is sulfided *in situ* for two hours with dimethyldisulfide (DMDS, Merck, >99%). DMDS is rapidly converted at elevated temperatures (623 K) in the presence of hydrogen (6.0 MPa). After the introduction of VO-TPP dissolved in *o*-xylene (total reaction volume: 125 ml), the reactor was filled to 0.30 MPa with a mixture of 15 mol% H<sub>2</sub>S in H<sub>2</sub> mixture, next H<sub>2</sub> was added to a total pressure of 5.0 MPa. The reactor was heated to a temperature of 578 K; when the reactor content reaches this temperature the stirrer was switched on to 2000 rpm to avoid any mass transfer limitations (7). From this point, liquid samples were taken to determine the porphyrin concentration. Inevitably, during heating of the reactor already some intermediates are formed.

The HDM reaction was carried out at industrial conditions, *viz.* 578 K and 10.0 MPa H<sub>2</sub> pressure. At certain time intervals a liquid sample was taken from the autoclave and analysed *ex-situ* with UV/Vis spectroscopy to determine the porphyrin concentrations. Details on sampling and determination of concentrations are given elsewhere (7). Kinetic parameters were obtained by evaluation of concentration-time data according to a two-site Langmuir-Hinshelwood model with competitive adsorption of hydrogen (3).

### 3. RESULTS

#### 3.1. Temperature Programmed Reduction and Sulfiding

The TPR patterns of all catalysts, including the supports and bulk  $V_2O_5$  (Aldrich, >99.6%), have been recorded. Figure 2 shows the TPR patterns of two alumina and silica supported vanadium catalysts, the supports and bulk  $V_2O_5$ . The alumina support shows a broad reduction peak with a maximum reduction rate at 952 K, which is due to impurities present in the material. Bulk  $V_2O_5$  and all  $V/Al_2O_3$  and  $V/SiO_2$  catalysts show a sharp reduction peak, indicating that the reduction is kinetically controlled.

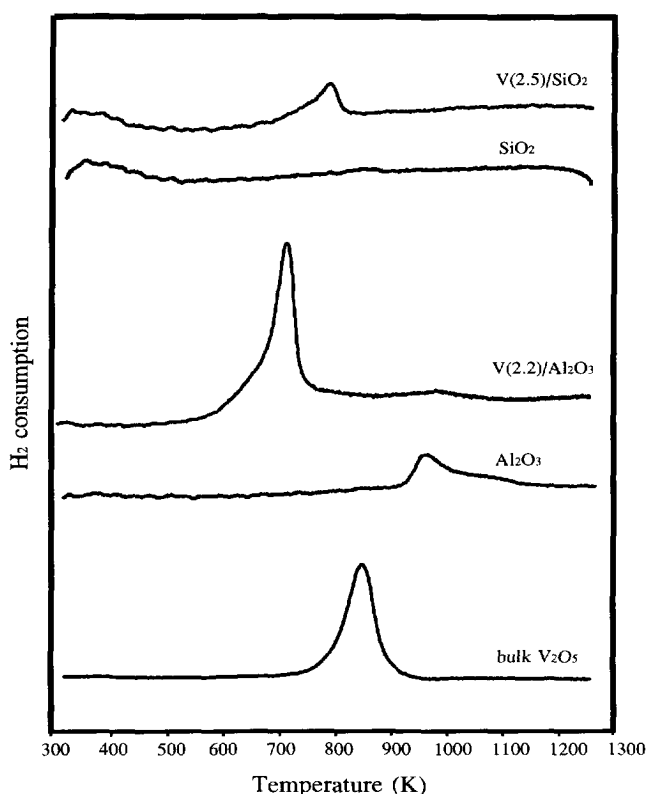


**Figure 2.** TPR patterns of the supports, vanadium catalysts and bulk  $V_2O_5$ .  
(the TPR profiles for alumina and silica supported vanadium catalysts are normalized to 150 mg sample, for bulk  $V_2O_5$  to 5 mg sample)

Figure 3 shows the temperature at which maximum reduction rate ( $T_{\max}$ ) is observed as a function of the vanadium loading for the investigated catalysts. As can be observed for the alumina supported vanadium catalysts,  $T_{\max}$  shifts to a lower value when the vanadium loading is increased from 1.2 to 2.2 at./nm<sup>2</sup>.  $T_{\max}$  shows a slight increase when the loading is increased from 2.2 to 3.0 at./nm<sup>2</sup>. The values for  $T_{\max}$  for the silica supported vanadium catalysts are 30 to 50 K higher than those of the alumina supported catalysts and show an identical course as the alumina supported vanadium catalysts.

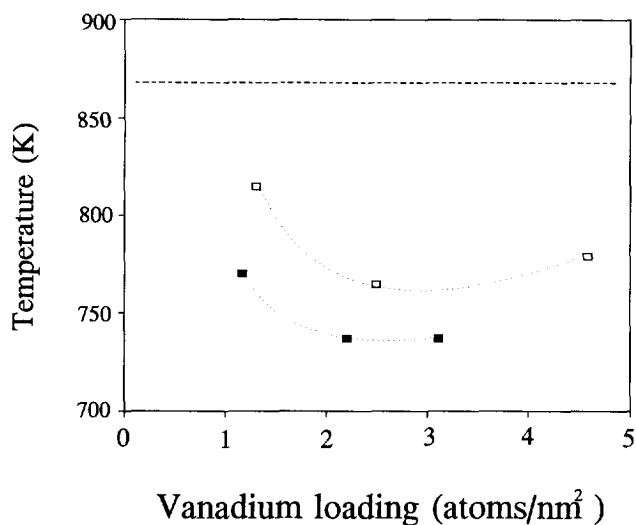


**Figure 3.** Temperature of observed maximum reduction rate ( $T_{\max}$ ) versus vanadium loading. (■ alumina supported vanadium catalysts, □ silica supported vanadium catalysts and ---- bulk V<sub>2</sub>O<sub>5</sub>)

Table 2 summarizes the amount of reducible oxygen per vanadium atom for bulk V<sub>2</sub>O<sub>5</sub> and the investigated catalysts. Bulk V<sub>2</sub>O<sub>5</sub> shows a complete reduction to V<sub>2</sub>O<sub>3</sub>, 1 oxygen atom is removed per vanadium atom. In contrast, the alumina and silica supported vanadium catalysts show incomplete reduction from V<sup>5+</sup> to V<sup>3+</sup>. Values ranging from 0.5 to 0.8 oxygen removal per vanadium are observed for both supports.



TABLE 2

Amount of reducible oxygen per vanadium atom of the alumina and silica supported vanadium catalysts as estimated from TPR  
(corrected for the H<sub>2</sub> consumption of the support).

catalyst	O <sub>red</sub> /V	catalyst	O <sub>red</sub> /V
bulk V <sub>2</sub> O <sub>5</sub>	1.0		
V(1.2)/Al <sub>2</sub> O <sub>3</sub>	0.5	V(1.3)/SiO <sub>2</sub>	0.7
V(2.2)/Al <sub>2</sub> O <sub>3</sub>	0.8	V(2.5)/SiO <sub>2</sub>	0.5
V(3.1)/Al <sub>2</sub> O <sub>3</sub>	0.8	V(4.6)/SiO <sub>2</sub>	0.6

The TPS patterns of two supported catalysts and bulk V<sub>2</sub>O<sub>5</sub> are depicted in Figure 4. The TPS patterns of all samples sulfided up to 1273 K can be divided into five stages, which are depicted in Figure 4; (1) isothermal sulfiding at room temperature, (2) H<sub>2</sub>S desorption, (3) low temperature sulfiding, (4) hydrogenation of non stoichiometric sulfur, S<sub>x</sub>, and (5) high temperature sulfiding.

At room temperature, all samples show a small amount of H<sub>2</sub>S consumption (stage 1). Compared to bulk V<sub>2</sub>O<sub>5</sub> and the supports, a much larger H<sub>2</sub>S uptake is observed during isothermal sulfiding at room temperature for the supported vanadium catalysts. Together with the colour change from yellow to black, this shows that sulfiding already takes place at room temperature.

By increasing the temperature a small amount of H<sub>2</sub>S desorbs at 300 to 320 K (stage 2). This is due to desorption of physisorbed H<sub>2</sub>S on the catalyst samples.

At higher temperatures, both bulk V<sub>2</sub>O<sub>5</sub> and V/SiO<sub>2</sub> catalysts show a two-step sulfiding process at 450 and 580 K (stage 3), whereas V/Al<sub>2</sub>O<sub>3</sub> catalysts show a single step sulfiding. This is followed by H<sub>2</sub>S production together with H<sub>2</sub> consumption in stoichiometric amounts at 620-640 K (stage 4). All samples show further sulfiding at higher temperatures (> 673 K, stage 5), which indicates that sulfiding is not complete at 673 K.

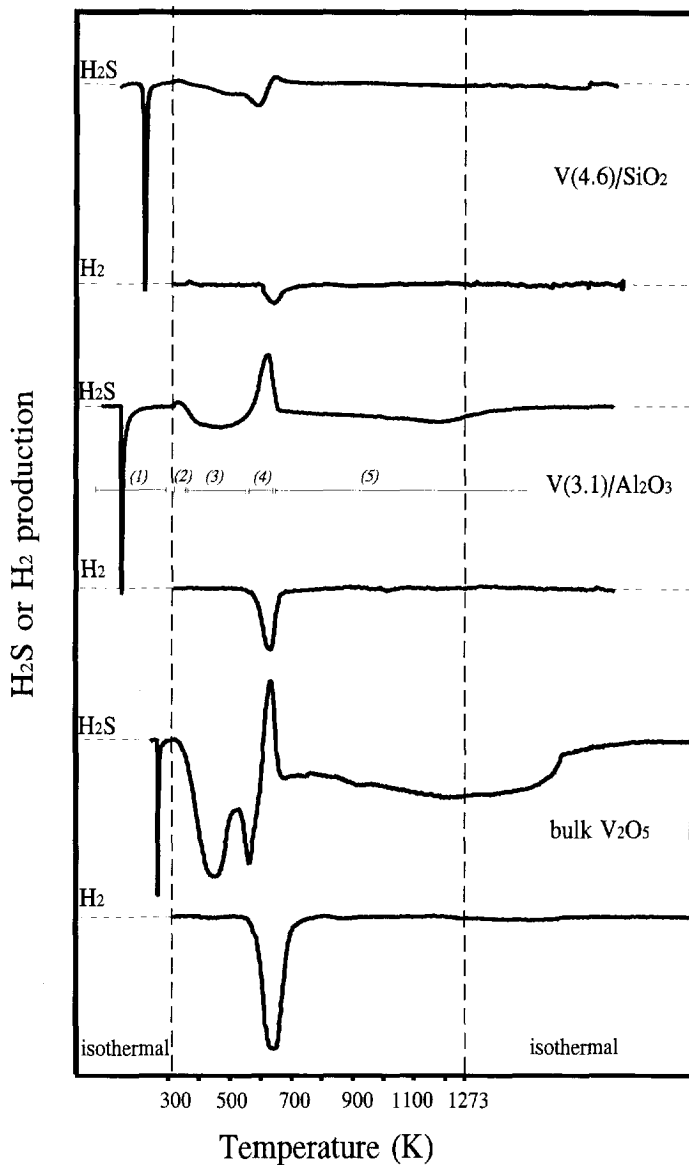


**Figure 4.** TPS patterns of vanadium catalysts and bulk V<sub>2</sub>O<sub>5</sub>.  
(the TPS profiles are normalized to 100 mg sample)

During sulfiding up to 1273 K elemental sulfur is sublimated from the catalyst samples and condensed in the cold part of the reactor, which makes quantitative TPS very difficult. Bulk  $V_2O_5$  is completely sulfided to  $V_2S_3$  at 1273 K. Since bulk sulfiding phenomena are predominant at these high temperatures, it is concluded that the catalyst samples are also sulfided to  $V_2S_3$ .

### 3.2. Catalyst activity

#### 3.2.1. Thiophene HDS activity

Figure 5 shows the first order reaction rate constant for the thiophene conversion (after 3 hours time on stream) for the alumina and silica supported vanadium catalysts. These reaction rate constants are normalized to the amount of vanadium present on the catalyst.

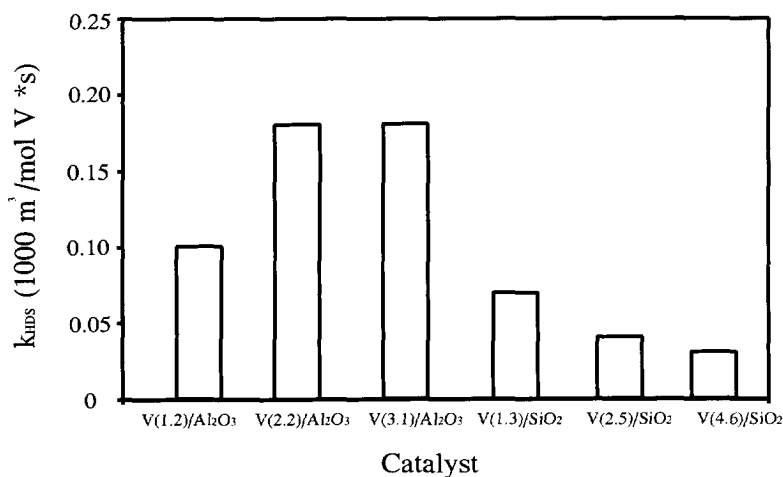


**Figure 5.** First order reaction rate constants ( $k_{HDS}$ ) for thiophene HDS of vanadium catalysts.

As can be observed, the alumina supported catalysts show a larger thiophene HDS activity than the silica supported catalysts. The reaction rate constants of alumina supported vanadium catalysts are a factor 1.5 to 6 larger than for silica supported vanadium catalysts. The  $k_{HDS}$  of alumina increases with increasing vanadium loading and stabilizes above 2.2 atoms/nm<sup>2</sup>. The silica supported vanadium catalysts show a decrease in  $k_{HDS}$  with increasing vanadium loading.

### 3.2.2. VO-TPP HDM activity

Figure 6 depicts the concentration versus time profiles for both catalysts systems as determined in the batch autoclave. Figure 6 a shows the profile for an alumina supported vanadium catalyst. A decreasing concentration of the reactant VO-TPP can be observed, the first intermediate VO-TPC is passing through a maximum and approaching zero. The second intermediate VO-TPiB, which is irreversibly converted to ring fragments and vanadium deposits, is also passing through a maximum. The concentration of VO-TPiB, depicted in Figure 6 b, for the silica supported vanadium catalysts remains always very low.

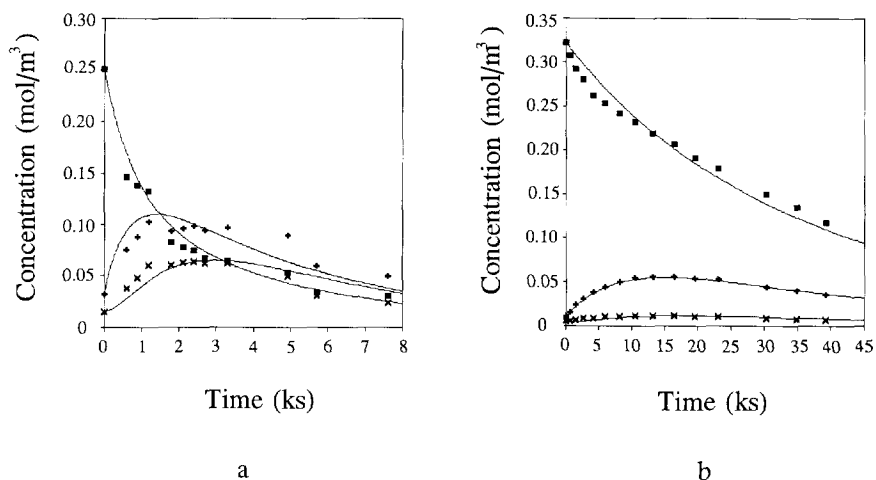


**Figure 6.** Concentration-time profiles for VO-TPP HDM for alumina and silica supported vanadium catalysts, a- V(3.1)/Al<sub>2</sub>O<sub>3</sub> and b- V(2.5)/SiO<sub>2</sub>.

(■ : VO-TPP, + : VO-TPC, x : VO-TPiB and — : fit according to two-site model (3))

Kinetic parameters were obtained by evaluation of concentration-time data according to a two-site Langmuir-Hinshelwood model with competitive adsorption of hydrogen (3). The solid lines in Figure 6 represent the calculated concentrations according to this model. Some irregularities are observed between the experimental and calculated concentrations in Figure 6 a which are due to a non optimized liquid sampling procedure.

Figure 7 shows the intrinsic reaction rate constants as a function of the vanadium loading and the support at 578 K. Two hydrogenation reaction rate constants,  $k_1$  and  $k_3$ , and the ring cleavage reaction rate constant,  $k_5$ , are normalized to the amount of active phase present in the reactor.

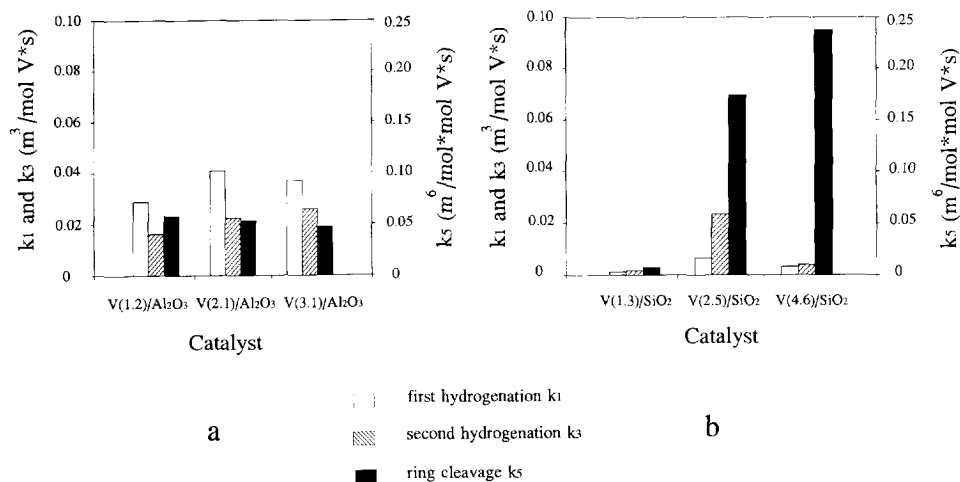


**Figure 7.** Reaction rate constants for VO-TPP HDM of vanadium catalysts, a- alumina supported vanadium catalysts and b- silica supported vanadium catalysts.

The alumina supported vanadium catalysts show a much higher hydrogenation activity in VO-TPP HDM than the silica supported catalyst. The hydrogenation rate constants for alumina supported vanadium catalysts are one order of magnitude higher than for silica supported vanadium catalysts.

A striking difference between the two catalyst systems is the hydrogenation-ring cleavage selectivity. The silica supported catalysts show a much lower selectivity than the alumina supported catalysts, which is depicted in Figure 8.

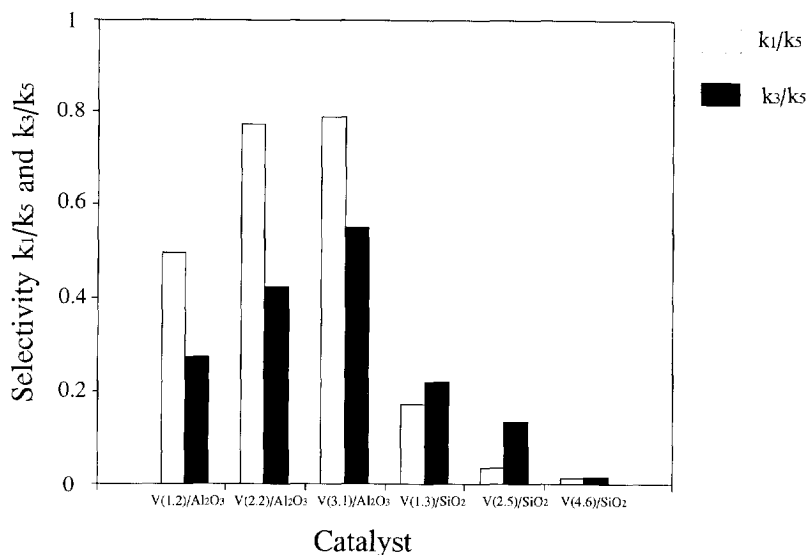


**Figure 8.** Hydrogenation-ring cleavage selectivities,  $k_1/k_5$  and  $k_3/k_5$ , for alumina and silica supported vanadium catalysts.

## 4. DISCUSSION

### 4.1. Catalyst characterisation

Hanke et al. (8) investigated the formation of vanadium oxide surface species on SiO<sub>2</sub>. His work shows that at low vanadium loadings tetrahedrally coordinated vanadium is formed by the reaction of the precursor with surface hydroxyl groups. After depletion of the hydroxyl groups, increasing vanadium loadings lead to the formation of octahedral vanadium species. Both the tetrahedrally and octahedrally coordinated vanadium species have an intimate interaction with the support, so that relatively high temperatures are required for reduction.. Upon increase of the vanadium loading, these species polymerize until a monolayer coverage at about 2 atoms V/nm<sup>2</sup> is reached (9). This monolayer has a less intimate interaction with the support and is, therefore, more easily reduced. Further increase of the vanadium loading leads to the formation of V<sub>2</sub>O<sub>5</sub> crystallites, which are more difficult to reduce (10). This explains the course of the T<sub>max</sub> curve in Figure 3.

Values for  $T_{\max}$  for the silica supported vanadium catalysts are 30 to 50 K higher than for the alumina supported vanadium catalysts and closer to the  $T_{\max}$  value of bulk  $V_2O_5$ . This is probably due to the presence of larger vanadium crystallites on the silica surface. This corresponds to the observation that the silica support has a relatively low vanadiumoxide monolayer capacity due to the weak interaction of the vanadium ions with the support (11).

The incomplete reduction of  $V^{5+}$  to  $V^{3+}$  for the alumina and silica supported vanadium catalysts is also reported by Bonné (10), who found amounts for the reducible oxygen per vanadium atom to vary from 0.5 to 0.7, for a loading range of 0.7-2.0 atoms V/nm<sup>2</sup>. Similar values are found for the silica supported vanadium catalysts. Stobbe-Kreemers (12) also found incomplete reduction of  $V^{5+}$  to  $V^{3+}$  for the alumina and silica supported vanadium catalysts.

The sulfiding mechanism of bulk  $V_2O_5$  consists essentially of two steps. In the first step  $V^{5+}$  is reduced to  $V^{3+}$ . The reaction proceeds through O-S exchange. Part of the elemental sulfur formed in the sulfiding process sublimates and condenses in the cold part of the reactor, while the remaining part is hydrogenated to  $H_2S$ . In the second step, the *in situ* formed  $V^{3+}$  is sulfided to  $V_2S_3$ , as well through O-S exchange. This step, the actual sulfiding step, occurs in the high temperature region (673 to 1273 K). This O-S exchange mechanism has been found for other systems like  $CrO_3$  (13, 14), and  $MoO_3$  (6).

The alumina supported vanadium catalysts are sulfided via a similar mechanism as bulk  $V_2O_5$ . The  $H_2S$  and  $H_2$  consumption and/or production peaks, as found in TPS of the alumina supported catalysts, agree with the sulfiding mechanism as described by Bonné et al. (15). However, the two separate sulfiding steps at low temperatures are convoluted in a single broad step due to small temperature differences between both steps.

Little is known about the sulfiding mechanism of silica supported vanadium catalysts. It has been assumed that the sulfiding mechanism is analogous to that of bulk  $V_2O_5$ . The TPS patterns of silica supported catalysts show indeed similar phenomena as observed in TPS of bulk  $V_2O_5$  at temperatures below 673 K, in accordance with this presumption.

So, when comparing the TPS patterns of the bulk material and the supported catalysts we can state that the sulfiding pattern of the silica supported vanadium catalysts is similar to the sulfiding of bulk material due to the presence of the larger crystallites as compared to alumina. Alumina supported vanadium catalysts are more easily sulfided (at lower temperatures) due to a higher dispersion.

Quantitative TPS is obscured by (a) sublimation of elemental sulfur, which was also observed by Bonné et al. (15), and (b) the presence of small amounts of the active phase, which are close to the detection limit of the sulfiding equipment. For bulk  $V_2O_5$  a sulfur-vanadium ratio of 0.5 was found at 673 K, which indicates partial sulfiding and the presence of an oxy-sulfide.

The amount of hydrogenated sulfur for the silica supported catalysts is relatively low as compared to the alumina supported catalysts, which implies that the amount of non stoichiometric sulfur  $S_x$  on the surface of V/SiO<sub>2</sub> catalysts is much less than that of V/Al<sub>2</sub>O<sub>3</sub>.

#### *4.2. Catalyst activity*

##### *4.2.1. Thiophene HDS activity*

The alumina supported vanadium catalysts are more active for thiophene HDS than the silica supported vanadium catalysts. This can be explained as follows. It is a known fact that surface vanadium compounds are more active than bulk phase compounds for thiophene HDS. From TPR, it can be concluded that on silica more crystalline vanadium is formed, obviously because of the lower amount of surface hydroxyl groups as compared to alumina. Therefore, silica supported vanadium catalysts are expected to be less active than alumina supported catalysts.

TPS of the vanadium catalysts showed that lower amounts of  $S_x$  were hydrogenated on silica than on alumina supported catalysts. The relation between the amount of non-stoichiometric sulfur and thiophene HDS activity proposed by Mangnus et al. (16) is supported by the present work.

The trend between  $k_{HDS}$  and the vanadium loading can be explained as follows. Probably, at low loading the vanadium is strongly bonded to the support which gives a lower HDS activity. Above monolayer coverage ( $> 2$  atoms/nm<sup>2</sup>), the support-vanadium interaction becomes weaker resulting in a higher HDS activity. The presence of vanadium crystallites on silica catalysts, as can be inferred from TPR, results in a decreasing  $k_{HDS}$  with increasing vanadium loading. It is tentatively concluded that the presence of large clusters have a lower ratio of edge sites per mol vanadium, and therefore a lower intrinsic thiophene HDS activity.

A comparison between the thiophene HDS activity of vanadium catalysts and CoMo- and NiW-catalysts shows that bimetallic catalysts are far more active. Vanadium has similar thiophene HDS activity as tungsten (18).

##### *4.2..2. VO-TPP HDM activity*

Bonné et al. (3) showed that a two-site model applies for the HDM of VO-TPP. In this model, hydrogenation reactions occur on sites which are thought to consist of sulfur vacancies or coordinatively unsaturated (Lewis acid) sites (CUS), whereas the ring cleavage reaction occurs on Brønsted acid sites (18, 19).



Our results show that the hydrogenation-ring cleavage selectivity is higher for the alumina supported catalysts than for the silica supported catalysts. For silica supported catalysts, ring cleavage is the fastest step in the HDM reaction, whereas for alumina supported catalysts the hydrogenation and ring cleavage rates are of the same order of magnitude. The selectivity difference between both catalyst systems corroborates the conclusion that hydrogenation and ring cleavage reactions occur on different types of sites. Apparently, the hydrogenation sites in VO-TPP HDM are more susceptible to the structure and dispersion of the active phase than the ring cleavage sites, this results in a higher hydrogenation rate on alumina as compared to silica. Rajagopal et al. (20) recently reported an increasing ratio of Brønsted to Lewis acid site concentration with increasing loading or crystallite size for  $\text{MoO}_3/\text{Al}_2\text{O}_3$  catalysts. An increase in Mo loading ( $\geq 4$  wt.%  $\text{MoO}_3$ ) or crystallite size generated new Brønsted acid sites (originating from multiple layers of octahedrally Mo species) and decreased the Lewis acid site concentration (originating from tetrahedrally coordinated Mo species and CUS of the support). Their observations could also explain the selectivity differences we find in the hydrodemetallisation of VO-TPP on silica and alumina supported vanadium catalysts.

In general we can state that both hydrodesulfurisation of thiophene and hydrogenation of VO-TPP and VO-TPC are structure and dispersion sensitive reactions, which can be related very well to the results of the characterisation methods such as temperature programmed reduction and sulfiding. The ring cleavage reaction in the hydrodemetallisation of VO-TPP is associated with larger structures of active phase or the type of support material.

## 5. CONCLUSIONS

Characterisation of silica and alumina supported vanadium catalysts with temperature programmed techniques shows differences in the dispersion of the active phase. Vanadium on alumina has a higher dispersion than on silica.

This dispersion effect is clearly noticeable in catalysts activities, the silica supported catalysts show a much lower activity for thiophene HDS and a lower hydrogenation rate in VO-TPP HDM than the alumina supported catalysts.

The two catalyst systems show large differences in the hydrogenation-ring cleavage selectivity for VO-TPP HDM. For alumina supported vanadium catalysts a much higher selectivity is found than the silica supported catalysts, which is due to the presence of at least two different types of reactive sites. Hydrogenation reactions in VO-TPP HDM take place on structure or dispersion sensitive sites, whereas ring cleavage is associated with large clusters of active phase or the type of support material.

Alumina and silica supported vanadium catalysts sulfide according to the same sulfiding mechanism. All catalyst samples were completely sulfided at 1273 K, at 673 K the catalysts were partially sulfided (oxy-sulfide).

## ACKNOWLEDGMENTS

This study was supported with financial aid from the Shell Research and Technology Centre, Amsterdam (SRTCA) and the European Community (contract number JOUF 0049).

## REFERENCES

1. Sie, S.T., in 'Catalyst deactivation', Delmon, B. and Froment G.F. (Eds.), Elsevier Scientific Publishing Company, Amsterdam (1980) 545.
2. Quann, R.J., Ware, R.A., Hung, C.W., and J. Wei, *Adv. Chem. Eng.*, **14** (1988) 95.
3. Bonné, R.L.C., Steenderen, P. van, and J.A. Moulijn, *Bull. Soc. Chim. Belg.*, **100**(11-12) (1991) 877.
4. Hengstum, A.J. van, Ommen, J.G. van, Bosch, H., and P.J. Gellings, *Appl. Catal.*, **5** (1983) 207.
5. Arnoldy, P., and Moulijn, J.A., *J. Catal.*, **93** (1985) 38.
6. Arnoldy, P., Heijkant, J.A.M. van den, Bok, G.D. de, and J.A. Moulijn, *J. Catal.*, **92** (1985) 35.
7. Chapter 2 of this thesis.
8. Hanke, W., Bienert, R., and H.G. Jerschke, *Z. Anorg. Allg. Chem.*, **414** (1975) 109.
9. Eckert, H., and Wachs, I.E., *J. Phys. Chem.*, **93** (1989) 6796.
10. Bonné, R.L.C., Ph.D thesis University of Amsterdam, Chapter 6 (1992).
11. Roozeboom, F., Fransen, T., Mars, P., and P.J. Gellings, *Z. Anorg. Allg. Chem.*, **449** (1979) 25.
12. Stobbe-Kreemers, A.W., Ph.D thesis Delft University of Technology, Chapter 6 (1993).
13. Scheffer, B., Dekker, N.J.J., Mangnus, P.J., and J.A. Moulijn, *J. Catal.*, **121** (1990) 31.
14. Mangnus, P.J., Ellison, A., Scheffer, B., and J.A. Moulijn, *Bull. Soc. Chim. Belg.*, **96** (1987) 977.
15. Bonné, R.L.C. Langeveld, A.D. van, and J.A. Moulijn, *J. Catal.*, **154** (1995) 115.
16. Mangnus, P.J., Riezebos, A., Langeveld, A.D. van, and J.A. Moulijn, *J. Catal.*, **151** (1995) 178.
17. Scheffer, B., Ph.D thesis University of Amsterdam, Appendix (1988).
18. Yang, S.H., and C.N. Satterfield, *J. Catal.*, **81** (1983) 168.
19. Yang, S.H., and C.N. Satterfield, *Ind. Eng. Chem. Process Des. Dev.*, **23** (1984) 20.
20. Rajagopal, S., Marzari, J.A., and Miranda, R., *J. Catal.*, **151** (1995) 192.



# Chapter 4

## Influence of Hetero-atom Containing Compounds on the Hydrodemetallisation of Vanadyl- tetraphenylporphyrin

### ABSTRACT

---

Heavy oil residua contain large amounts of hetero-atoms, such as sulfur, nitrogen, oxygen and metals. The metals, mainly vanadium and nickel, are removed by catalytic hydrotreatment. The presence of sulfur, nitrogen and oxygen containing compounds in heavy oil residua can influence the rate at which these metals are removed, since they can adsorb competitively on the active site of the catalyst and decrease the rate of hydrogenation and ring cleavage reactions of organo-metallic compounds.

In the present work the influence of hetero-atom containing compounds, *i.e.*, quinoline, ammonia, benzofuran, water, dibenzothiophene, and anthracene on the hydrodemetallisation (HDM) of vanadyl-tetraphenylporphyrin (VO-TPP) has been investigated. The spiked amount of hetero-atoms has been chosen near to that occurring in oil residua.

The added compounds appeared to decrease the overall rate of metal removal. The hydrogenation reaction rates decreased in the following sequence: water ~ ammonia > benzofuran ~ anthracene > quinoline > dibenzothiophene. The reaction rates of the lumped ring cleavage step decreased in the following sequence: water > ammonia > benzofuran ~ quinoline > anthracene ~ dibenzothiophene.

The decrease in reaction rates due to the addition of quinoline, benzofuran, dibenzothiophene and anthracene is caused by competitive adsorption with vanadyl-tetraphenylporphyrin on the active sites of the catalyst. Water and ammonia proved to coordinate with the vanadyl group in the porphyrin and, therefore, stabilize the porphyrin for metal removal.

It is concluded that competitive adsorption of reaction products from the ring cleavage of VO-TPP is negligible and that the presence of hetero-atom containing compounds in realistic feedstocks can influence the rate of metal removal

---

## 1. INTRODUCTION

Hydrotreating processes can be used to upgrade oil residua by removing hetero-atoms, such as sulfur (hydrodesulfurisation, HDS), nitrogen (hydrodenitrogenation, HDN), oxygen (hydrodeoxygenation, HDO) and metals (hydrodemetallisation, HDM). These hetero-atoms in the feedstock are hydrogenated and removed as hydrogen sulfide, ammonia and water, respectively. The metals, mainly vanadium and nickel, are deposited as metal sulfides on the catalyst surface. These metal deposits cause an irreversible catalyst deactivation due to active site poisoning and pore plugging (1). Figure 1 depicts the ranges of hetero-atom content of various atmospheric residua (2).

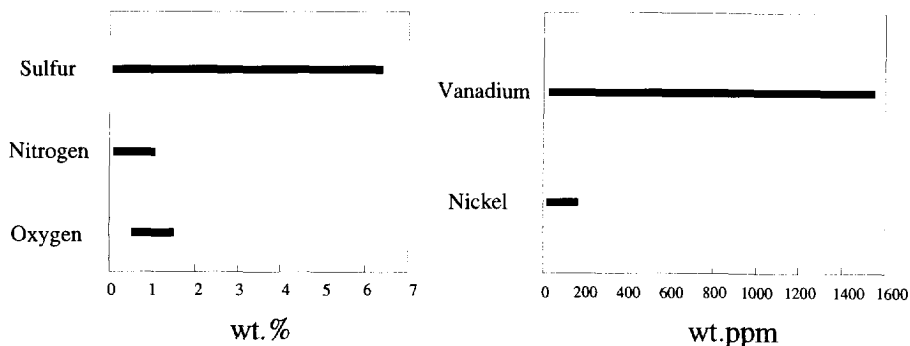


**Figure 1.** Ranges of hetero-atom content of various atmospheric residua.

From the organo-metallic compounds in heavy oil residua a part is complexed in porphyrinic compounds (2). These porphyrinic compounds are very suitable for reaction kinetics research due to the fact that the reaction mechanism of these compounds has been elucidated in some detail (2, 3).

Because HDM occurs in the presence of sulfur, nitrogen and oxygen containing compounds, it is of interest to investigate what is the influence of these hetero-atom containing compounds on the rate of metal removal. Apart from the fact that these hetero-atom containing compounds may hinder the diffusion of organo-metallic compounds in catalyst pores, physical and chemical effects may be expected as well. The hetero-atom containing compounds may adsorb competitively with the organo-metallic compounds on the active sites of the catalyst

and thus decrease the rate of metal removal. The use of model compounds, such as dibenzothiophene, quinoline, benzofuran, water and ammonia enables a clearer picture of the reactions to be ascertained.

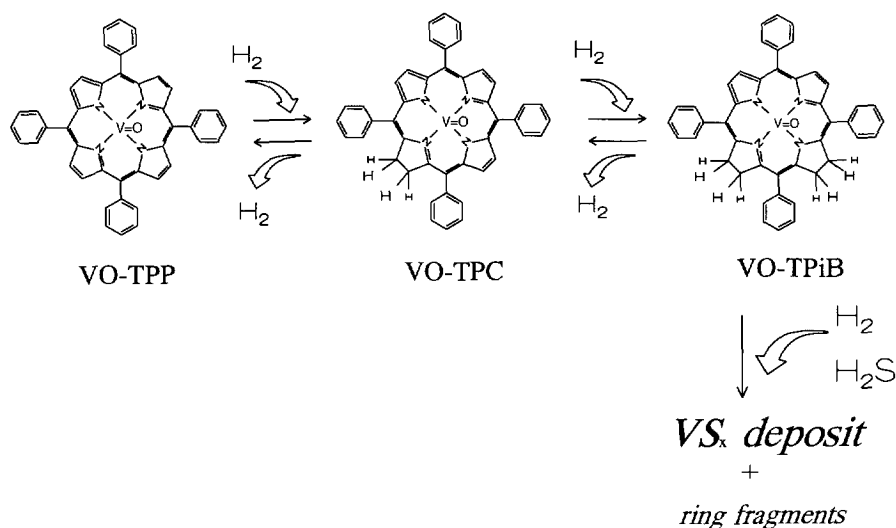


**Figure 2.** Hydrodemetallisation reaction mechanism of vanadyl-tetraphenylporphyrin (VO-TPP).

(VO-TPC: vanadyl-tetraphenylchlorin and VO-TPiB: vanadyl-tetraphenylisobacteriochlorin)

In the present work, the hydrodemetallisation of vanadyl-tetraphenylporphyrin (VO-TPP) is investigated. The simplified reaction scheme of this porphyrinic model compound is depicted in Figure 2 (3). The reactant VO-TPP is reversibly hydrogenated to vanadyl-tetraphenylchlorin (VO-TPC), which can be reversibly hydrogenated to vanadyl-tetraphenylisobacteriochlorin (VO-TPiB). The last step in the reaction mechanism, the ring cleavage, is a lumped step. In this step the porphyrin is further hydrogenated and cleaved into ring fragments. Vanadium is removed from the porphyrin and deposited on the catalyst surface. Therefore, the lumped ring cleavage step consists of both hydrogenation and hydrogenolysis reactions.

The research presented in this paper deals with the influence of hetero-atom containing compounds in HDM of VO-TPP. The studied compounds or competitors are depicted in Figure 3.

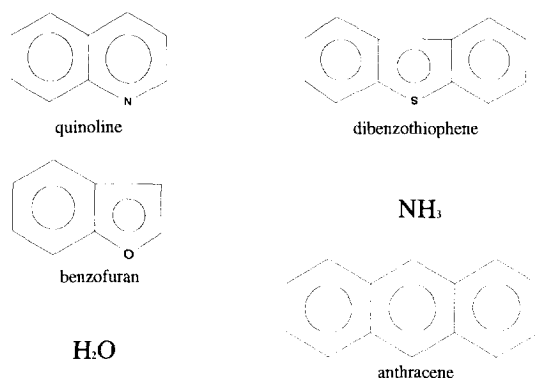


**Figure 3.** Compounds used in present work.

## 2. EXPERIMENTAL

### 2.1. Catalyst preparation

A  $\gamma$ -Al<sub>2</sub>O<sub>3</sub> (supplied by Shell Research and Technology Centre, Amsterdam) supported vanadium catalyst was prepared by multiple-step wet impregnation with an aqueous solution of ammoniummetavanadate (Aldrich, 99%) (4). After impregnation the catalyst was dried overnight in an oven of 353 K. Subsequently, the catalyst was calcined at 753 K with a heating rate of 0.083 K/s. The temperature remained constant at 753 K for 2 h. Particles of 63-160  $\mu$ m were used. The characteristics of the catalyst used are summarized in Table 1.

This catalyst was used since vanadium is the most abundant metal in oil residua and deposits on the internal catalyst surface during hydrodemetallisation. In order to assess the (auto)catalytic activity of vanadium and to minimize deactivation effects this vanadium catalyst was applied for present work.

**TABLE 1**  
 Characteristics of  $\gamma$ -Al<sub>2</sub>O<sub>3</sub> supported vanadium catalysts.

Catalyst	loading (at.V/nm <sup>2</sup> )	(wt.% V)	surface area (m <sup>2</sup> /g)	pore volume (cm <sup>3</sup> /g)	pore radius (nm)
V(2.2)/Al <sub>2</sub> O <sub>3</sub>	2.2	3.4	180	0.61	7

The surface area and pore volume are determined by N<sub>2</sub> adsorption, the pore radius is calculated by assuming cylindrical pores. Approximately 10% of the pore volume can be attributed to macro pores.

## 2.2. Hydrodemetallisation of VO-TPP

The HDM experiments were carried out with VO-TPP and *o*-xylene (Janssen Chimica, p.a. grade) as solvent in a 250 ml batch autoclave. Approximately 80 to 100 mg catalyst was introduced in the reactor. The catalyst was sulfided *in situ* for two hours with dimethyl-disulfide (DMDS, Merck, >99%). DMDS is rapidly converted at elevated temperatures (623 K) in the presence of hydrogen (6.0 MPa). After introduction of VO-TPP dissolved in *o*-xylene (total reaction volume: 125 ml), the reactor was filled to 0.4 MPa with a mixture of 15 mol% H<sub>2</sub>S in H<sub>2</sub>. Next H<sub>2</sub> was added to a total pressure of 5.0 MPa. The reactor was heated to 578 K, when the reactor contents reaches this temperature the stirrer is switched on to 2000 rpm to avoid mass transfer limitations (5).

The HDM reaction was carried out under industrial conditions, 578 K and 10.0 MPa H<sub>2</sub> pressure. At certain time intervals a liquid sample was taken from the autoclave and analysed *ex-situ* with UV-VIS spectroscopy to determine the porphyrin concentrations.

Kinetic parameters were obtained by evaluation of concentration-time data according to a two-site Langmuir-Hinshelwood model with competitive adsorption of hydrogen (3). Details on sampling, determination of reactant and intermediates concentrations and reaction kinetics evaluation are given elsewhere (5).



## Chapter 4

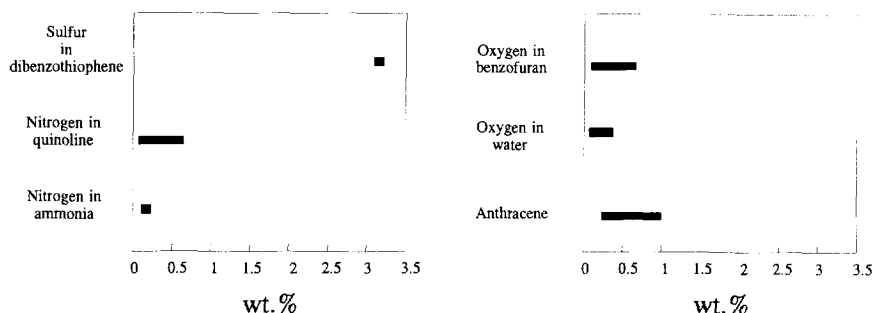


**Figure 4.** Ranges of competitor content (in wt.%) added to the reaction mixture.

In order to investigate the influence of hetero-atom containing compounds certain amounts were added to the reaction mixture. Figure 4 depicts the ranges of the competitor content added to the reaction mixture. The spiked amount of hetero-atoms are chosen near to those occurring in oil residua. Table 2 summarizes the concentrations of competitors in the reaction mixture.

**TABLE 2**  
Amounts of competitors added to the reaction mixture.

Reactant	molar concentration (mol/m <sup>3</sup> <sub>solvent</sub> )			hetero-atom content		
vanadyl-tetraphenylporphyrin		1.0		55		wt.ppm V
<b>Competitor</b>						
quinoline (Merck, >97 %)	71	141	361	0.11	0.22	0.57 wt.% N
ammonia (DAP, Aldrich >99 %)	76			0.12		wt.% N
dibenzothiophene (Aldrich, >98 %)			849	3.1		wt.% S
benzofuran (Aldrich, 99.5 %.)	67	118	298	0.12	0.21	0.54 wt.% O
water	15	30	149	0.03	0.05	0.27 wt.% O
anthracene (Merck, >96 %)	10	50				

### 3. RESULTS

#### 3.1. Blank test of VO-TPP hydrodemetallisation

In order to determine the effects of competitors on the hydrodemetallisation of VO-TPP, a test in the absence of the competitors was carried out to assess the reference reaction rate constants. Table 3 summarizes the values of the reaction rate constants of this blank test, which are normalized on the amount of active phase present in the reactor. In the kinetic analysis, the hydrogenation and dehydrogenation rate constants were not taken as independent variables, but the ratios  $k_1/k_2$  and  $k_3/k_4$ , which are the equilibrium constants  $K_{12}$  and  $K_{34}$ , were kept constant. The effects of competitors were expressed as the change in the absolute values of  $k_1$  (first hydrogenation),  $k_3$  (second hydrogenation), and  $k_5$  (lumped ring cleavage).

**TABLE 3**  
Blank test values for VO-TPP hydrodemetallisation reaction rate constants.

	first hydrogenation $k_1$ ( $\text{m}^3/\text{mol V}\cdot\text{s}$ )	second hydrogenation $k_3$ ( $\text{m}^3/\text{mol V}\cdot\text{s}$ )	ring cleavage $k_5$ ( $\text{m}^6/\text{mol}\cdot\text{mol V}\cdot\text{s}$ )
reaction rate constants	$1.28\cdot 10^{-2}$	$2.06\cdot 10^{-2}$	$7.19\cdot 10^{-2}$

#### 3.2. Influence of the nitrogen containing compounds quinoline and ammonia

Figure 5 shows the concentration-time profiles obtained from the batch autoclave for the blank test (without competitor) and for the test with quinoline added to the reaction mixture.

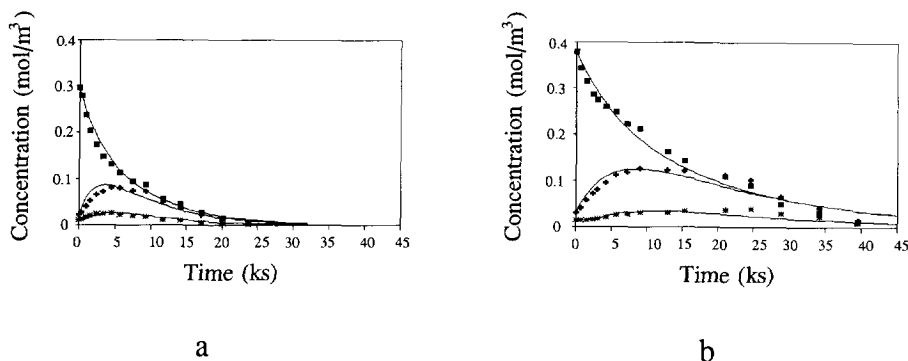


**Figure 5.** Concentration-time profiles for VO-TPP hydrodemetallisation at 578 K and 10.0 MPa  $H_2$  pressure, a- blank test and b- with addition of quinoline ( $361 \text{ mol/m}^3$ ).

(■: VO-TPP, +: VO-TPC, \*:VO-TPiB and — fit according to two-site model (3))

The competition effect of the nitrogen containing compound quinoline on the HDM reaction kinetics of VO-TPP can be clearly seen. The reactant and intermediates react much slower with the addition of quinoline to the reaction mixture. Figure 6 shows the reduction in the reaction rate constants for the two hydrogenation steps,  $k_1$  and  $k_3$ , and the lumped ring cleavage step,  $k_5$  as a function of the quinoline amount added. An almost identical reduction in all reaction rate constants can be observed with increasing amount of quinoline added.

During the HDM reaction in the presence of quinoline significant conversion of quinoline was observed. Quinoline is converted into tetrahydroquinoline as can be seen from Figure 7, no hydrodenitrogenation of tetrahydroquinoline to form ammonia was observed.

The influence of ammonia on VO-TPP hydrodemetallisation was studied by *in situ* formation from diaminopropane, which decomposes rapidly under reaction conditions to ammonia and hydrocarbon products. The competition by ammonia is shown in Figure 8. The competition effect is large and it is striking that all reaction rates are reduced with the same factor.

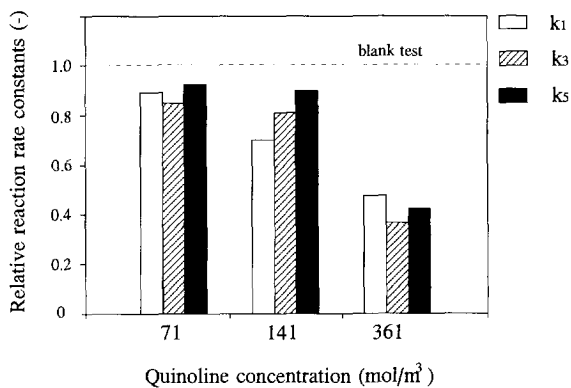


**Figure 6.** Influence of quinoline addition on VO-TPP hydrodemetallisation.  
(k<sub>1</sub> and k<sub>3</sub>: hydrogenation reaction rate constants, k<sub>5</sub>: lumped ring cleavage reaction rate constants)

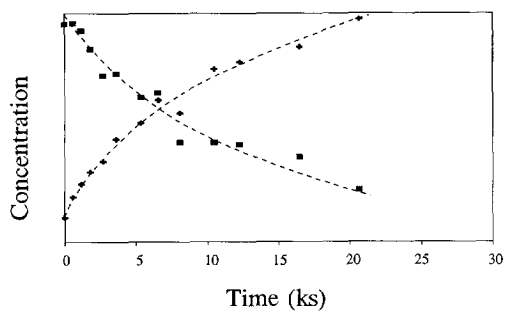


**Figure 7.** Quinoline conversion into tetrahydroquinoline during HDM of VO-TPP.  
(■: quinoline and +: tetrahydroquinoline)

A similar ammonia competition experiment was carried out for the hydrodemetallisation of nickel-tetraphenylporphyrin (Ni-TPP). In that case no significant decrease in reaction rate constants was observed.

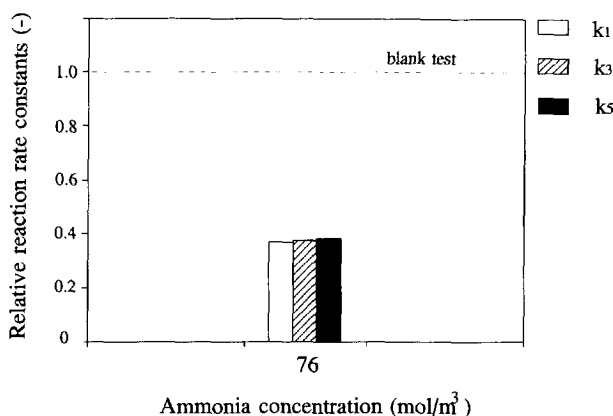


**Figure 8.** Influence of ammonia addition on VO-TPP hydrodemetallisation.

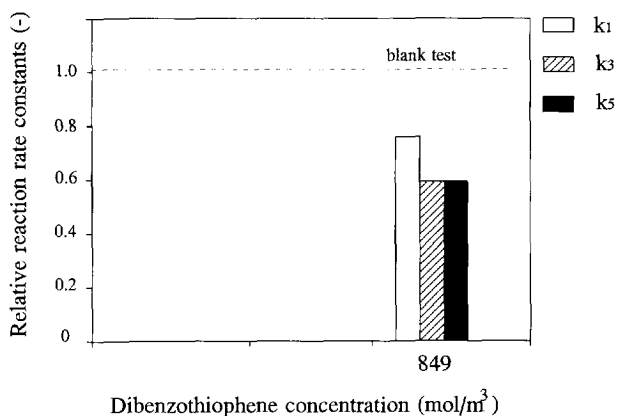
( $k_1$  and  $k_3$ : hydrogenation reaction rate constants,  $k_s$ : lumped ring cleavage reaction rate constants)

### 3.3. Influence of the sulfur containing compound dibenzothiophene

Figure 9 shows the influence of the sulfur containing compound dibenzothiophene addition on the HDM reaction kinetics of VO-TPP. Again a reduction in reaction rate constants is observed. The observed decrease in reaction rate constants is smaller than for the quinoline or ammonia competition experiments. The hydrodesulfurisation of dibenzothiophene was found to be on a much larger time scale than the VO-TPP hydrodemetallisation reaction.

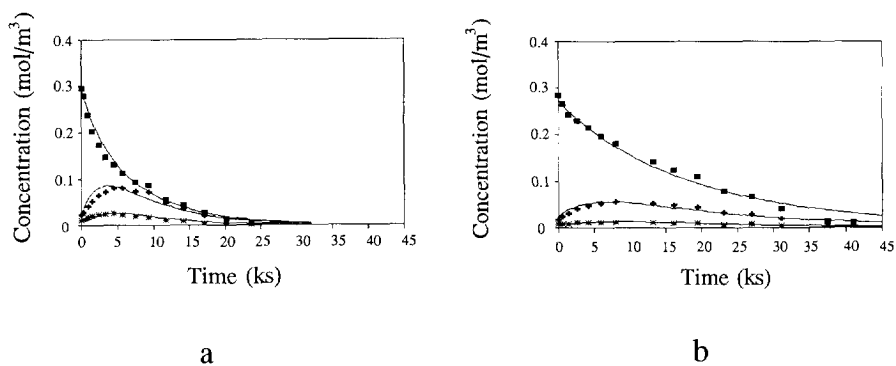
### 3.4. Influence of the oxygen containing compounds benzofuran and water

Figure 10 shows the concentration-time profiles obtained from the batch reactor for the blank test (without competitor) and for the test with benzofuran added to the reaction mixture. Again competition is observed for the HDM of VO-TPP. However, there is no equal competition effect in the hydrogenation and ring cleavage reactions. The rate of the first hydrogenation step, the conversion of VO-TPP in VO-TPC, is relatively more decreased than the rate of the second hydrogenation and the ring cleavage step. The hydrodeoxygenation of benzofuran in water was not experimentally determined.



**Figure 9.** Influence of dibenzothiophene addition on VO-TPP hydrodemetallisation.

( $k_1$  and  $k_3$ : hydrogenation reaction rate constants,  $k_5$ : lumped ring cleavage reaction rate constants)



**Figure 10.** Concentration-time profiles for VO-TPP hydrodemetallisation at 578 K and 10.0 MPa H<sub>2</sub> pressure, a- blank test and b- with addition of benzofuran (118 mol/m<sup>3</sup>).

Figure 11 and 12 show the reduction in the reaction rate constants for the two hydrogenation steps,  $k_1$  and  $k_3$ , and the lumped ring cleavage step,  $k_5$  as a function of the amount of benzofuran and water added.

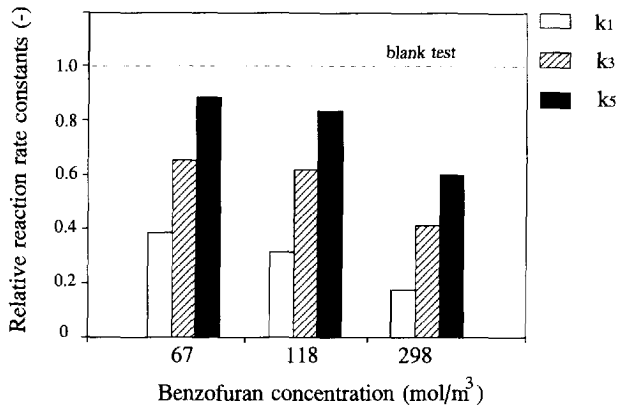


**Figure 11.** Influence of benzofuran addition on VO-TPP hydrodemetallisation. ( $k_1$  and  $k_3$ : hydrogenation reaction rate constants,  $k_s$ : lumped ring cleavage reaction rate constants)

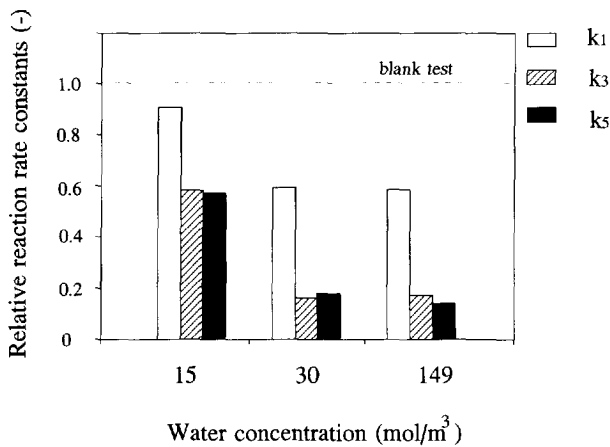


**Figure 12.** Influence of water addition on VO-TPP hydrodemetallisation. ( $k_1$  and  $k_3$ : hydrogenation reaction rate constants,  $k_s$ : lumped ring cleavage reaction rate constants)

A reduction in the reaction rate constants is observed with increasing amount of benzofuran added. As already observed in the concentration-time profiles, the rate of the first hydro-

generation step is more decreased than the rate of the second hydrogenation and lumped ring cleavage step, resulting in a relatively lower reaction rate constant.

In the water addition experiments, an initially sharp reduction in the reaction rate constants for hydrodemetallisation of VO-TPP is observed, but above a water concentration of 30 mol/m<sup>3</sup> the reaction rate constants remain constant. In contrast to the case of benzofuran addition, the rate of the first hydrogenation step is less decreased than the rate of the second hydrogenation and lumped ring cleavage step.

A similar experiment of water addition was carried out with Ni-TPP. This showed that water does not lower the reaction rate of Ni-TPP hydrodemetallisation.

### 3.5. Influence of anthracene

Figure 13 shows the reduction in the reaction rate constants for VO-TPP hydrodemetallisation as a function of the amount of anthracene added. Again an increasing competition effect is observed with increasing amount of anthracene added to the reaction mixture. The rate of the first hydrogenation step is decreased, whereas the effect on the rate of the second hydrogenation and the lumped ring cleavage step is small.

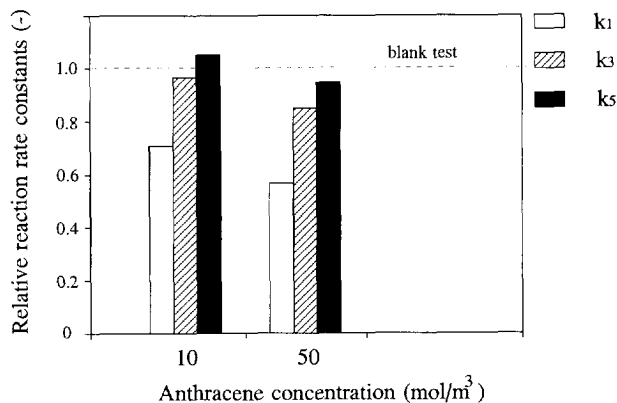


**Figure 13.** Influence of anthracene addition on VO-TPP hydrodemetallisation.

(k<sub>1</sub> and k<sub>3</sub>: hydrogenation reaction rate constants, k<sub>5</sub>: lumped ring cleavage reaction rate constants)



## 4. DISCUSSION

The competition effects of hetero-atom containing compounds on model compound HDS, HDN and HDO reactions have been studied by various researchers (6-18). Studies on competition effects on hydrodemetallisation reactions are scarce. The effect of pyridine addition was investigated by Ware & Wei (19). For the hydrodemetallisation of nickel-tetra(3-methylphenyl)porphyrin (Ni-T3MPP) over an oxidic CoMo/Al<sub>2</sub>O<sub>3</sub> catalyst, pyridine strongly decreased the rate of the hydrogenation reactions and showed less effect on the ring cleavage reaction rate. This result was explained by the assumption that hydrogenation and ring cleavage reactions occur on two different sites. Hydrogenation reactions are associated with Lewis acid sites, whereas ring cleavage reactions occur on Brønsted acid sites.

Our work shows that all competitors, *i.e.*, quinoline, ammonia, benzofuran, water, dibenzothiophene, and anthracene, decrease the rate of hydrodemetallisation of vanadyl-tetraphenylporphyrin; both the rate of the hydrogenation ( $k_1$  and  $k_3$ ) and the lumped ring cleavage ( $k_5$ ) reaction step are decreased. This competition observed is relevant for industrial practice, it occurs at concentrations representative for realistic feedstocks. When the competition is quantified according to a Langmuir-Hinshelwood adsorption concept (taking into account the initial competitor concentrations, which are assumed to remain constant), an competition effect on the hydrogenation reactions ( $k_1$  and  $k_3$ ) is found in the following sequence: water ~ ammonia > benzofuran ~ anthracene > quinoline > dibenzothiophene. The competition sequence for the lumped ring cleavage reaction ( $k_5$ ) is: water > ammonia > benzofuran ~ quinoline > anthracene ~ dibenzothiophene. Table 4 lists the calculated values of adsorption coefficients for the added compounds.

Water and ammonia are the strongest competitors for VO-TPP hydrodemetallisation. However, the addition of water and ammonia showed no significant decrease in Ni-TPP hydrodemetallisation rate. At first sight this is surprising when competition takes place by competitive adsorption between the reactant/intermediates and the competitor on the active sites of the catalyst. However, an alternative explanation is postulated for this observation. It is assumed that the decrease in VO-TPP HDM reaction rate due to water and ammonia addition takes place by coordination as axial ligands with the vanadyl group in the centre of the porphyrin rather than at the active sites of the catalyst. This coordination is caused by hydrogen bonding (20, 21). The coordination stabilizes the reactant and intermediates and the hydrodemetallisation reaction rate is decreased. The observation that the Ni-TPP hydrodemetallisation is not significantly influenced by water and ammonia corroborates this interpretation. Literature on ammonia competition in thiophene hydrodesulfurisation (15) supports the present observation, the effect of ammonia by competitive adsorption was found to be very weak.

**TABLE 4**  
 Calculated adsorption coefficients for the added competitors  
 in the hydrodemetallisation of VO-TPP.

Compound	adsorption coefficient in hydrogenation steps (m <sup>3</sup> /mol)	adsorption coefficient in lumped ring cleavage step (m <sup>3</sup> /mol)
Water	2.0·10 <sup>-2</sup>	4.0·10 <sup>-2</sup>
Ammonia	2.0·10 <sup>-2</sup>	2.0·10 <sup>-2</sup>
Benzofuran	1.0·10 <sup>-2</sup>	2.0·10 <sup>-3</sup>
Quinoline	4.0·10 <sup>-3</sup>	3.5·10 <sup>-3</sup>
Anthracene	8.0·10 <sup>-3</sup>	1.0·10 <sup>-3</sup>
Dibenzothiophene	4.0·10 <sup>-4</sup>	8.0·10 <sup>-4</sup>

Competition is quantified according to:  $k_{\text{blank test}}/k_{\text{with competitor}} = 1 + \text{adsorption coefficient} \cdot \text{concentration}$ . Errors up to 25% should be expected in the values for the adsorption coefficients.

In the VO-TPP hydrodemetallisation kinetic analysis, quinoline and dibenzothiophene did not change the hydrogenation-ring cleavage selectivity significantly, whereas benzofuran and anthracene showed a stronger competition effect on the hydrogenation reactions, resulting in a lower hydrogenation-ring cleavage selectivity. These selectivity differences of the various competitors are not fully understood at present. It is clear that hydrogenation and ring cleavage reactions occur on different sites, however, our results are obscured by the lumped ring cleavage step in the VO-TPP HDM reaction mechanism. It is possible that an observed decrease in the rate of the last ring cleavage step is caused by competition in the hydrogenation reaction lumped in this step. Competition effects of quinoline, benzofuran, dibenzothiophene, and anthracene in the hydrodemetallisation of Ni-TPP are not determined experimentally. However, it is postulated that these compounds also decrease the hydrodemetallisation reaction rate of Ni-TPP due to competitive adsorption.

Benzofuran is found to be a stronger competitor than dibenzothiophene for VO-TPP hydrodemetallisation. This is in agreement with the work of Lee & Ollis (11) who studied the competition of benzofuran on HDS of dibenzothiophene over a sulfided CoMo/Al<sub>2</sub>O<sub>3</sub> catalyst and concluded that the adsorption of benzofuran is stronger than that of dibenzothiophene. Therefore, the decrease in reaction rates caused by competitive adsorption of benzofuran is expected to be larger than of dibenzothiophene.

The effect of anthracene is concluded to be due to the competitive adsorption of anthracene on active sites, because it is a strong adsorbing molecule due to the presence of a large number of  $\pi$ -electrons.

Studies on competition effects of nitrogen containing compounds on thiophene HDS have shown that quinoline has a stronger competition effect than ammonia (15). Quinoline is probably stronger competitively adsorbed on the active sites than ammonia and therefore causes a larger reduction in the HDS activity. In present work, we find that ammonia is a stronger competitor than quinoline. This can be explained by the different ways of competition of both nitrogen containing compounds. Ammonia stabilizes the porphyrin due to axial ligand formation on the vanadyl group, whereas quinoline decreases the hydrodemetallisation reaction rate due to competitive adsorption. According to the literature, quinoline is expected to show more affinity to hydrogenation sites than hydrogenolysis sites (22, 23). Our results show an almost identical reduction in the rate constants for the hydrogenation and lumped ring cleavage steps. Two possible explanations arise (i) quinoline decreases the rate of the hydrogenation reactions in the lumped ring cleavage step and (ii) quinoline is converted into tetrahydroquinoline which apparently shows more affinity to ring cleavage reaction.

Competition effects are observed for spiked amounts of hetero-atom containing compounds near to the content occurring in oil residua. It should be kept in mind that the concentrations of these hetero-atom containing compounds are much higher than the concentration of VO-TPP. Hetero-atom containing compounds concentrations close to the VO-TPP concentration did not show any significant competition. This leads to the conclusion that the presence of hetero-atom containing compounds in real feedstocks can indeed influence the rate of metal removal. In contrast, competition by reaction products from the ring cleavage of VO-TPP (mono-pyrrole rings with one or two phenyl groups (24)) can be neglected due to the fact that these are present in low concentrations.

## 5. CONCLUSIONS

The presence of hetero-atom containing compounds, *i.e.*, quinoline, ammonia, benzofuran, water, dibenzothiophene, and anthracene decreases the rate of the hydrodemetallisation reaction of vanadyl-tetraphenylporphyrin when added in concentrations near to those in oil residua.

The rate of the hydrogenation reactions in the hydrodemetallisation of vanadyl-tetraphenylporphyrin are decreased in the following sequence: water ~ ammonia > benzofuran ~ anthracene > quinoline > dibenzothiophene. The rate of the lumped ring cleavage reaction in

the hydrodemetallisation of vanadyl-tetraphenylporphyrin is decreased in the sequence: water > ammonia > benzofuran ~ quinoline > anthracene ~ dibenzothiophene.

The decrease in the rate of metal removal is caused by two effects, (a) competitive adsorption of the added compound and the organo-metallic compound on the active sites of the catalyst and (b) axial ligand formation between the vanadyl group of the metallo-porphyrin and the added compound.

The influence of water and ammonia addition on the hydrodemetallisation of VO-TPP is the strongest due to the stabilization of the porphyrin by ligand formation with the vanadyl group. Quinoline, benzofuran, dibenzothiophene and anthracene decrease the rate of the hydrodemetallisation reaction of vanadyl-tetraphenylporphyrin by competitive adsorption on the active sites of the catalyst.

The rate of metal removal in realistic feedstocks can be influenced due to the presence of hetero-atom containing compounds. The reaction products from the ring cleavage of vanadyl-tetraphenylporphyrin, which are present in low concentrations, do not influence the rate of metal removal.

## ACKNOWLEDGMENTS

This work was financially supported by the Shell Research and Technology Centre, Amsterdam (SRTCA).

## REFERENCES

1. Sie, S.T., in 'Catalyst Deactivation', Delmon, B. and Froment, G.F. (Eds.), Elsevier Scientific Publishing Company, Amsterdam (1980) 545.
2. Quann, R.J., Ware, R.A., Hung, C.W., and Wei, J., *Adv. Chem. Eng.*, **14** (1988) 95.
3. Bonné, R.L.C., Steenderen, P. van, and Moulijn, J.A., *Bull. Soc. Chim. Belg.*, **100** (11-12) (1992) 877.
4. Chapter 3 of this thesis.
5. Chapter 2 of this thesis.
6. Satterfield, C.N., and Cocchetto, J.F., *Ind. Eng. Chem. Process Des. Dev.*, **15** (1976) 272.
7. Cowley, S.W., and Massoth, F.E., *J. Catal.*, **51** (1978) 291.
8. Satterfield, C.N., Modell, M., and Wilkens, J. A., *Ind. Eng. Chem. Proc. Des. Dev.* **19** (1980) 154.
9. Satterfield, C.N. and Carter, D.L., *Ind. Eng. Chem. Process Des. Dev.*, **20** (1981) 538.
10. Satterfield, C.N., and Yang, S.H., *J. Catal.*, **81** (1983) 335.

#### Chapter 4

11. Lee, C-L, and Ollis, D.F., *J. Catal.*, **87** (1984) 332.
12. Satterfield, C.N., Smith, C.M., and Ingalls, M., *Ind. Eng. Chem. Process Des. Dev.*, **24** (1985) 1000.
13. Nagai, M., Sato, T., and Aiba, A., *J. Catal.* **97** (1986) 52.
14. Massoth, F.E., and Miciukiewicz, J., *J. Catal.*, **101** (1986) 505.
15. LaVopa, V., and Satterfield, C.N., *J. Catal.*, **110** (1988) 375.
16. Laurent E. and Delmon B. *Ind. Eng. Chem. Res.* **32** (1993) 2516.
17. Ishihara, A., Itoh, T., Hino, T., Nomura, M., Qi, P., and Kabe, T., *J. Catal.*, **140** (1993) 184.
18. Laurent E. and Delmon B., *J. Catal.*, **146** (1994) 281.
19. Ware, R.A., and Wei, J., *J. Catal.*, **93** (1985) 122.
20. Flynn, J.S., and Freeman, D.H., *J. Chromatogr.*, **386** (1987) 111.
21. Xu, H., and Lesage, S., *J. Chromatogr.*, **607** (1992) 139.
22. Yang, S.H., and Satterfield, C.N., *J. Catal.*, **81** (1983) 168.
23. Yang, S.H., and Satterfield, C.N., *Ind. Eng. Chem. Process Des. Dev.*, **23** (1984) 20.
24. Chapter 7 of this thesis, accepted for publication in *Recueil*.

# Chapter 5

## Catalyst Deactivation in the Hydrodemetallisation of Vanadyl-tetraphenylporphyrin under Industrial Conditions

### ABSTRACT

---

Heavy oil residua contain organically bound metals, primarily vanadium and nickel. Hydrodemetallisation (HDM) generates metal deposition in catalyst pellets and this is one of the most important phenomena causing, in principle, irreversible catalyst deactivation.

Present work focuses on the modelling of HDM catalyst deactivation by vanadyl-tetraphenylporphyrin (VO-TPP). Intrinsic reaction kinetics, restrictive diffusion and the changing catalyst porous texture are the relevant phenomena to describe this deactivation process.

The changing catalyst porous texture during metal deposition can be described successfully by percolation concepts using a tessellation model. The behaviour of the tessellation model corresponds closely to the realistic deactivation behaviour of hydrotreating catalysts and is favoured over the conventional single cylindrical pore model.

Comparison of HDM catalyst deactivation model simulations of VO-TPP and experimental vanadium deposition profiles in catalyst pellets of an industrial feedstock show qualitative agreement. The similarity between the results for the model compound and the industrial feedstock implies that the use of these model compounds is a convenient tool in deactivation studies of hydrotreating catalysts.

---

## 1. INTRODUCTION

In the hydrotreating processing of heavy oils hetero-atoms, such as sulfur, nitrogen, oxygen and metals, are catalytically removed. Sulfur, nitrogen and oxygen leave the reactor as hydrogen sulfide, ammonia and water respectively. The metals, mainly vanadium and nickel, remain in the reactor as solid deposits accumulating on the catalyst surface after decomposition of the organo-metallic compounds. The removal of metals from heavy oil by catalytic hydrotreatment is called hydrodemetallisation (HDM).

Selection of the reactor type and the catalyst system used for hydrotreating is based on the type of feedstock and the metal content in the feedstock (1). This selection also determines the catalyst deactivation phenomena.

Deactivation of CoMo- or NiMo/ $\text{Al}_2\text{O}_3$  hydrodesulfurisation (HDS) catalysts is mainly caused by the interaction of the deposited metals with the original active sites of the catalyst ('*active site poisoning*') and the loss of pore volume due to the obstruction of catalyst pores ('*pore plugging*') (2).

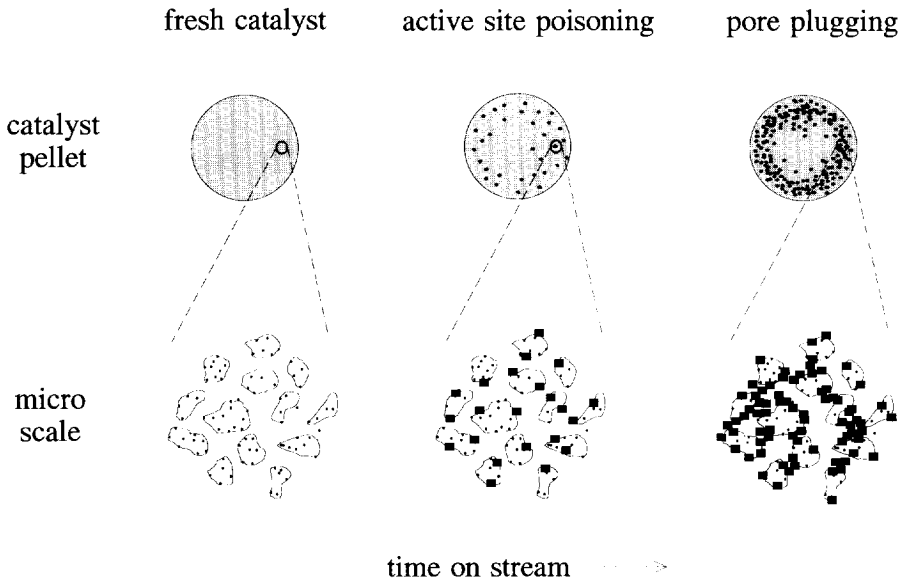


**Figure 1.** Metal deposition process in HDS catalyst.

Metal deposition on a wide-pore silica HDM catalyst can cause an increase in catalyst activity for HDM due to the autocatalytic effect of the deposited nickel and vanadium ('*active site generation*'). Eventually, at high metal loadings *pore plugging* becomes the dominant deactivation phenomenon. The catalyst deactivation phenomena for both catalyst systems are depicted in Figures 1 and 2 respectively.

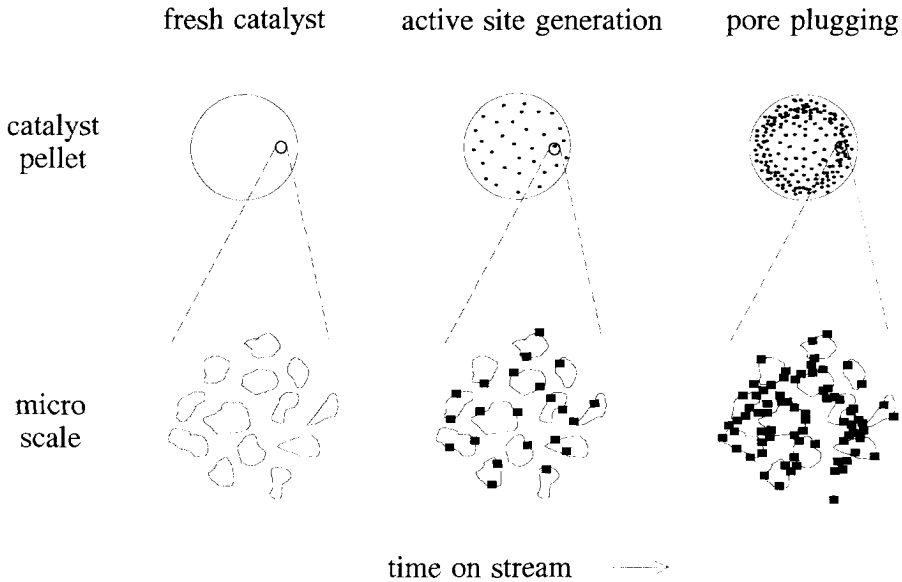


**Figure 2.** Metal deposition process in wide-pore HDM catalyst, starting from bare support.

Key-issue in HDM process design and operation is the development of catalyst deactivation models which give reliable predictions of catalyst life-time and activity, thus providing a convenient tool for designing optimized catalysts. The present work proposes a general approach for the modeling of catalyst deactivation. A HDM catalyst deactivation model is developed based on percolation concepts and compared with experimental catalyst deactivation results.



## 2. APPROACH FOR MODELLING HDM CATALYST DEACTIVATION

The general approach for modelling catalyst deactivation is schematically organised in Figure 3. The core of the model consists of the mass balances of reactants, intermediates, and metal deposits. In these mass balances, coefficients are present to describe reaction kinetics (reaction rate constant), mass transfer (diffusion coefficient), and catalyst porous texture (accessible porosity and effective transport properties). The mass balances together with the boundary conditions define the catalyst deactivation model. The boundary conditions are determined by the axial position in the reactor. Simulations result in metal deposition profiles in catalyst pellets and catalyst life-time predictions.

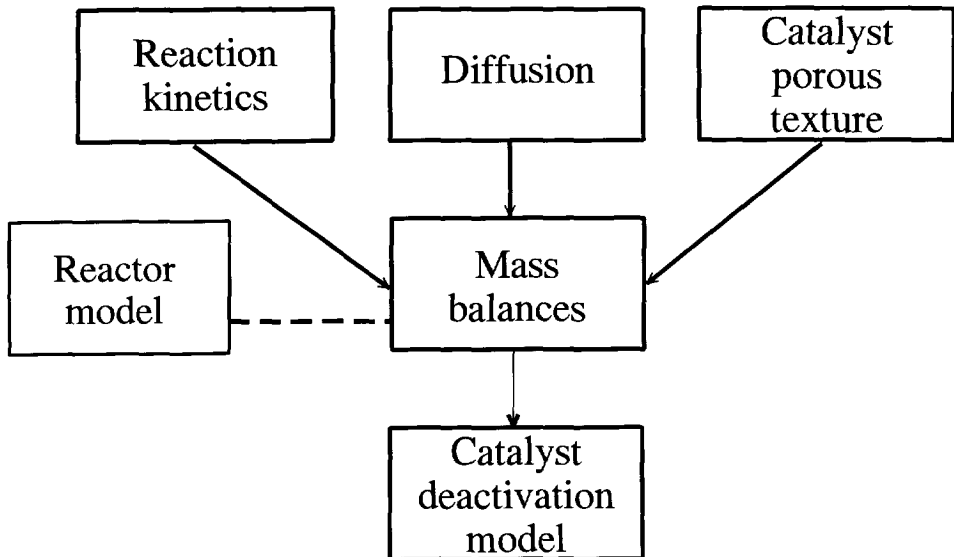


**Figure 3.** General approach for modelling HDM catalyst deactivation.

In the successive paragraphs of this chapter, each independent part of the modelling approach will be discussed.

### 2.1. HDM reaction kinetics and diffusion

A significant proportion of the metal compounds in heavy oil residua is complexed in porphyrins (3). The use of porphyrinic model compounds in reaction kinetics research eliminates many of the complicated and competing reactions encountered with heavy oil residua, thus enabling a clearer picture of the reactions to be ascertained. The hydrodemetallisation of porphyrinic model compounds involves a sequence of hydrogenation steps and a ring cleavage. Figure 4 depicts the HDM reaction mechanism for model compound vanadyl-tetraphenylporphyrin (VO-TPP) (4). VO-TPP is reversibly hydrogenated to vanadyl-tetraphenylchlorin (VO-TPC), which can be reversibly hydrogenated to vanadyl-tetraphenylisobacteriochlorin (VO-TPiB). The last step in the reaction mechanism, the ring cleavage, is a lumped step. The porphyrin is further hydrogenated and broken up into ring fragments. Vanadium is removed from the porphyrin and deposited on the catalyst surface. Therefore, the lumped ring cleavage step consists of both hydrogenation and hydrogenolysis reactions.

Bonné et al. (4) studied reaction kinetics of tetraphenylporphyrin model compounds over several catalysts and concluded that hydrogenation and ring cleavage occur on two different sites. Therefore, the reaction mechanism of VO-TPP hydrodemetallisation is described by a two-site model. It was also found that a Langmuir-Hinshelwood type of kinetics applies with competitive adsorption of hydrogen.

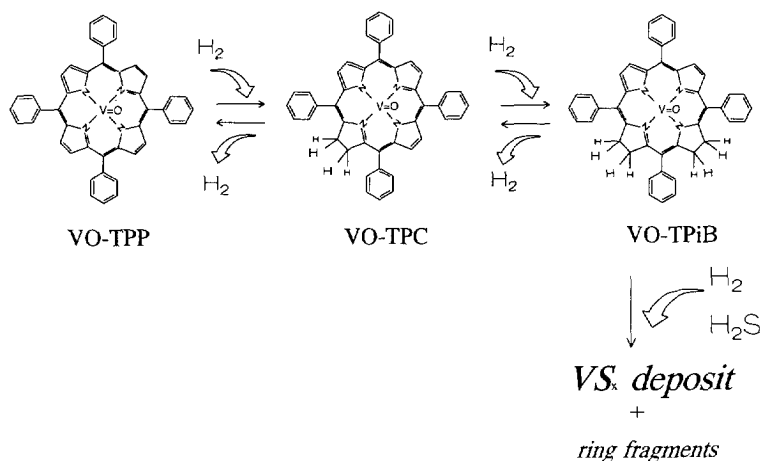


**Figure 4.** HDM reaction mechanism of model compound vanadyl-tetraphenylporphyrin.

(TPP: tetraphenylporphyrin, TPC: tetraphenylchlorin, TPiB: tetraphenylisobacteriochlorin)

Prerequisite for hydrodemetallisation is the diffusion of these large porphyrins into the catalyst porous texture. Diffusion of these molecules can be limited by geometric exclusion and hydrodynamic drag. When the solute molecular size is significant as compared to the pore dimensions, a restrictive factor should be introduced to account for the reduced diffusivity (5). As a consequence, detailed HDM reaction kinetics may be obscured by diffusion limitations.

## 2.2. Catalyst porous texture

The initial porous texture of a catalyst pellet and the change in texture caused by metal deposition can be described using the percolation theory. In the percolation approach the pellet is constructed as a binary interdispersion of void space and (deposited) solid material. In this binary interdispersion, the void space can exist as (a) isolated clusters surrounded by solid material or (b) sample overspanning void space that allows mass transport from one side to the other. The total void space  $\epsilon$  can be split into the sum of the volume fraction of isolated non-accessible void space  $\epsilon^I$  and the volume fraction of accessible void space  $\epsilon^A$ . If  $\epsilon$  is below a critical value, the so-called percolation threshold  $\epsilon_c$ , all the void space consists of isolated clusters and transport through the pellet is impossible .

A quantity relevant for diffusional transport is the effective transport void space  $\epsilon^E$ . If the accessible void space was arranged in parallel layers, then  $\epsilon^E$  equals  $\epsilon^A$ . However, in disordered interdispersions the accessible void space for transport may be tortuous and have inactive dead-ends, so that in general  $\epsilon^E \leq \epsilon^A$ .

Two types of percolation models are mentioned in the literature to describe the local porosity in catalyst pellets, (a) topologically-disordered networks in a continuous system (tessellation models) and (b) regular discrete networks (Bethe networks) (6).

In tessellation models, the interdispersion represents void and solids distributed as for example cubes. The composite shown in Figure 5 a is a random tessellated space with identical cubes. The metal deposition process can be envisaged as an increase in the number of randomly tessellated cubes.

A Bethe network is a branching structure defined by nodes and bonds, as shown in Figure 5 b. The metal deposition process can be envisaged as a uniform deposition of metals in the pores of the network. The dependence of  $\epsilon^I$ ,  $\epsilon^A$ , and  $\epsilon^E$  on the total void space  $\epsilon$  during the metal deposition process can be determined by analytical relations (7).

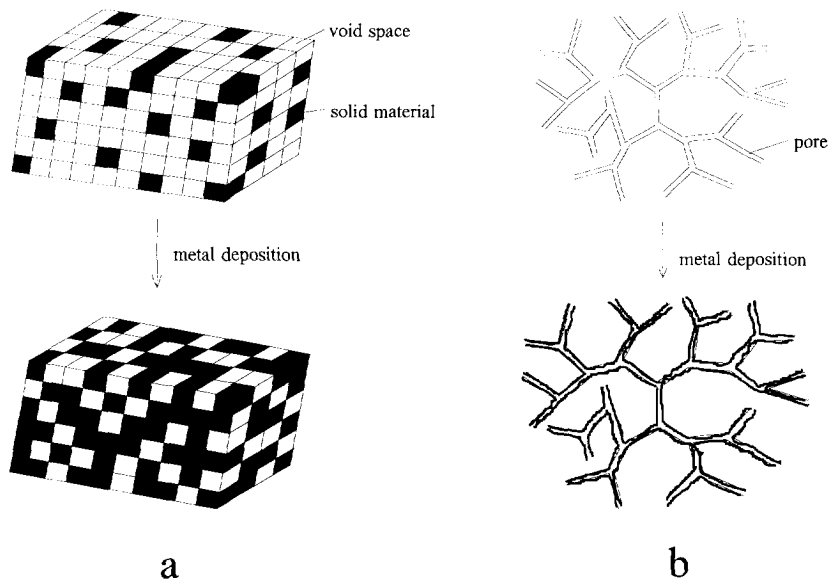


**Figure 5.** Catalyst porous texture as described by a- the cubic tessellation model and b- the Bethe network.

A disadvantage of the Bethe network is that it lacks physical reality, e.g. the presence of closed loops, which are present in practical porous materials. In contrast with this, in tessellation models closed loops are present. The presence of closed loops is an important aspect in describing the metal deposition process in catalyst pellets and therefore the tessellation approach is favoured over the Bethe network.

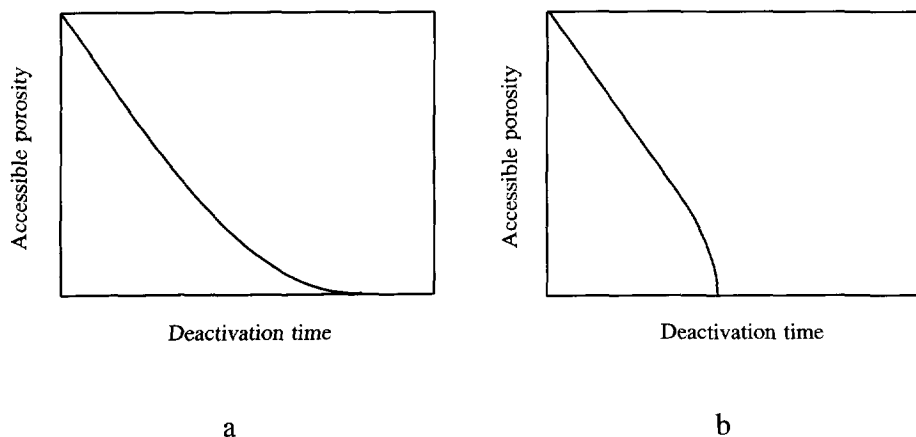


**Figure 6.** Accessible porosity as a function of the deactivation time for a- conventional single cylindrical pore model and b- cubic tessellation model.

A comparison between the cubic tessellation model and the conventional single cylindrical pore model shows a fundamentally different behaviour during the metal deposition process. In Figure 6 the accessible porosity is plotted versus the time on stream of a catalyst pellet. As can be observed, both models show initially an identical, almost linear decrease of the accessible porosity. At a larger time on stream, the two models start to differ. The single cylindrical pore model shows a continuing gradual decrease of the accessible porosity, whereas the tessellation model shows a more rapid decline. This rapid decline in the accessible porosity is attributed to the formation of isolated void space in which mass transport is impossible.

The rapid decline in accessible porosity or activity is found in experimental deactivation curves for heavy oil hydrotreating catalysts (8). The behaviour of the tessellation model corresponds more closely to the realistic deactivation behaviour of hydrotreating catalysts and is therefore favoured over the conventional single cylindrical pore model.

### 2.3. Mass balances and model equations

The mass balances of the reactants and intermediates in a spherical catalyst particle are given. The generalized mass balance consists of the accumulation term which equals the difference between diffusion and reaction

$$C \frac{\partial \epsilon^A}{\partial t} + \epsilon^A \frac{\partial C}{\partial t} = \frac{1}{r^2} \frac{\partial}{\partial r} \left[ r^2 \epsilon^E D_{eff} \frac{\partial C}{\partial r} \right] - S_v \mathfrak{R} \quad (1)$$

The mass balance of the metal deposits consists of the accumulation term which equals the reaction term

$$\frac{\partial W_M}{\partial t} = \alpha M_M S_v \mathfrak{R} \quad (2)$$

The initial and boundary conditions are:

$$\begin{array}{ll} t = 0, 0 \leq r \leq R_c: & t > 0, r = R_c: C = C_{bulk} \\ C = 0 \text{ and } W_M = 0 & r = 0: \frac{\partial C}{\partial r} = 0 \end{array}$$

In the mass balances, the variables  $S_v$ ,  $\epsilon^A$ , and  $\epsilon^E$  occur. These are the variables characterizing the changing porous texture of the catalyst pellet during metal deposition and are described using the percolation approach. The catalyst pellet textural properties can be calculated from a network model, which equivalent to a finite difference approximation to the continuum problem (7). Figure 7 shows the isolated, accessible porosity ( $\epsilon^I$ ,  $\epsilon^A$ ) and effective transport coefficient ( $\epsilon^E$ ) as a function of the total catalyst pellet porosity. In the present work, deactivation by metal deposition is caused only by a decrease in porosity, pore volume and surface area. For details on percolation concepts and model equations is referred to Mohanty et al. (7).

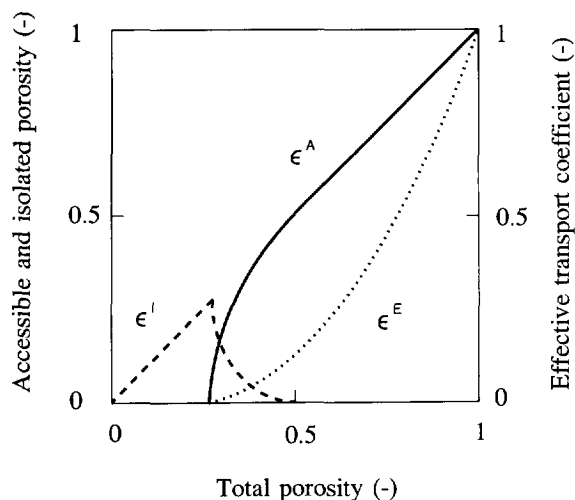


**Figure 7.** Isolated, accessible porosity ( $\epsilon^I$ ,  $\epsilon^A$ ) and effective transport coefficient ( $\epsilon^E$ ) as a function of the total catalyst pellet porosity.

### 3. EXPERIMENTAL

#### 3.1. HDM reaction kinetics

Intrinsic reaction kinetics parameters for the hydrodemetallisation of VO-TPP on a sulfided vanadium on a wide-pore silica support have been determined. The experiments were carried out in a 250 ml batch autoclave with *o*-xylene as solvent. The properties of the catalyst used in this study are summarized in Table 1.

**TABLE 1**  
Properties of catalyst used in this study.

catalyst	V/SiO <sub>2</sub>
loading active phase	
(vanadium atoms/nm <sup>2</sup> )	4.6
(wt.% V)	1.34
initial surface area (m <sup>2</sup> /kg)	24·10 <sup>3</sup>
initial pore radius (m)	43·10 <sup>-9</sup>
initial accessible porosity (-)	0.57
catalyst pellets radius (m)	75·10 <sup>-6</sup>

The textural properties are determined with Hg porosimetry. Approximately 25% of the pore volume can be attributed to macro pores.

The two-site reaction kinetics model proposed by Bonné et al. (4) was used to evaluate the kinetic parameters. Activation energies and pre-exponential factors were determined from experiments between 570-630 K at 10 MPa H<sub>2</sub> pressure.

Experimental and theoretical details on HDM reaction kinetics are given elsewhere (9).

### 3.2. Catalyst deactivation

Catalyst deactivation experiments were carried out in a micro-flow reactor using a wide- and a narrow-pore silica (pore radii of 30 and 5 nm respectively) with a pellet radius of 0.85 mm. A heavy oil containing 61 ppmw V was used as feedstock and continuously fed to the reactor at 15 MPa H<sub>2</sub> pressure and 673 K. After the run a vanadium deposition profile was determined in a catalyst pellet with Electron Probe Micro Analysis (EPMA). This profile can be considered to represent that of a catalyst at an average position in the reactor.

The description of the proposed HDM catalyst deactivation model includes a system of nonlinear parabolic partial differential equations in one space variable. These equations are numerically solved with a CONVEX 3840 workstation. Subroutines to solve the set of PDEs are obtained from the NAG Fortran library (1988) (10).



## 4. RESULTS AND DISCUSSION

### 4.1. HDM reaction kinetics

Values for the pre-exponential factors at a reference temperature and activation energies are presented in Table 2. In order to decrease the strong intercorrelation between pre-exponential factors and activation energies, the reparametrisation method of Kittrell (11) was used.

**TABLE 2**  
Reaction kinetics parameters of VO-TPP HDM on sulfided V/SiO<sub>2</sub> catalyst.

Reaction:	first hydrogenation	second hydrogenation	ring cleavage
pre-exponential factor, $k_{T_{ref}}$ in	$(5.91 \pm 0.32) \cdot 10^{-8}$ $m^3/(m^2 \cdot s)$	$(9.55 \pm 0.97) \cdot 10^{-8}$ $m^3/(m^2 \cdot s)$	$(3.55 \pm 0.75) \cdot 10^{-7}$ $m^6/(m^2 \cdot mol \cdot s)$
Activation energy, $E_a$ (kJ/mol)	$80 \pm 10$	$55 \pm 18$	$88 \pm 41$
Reparametrisation method of Kittrell (11): $\ln k = \ln k_{T_{ref}} - (E_a/R) \cdot (1/T - 1/T_{ref})$ , $T_{ref} = 600$ K			

These results show that the second hydrogenation step seems to have a lower activation energy than the first hydrogenation step. The first hydrogenation step is apparently more difficult, obviously due to the resonance stability of the tetraphenylporphyrin. After the first hydrogenation the porphyrin becomes more vulnerable for hydrogenation and therefore shows a lower activation energy. The activation energy for the ring cleavage step is difficult to relate to the first and second hydrogenation due to the fact that this is a lumped step consisting of hydrogenation and hydrogenolysis reactions (12).

### 4.2. Catalyst deactivation: experimental and modelling

Figure 7 shows the influence of the bulk diffusion coefficient,  $D_b$ , on the vanadium deposition profiles using the reaction kinetics of VO-TPP and a wide pore silica catalyst. The simulations are performed at reactor inlet conditions, which implies that the concentration of

intermediates is equal to zero outside the catalyst pellet. Obviously, by decreasing the diffusivity the metal deposition process becomes more diffusion rate-limited, resulting in a less deep penetration into the catalyst pellet. According to literature (13), a bulk diffusion coefficient of  $10^{-8} \text{ m}^2/\text{s}$  is a reasonable value for the diffusion of porphyrins.

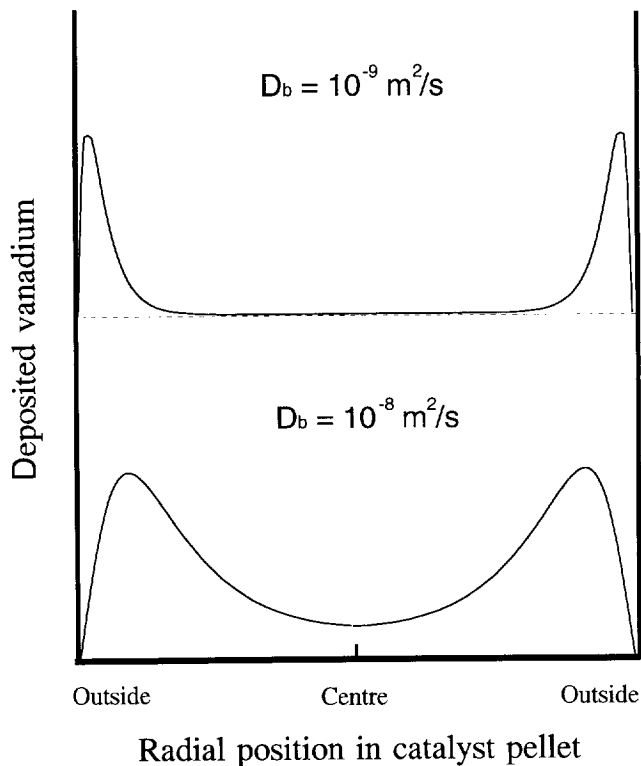


**Figure 7.** Influence of the bulk diffusion coefficient,  $D_b$ , on the vanadium deposition profile in a wide pore silica catalyst pellet at reactor inlet conditions.

(Model compound VO-TPP, 673 K, 10 MPa  $\text{H}_2$ , initial pore radius: 30 nm, catalyst pellet radius: 0.85 mm)

Figure 8 shows the influence of the axial position of the catalyst pellet in the reactor. As can be observed, the vanadium deposition profiles shift from a M-shaped profiles to a more U-shaped profile. This is due to the increasing presence of intermediates outside the catalyst pellet when going further downstream in the reactor. Experimental work by Ware & Wei (14) showed a similar shift in the shape of the metal deposition profile.

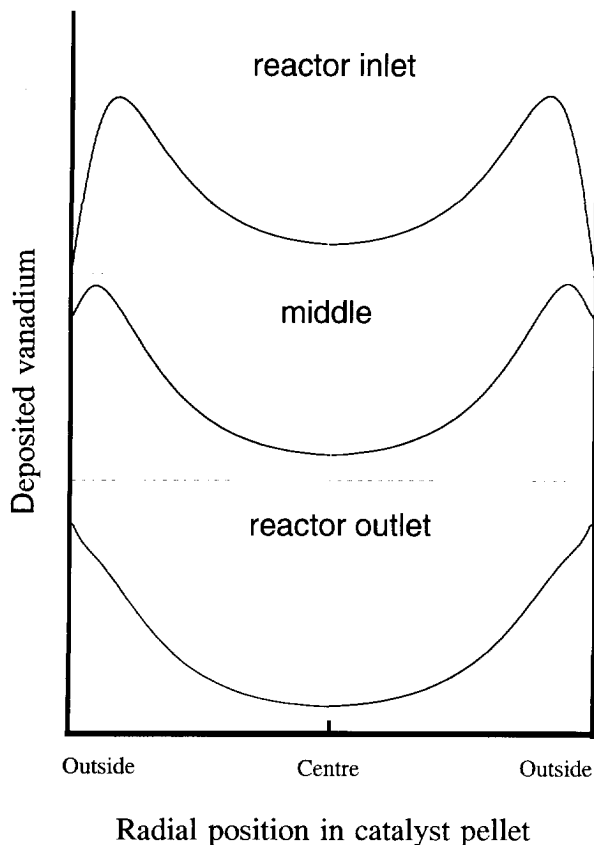


**Figure 8.** Influence of the axial position in the reactor on the vanadium deposition profile in a wide pore silica catalyst pellet.

(Model compound VO-TPP, 673 K, 10 MPa H<sub>2</sub>,  $D_b=10^{-8}$  m<sup>2</sup>/s, initial pore radius: 30 nm, catalyst pellet radius: 0.85 mm)

Figure 9 shows the influence of the initial pore radius, in the case of a wide- and narrow-pore silica catalyst, on the vanadium deposition profiles at an average axial position in the reactor. Both cases show the presence of deposition maxima, indicating that the deposition process is diffusion rate-limited. In the case of the narrow-pore silica the core volume of the pellet potentially available for vanadium deposition cannot be reached by reactant and intermediates and is lost for vanadium deposition.

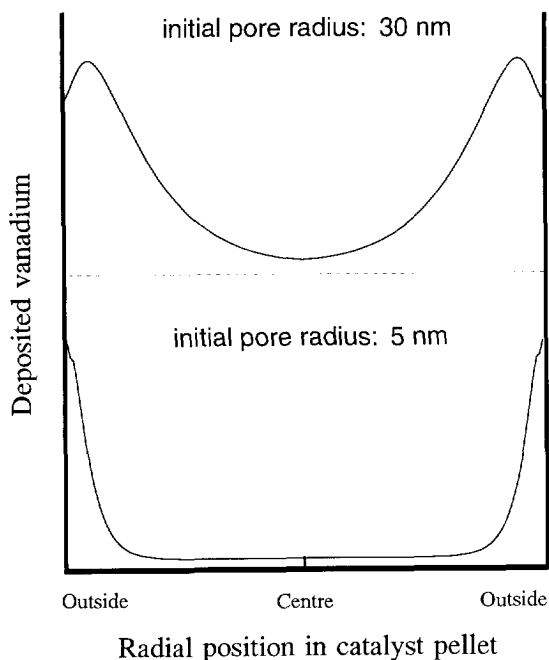


**Figure 9.** Influence of the initial pore radius on the vanadium deposition profile (wide- and narrow pore silica catalyst pellet) at an average axial position in the reactor.

(Model compound VO-TPP, 673 K, 10 MPa H<sub>2</sub>, D<sub>6</sub>=10<sup>-8</sup> m<sup>2</sup>/s catalyst pellet radius: 0.85 mm)

When the simulations shown in Figure 9 for the model compound VO-TPP are compared with the experimental vanadium deposition profiles from an industrial feedstock, depicted in Figure 10, it is clear that there is qualitative agreement. Apparently, model simulations using reaction kinetics of model compound VO-TPP give similar shaped vanadium deposition profiles.

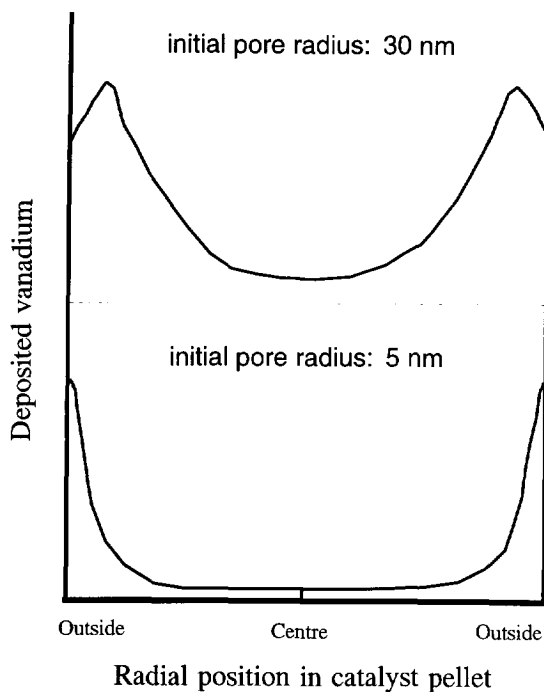


**Figure 10.** Experimental vanadium deposition profiles for wide- and narrow pore silica catalyst.

(Industrial feedstock containing 61 ppmw V, 673 K, 15 MPa H<sub>2</sub>, catalyst pellet radius: 0.85 mm)

At first sight it is surprising that model and experiment agree (at least qualitatively). An explanation for the similarly shaped vanadium deposition profiles is that the Thiele modulus, which determines the shape of the deposition profiles, is apparently equal for both cases. It is well documented that the bulk diffusion coefficient of an industrial feedstock is about two orders of magnitude lower than for a model compound (15). Therefore, the reaction rate of a model compound should be two orders of magnitude higher than for an industrial feedstock in order to preserve equal Thiele moduli.

Reaction rates of industrial feedstocks are lower than for model compounds which is due to *i*) the limited accessibility of metal compounds within asphaltenes to catalytic active site (16), *ii*) the competitive adsorption of hetero-atom species present in heavy oil (17) and *iii*) the intrinsically lower reactivities of vanadium containing structures in real feeds.

The observation that the simulated vanadium deposition profiles for model compound VO-TPP are similar to the experimental deposition profiles for an industrial feedstock is interesting from a catalyst screening and testing point of view. Research on deactivation of hydrotreating catalysts is time consuming and expensive. Since model compounds exhibit a much higher metal deposition rate than industrial feedstocks, the use of model compounds is a convenient tool to predict catalyst performance, thereby reducing the duration of deactivation tests and increasing the ability to screen more catalysts.

In Figure 11 the profiles of the reactant, VO-TPP, the intermediates, VO-TPC and VO-TPiB, and the vanadium deposits during the deactivation process in a flow reactor are depicted. Reactant VO-TPP is diffusing into the catalyst pellet and is converted into VO-TPC. The diffusion is too slow as compared to the reaction, which causes a lower concentration of VO-TPP in the centre of the pellet compared to the outside. The concentration of VO-TPP continues to decrease in time, which is due to the conversion into VO-TPC and the decreasing diffusivity caused by the deposition of vanadium in the catalyst pores.

Intermediates VO-TPC and VO-TPiB are produced by the conversion of VO-TPP and VO-TPC, respectively. VO-TPiB is converted into vanadiumsulfide deposits. The concentration profiles of VO-TPC and VO-TPiB are determined by the production or conversion and the diffusion in or out of the catalyst pellet. A maximum is observed in the concentration profiles which is dependent on the axial position in the reactor (see also Figure 8). This maximum in the concentration profiles is shifted to the outside of the pellet due to the decrease in diffusivity caused by vanadium deposition in the pores. The vanadium deposition profiles show a build-up in time. The shape of these profiles correspond to the concentration profiles of VO-TPiB, from which the metal deposits are irreversibly formed (sequential reaction mechanism (18)).

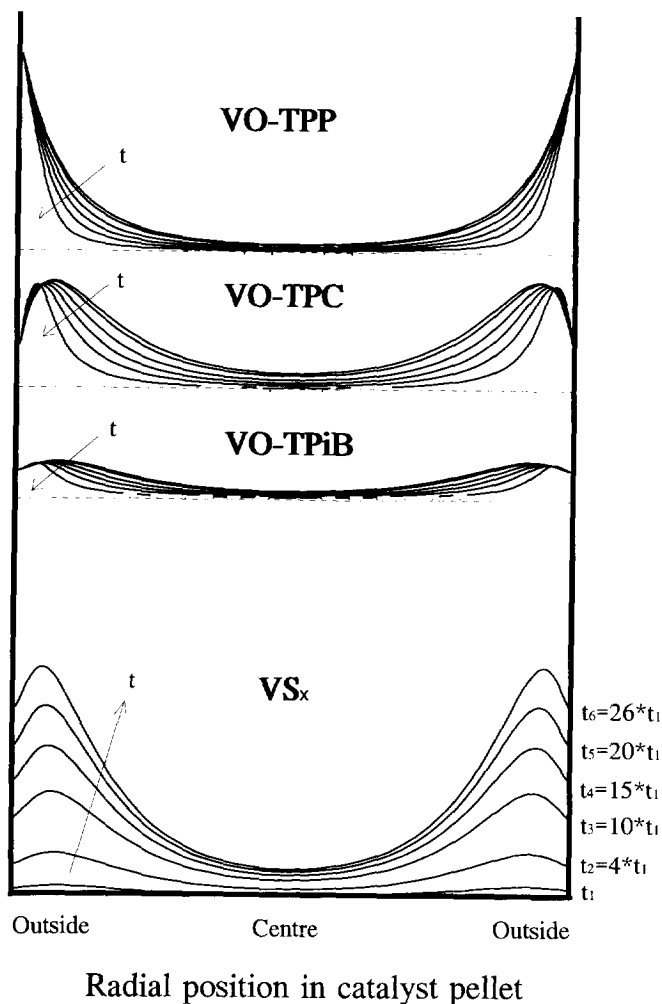


**Figure 11.** Evolution of concentration and vanadium deposits profiles in a wide pore silica catalyst at an average axial position in the reactor.

(Model compound VO-TPP, 673 K, 10 MPa H<sub>2</sub>,  $D_0 = 10^{-8}$  m<sup>2</sup>/s, initial pore radius: 30 nm, catalyst pellet radius: 0.85 mm)

## **5. CONCLUSIONS**

Intrinsic reaction kinetics, restrictive intraparticle diffusion and the (changing) catalyst porous texture are the relevant phenomena to describe HDM catalyst deactivation. Percolation concepts can be successfully applied to describe the changing catalyst porous texture during HDM. From the two percolation models, a tessellation approach is favoured over the Bethe network. The tessellation model corresponds closely to the realistic deactivation behaviour of hydrotreating catalysts in contrast to the conventional single cylindrical pore model.

Comparison of HDM catalyst deactivation model simulations of VO-TPP and experimental deposition profiles of an industrial feedstock in catalyst pellets show that the metal deposition process can be reproduced. The similarity between the results for the model compound and the industrial feedstock implies that the use of these model compounds in deactivation studies of hydrotreating catalysts is allowed.

## **ACKNOWLEDGMENTS**

The authors gratefully acknowledge the Shell Research and Technology Centre, Amsterdam (SRTCA) and the European Community (contract number JOUF 0049) for their financial support. Dr. B. Scheffer and Dr. J.C.C. den Ouden (SRTCA) are thanked for the stimulating discussions.



## NOTATION

$\alpha$	: ratio of number of metal atoms in deposit to number of metal atoms in porphyrin precursor	-
$C$	: concentration	mol/m <sup>3</sup>
$D_b$	: bulk diffusion coefficient in liquid phase	m <sup>2</sup> /s
$D_{\text{eff}}$	: effective or restrictive diffusion coefficient	m <sup>2</sup> /s
$E_a$	: activation energy	kJ/mol
$\epsilon$	: total void space or total porosity	-
$\epsilon^A$	: fraction of accessible void space or accessible porosity	-
$\epsilon_c$	: percolation threshold	-
$\epsilon^E$	: effective transport coefficient	-
$\epsilon^I$	: fraction of isolated void space or isolated porosity	-
$k$	: reaction rate constant	m <sup>3</sup> /m <sup>2</sup> ·s, m <sup>6</sup> /m <sup>2</sup> ·mol·s
$M_M$	: molecular weight of metal deposit	kg/mol
$r$	: radial length coordinate from centre of catalyst pellet	m
$R$	: universal gas constant	J/mol·K
$\mathcal{R}$	: reaction rate	mol/m <sup>2</sup> ·s
$R_c$	: radius of catalyst pellet	m
$\rho_M$	: density of metal deposit	kg/m <sup>3</sup>
$S_v$	: surface area per unit volume of catalyst pellet	m <sup>2</sup> /m <sup>3</sup>
$\sigma$	: dimensionless deposited vanadium, $W_M/\rho_M\epsilon^A$	-
$t$	: time	s
$T$	: temperature	K
$T_{\text{ref}}$	: reference temperature	K
$W_M$	: mass concentration of metal deposit	kg/m <sup>3</sup>
$z$	: coordination number	-

## REFERENCES

1. Stork, W.H.J., 'Catalyst for residue conversion', paper presented at first Shell workshop, Santa Domingo, March 10-11 (1983).
2. Sie, S.T., in 'Catalyst Deactivation', Delmon, B. and Froment, G.F. (Eds.), Elsevier Scientific Publishing Company, Amsterdam (1980) 545.
3. Quann, R.J., Ware, R.A., Hung, C.W., and Wei, J., *Adv. Chem. Eng.*, **14** (1988) 95.
4. Bonn , R.L.C., Steenderen, P. van, and Moulijn, J.A., *Bull. Soc. Chim. Belg.*, **100** (11-12) (1992) 877.
5. Satterfield, C.N., and Colton, C.K., *AIChE J.*, **19**(3) (1973) 628.

6. Sahimi, M., Gavels, G.R., and Tsotsis, T.T., *Chem. Eng. Sci.*, **45** (1990) 1443.
7. Mohanty, K.K., Ottino, J.M., and Davis, H.T., *Chem. Eng. Sci.*, **37** (1982) 905.
8. Tamm, P.W., Harnsberg, H.F., and Bridge, A.G., *Ind. Eng. Chem. Process Des. Dev.*, **20** (1981) 262.
9. Chapter 2 of this thesis.
10. NAG Fortran library (1988).
11. Kittrell, J.R., *Adv. Chem. Eng.*, **8** (1970) 97.
12. Chapter 7 of this thesis.
13. Chung, H. Tsai, Massoth, F.E., Lee, S.Y., and Seader, J.D., *Ind. Eng. Chem. Res.*, **30** (1991) 22.
14. Ware, R.A., and Wei, J., *J. Catal.*, **93** (1985) 100.
15. Chantong, A, and Massoth, F.E., *AIChE J.*, **29** (1983) 725.
16. Oxenreiter, M.F., Frye, C.G., Hoekstra, G.B., and Sroka, J.M., *Jpn. Petrol. Inst.*, Nov. 30 (1972)
17. Chapter 4 of this thesis.
18. Beeckman, J.W., and Froment, G.F., *Ind. Eng. Chem. Fundam.*, **21** (1982) 243.

# Chapter 6

## On the Metal Deposition Process during the Hydrodemetallisation of Vanadyl-tetraphenylporphyrin

### ABSTRACT

---

This chapter focuses on the metal deposition process during hydrodemetallisation (HDM) of vanadyl-tetraphenylporphyrin (VO-TPP) under industrial conditions. In catalyst pellets of a wide pore, low loaded molybdenum on silica, the vanadium deposition process was determined with EPMA and HREM. The effect of quinoline and  $H_2S$  on the vanadium deposition profile is studied and an attempt is made to simulate the deposition profiles based on intrinsic reaction kinetics and percolation concepts.

A reference vanadium deposition experiment is carried out in order to assess the influence of quinoline and  $H_2S$ . Quinoline showed to decrease the rate of metal removal, the amount of vanadium deposited is lower as compared to the reference experiment. The shape of the vanadium deposition profiles is similar in both cases. A deposition maximum is observed in the centre of the pellet, indicating that the vanadium deposition process is not diffusion limited and that a sequential reaction mechanism applies for VO-TPP HDM. Low  $H_2S$  partial pressure resulted in different vanadium deposition profiles as a function of the axial position in the reactor. At the inlet of the reactor, similarly shaped profiles as the reference experiment were found, however, at the outlet of the reactor a shift towards M-shaped profiles was found indicating a diffusion limited vanadium deposition process. This shift in vanadium deposition profiles is explained by the build up of the last intermediate resulting in a higher metal deposition rate.

Simulations of the vanadium deposition profiles showed reasonable results, at least at reactor inlet conditions. However, improvements should be made on the accuracy and determination of the input parameters of the proposed model. Since increasing discrepancies between model and experiment are observed in axial direction in the reactor.

With HREM, vanadium deposits were found in a layered structure both in the surrounding of the active phase, causing active site poisoning, and as isolated vanadium sulfide clusters, likely causing active site generation. In our vanadium deposition experiments (up to 9 wt.% vanadium) no significant catalyst deactivation occurred, indicating that both effects are compensated.

---

## 1. INTRODUCTION

Catalytic hydrotreating is a well established process for the removal of impurities or hetero-atoms, such as sulfur, nitrogen, oxygen and metals, from heavy oil residua. Sulfur, nitrogen and oxygen containing compounds are hydrogenated and removed as hydrogen sulfide, ammonia and water. The metals, however, remain in the reactor and deposit as metal sulfides on the internal catalyst surface. The removal of metals from heavy oil residua is called hydrodemetallisation (HDM).

Catalyst deactivation in hydrodemetallisation is caused by the interaction of the metal deposits with the original active phase (*'active site poisoning'*) and the loss of pore volume due to the obstruction of catalyst pores (*'pore plugging'*) (1). However, metal deposits also have an auto-catalytic effect on the hydrodemetallisation reaction, thus *'active site generation'* may occur in low active phase loaded or bare support catalyst systems.

Modelling of the metal deposition process is of great importance in process design and operation, in order to give reliable predictions on catalyst life-time and activity. A general approach for modelling the metal deposition process is proposed. Detailed knowledge of reaction kinetics and restrictive diffusion are indispensable, description of the catalyst porous texture during metal deposition is necessary and often neglected in literature. The catalyst deactivation model is an integration of reaction kinetics, diffusion and the catalyst porous texture in the mass balances. The reactor model essentially determines the boundary conditions of the mass balances.

The HDM reaction mechanism of Vanadyl-TetraPhenylPorphyrin (VO-TPP) is proposed by Bonné et al. (2). The reactant VO-TPP is reversibly hydrogenated to Vanadyl-TetraPhenyl-Chlorin (VO-TPC), which can be reversibly hydrogenated to Vanadyl-TetraPhenyliso-Bacteriochlorin (VO-TPiB). The last step in the reaction sequence is a lumped ring cleavage step in which VO-TPiB is further hydrogenated and broken into ring fragments. Vanadium is removed and deposited on the catalyst surface. A detailed study on this reaction mechanism is presented in Chapter 7 of this thesis (3, 4). Reaction kinetics of tetraphenylporphyrins over several catalysts can be described by a two-site model, in which hydrogenation and ring cleavage occur on two different sites (2). A Langmuir-Hinshelwood type of kinetics can be applied taking into account competitive adsorption of hydrogen.

Prerequisite for hydrodemetallisation is the diffusion of porphyrins into the catalyst porous texture. Diffusion of these large molecules can be limited by geometric exclusion and hydrodynamic drag. When the solute molecular size becomes comparable with the pore dimensions, a restrictive factor should be introduced to account for the reduced diffusivity (5). Since the catalyst porous texture is changing during hydrodemetallisation, detailed HDM

reaction kinetics may be obscured by diffusion limitations.

A previously proposed state-of-the-art catalyst deactivation model, based on percolation concepts (6, 7), is proposed to tackle the problem of the changing catalyst porous texture.

In present work, a study is performed on metal deposition profiles in a wide-pore silica catalyst using vanadyl-tetraphenylporphyrin (VO-TPP) as model compound. The intrinsic reaction kinetics parameters of the silica based catalyst system are determined in an autoclave reactor. Vanadium deposition profiles in the catalyst pellets are determined as a function of the axial position in a microflow reactor. The effect of a nitrogen containing compound (8), *i.e.* quinoline, and the presence of H<sub>2</sub>S on the vanadium deposition is assessed. An attempt is made to predict the experimentally found vanadium deposition profiles by the catalyst deactivation model based on percolation concepts. Furthermore, the vanadium deposits are localised using High Resolution Electron Microscopy (HREM).

## **2. EXPERIMENTAL AND COMPUTATIONAL TECHNIQUES**

### *2.1. Preparation and characterisation of fresh catalyst*

For the vanadium deposition experiments a molybdenum on silica catalyst is prepared. A molybdenum catalyst is used since it is active for the hydrodemetallisation of VO-TPP and it can be used as a reference component for determining the radial vanadium deposition in catalyst pellets.

The catalyst is prepared by high temperature batch adsorption (HTBA) (9) which ensures an uniform distribution of the active phase in the catalyst pellet. Molybdenyl acetylacetonate (Aldrich, [CH<sub>3</sub>COCH=C(O-)CH<sub>3</sub>]<sub>2</sub>·MoO<sub>2</sub>) was used as precursor, 7.1 g was dissolved in 500 ml toluene (Aldrich, 99.8 %). Approximately 50 g of a wide-pore SiO<sub>2</sub> support material (supplied by Shell Research and Technology Centre, Amsterdam), with pellet diameter of 2.1 mm, was added and the solution was stirred for 4 hours at 380 K. After this adsorption step, the solution was cooled to room temperature and filtered. The impregnated catalyst pellets were dried at 393 K for 100 hours and calcined at 798 K for 4 hours. The characteristics of the prepared catalyst are summarized in Table 1.

**TABLE 1**  
 Characteristics of Mo/SiO<sub>2</sub> catalyst.

	surface area m <sup>2</sup> /g	pore volume cm <sup>3</sup> /g	pore radius nm	Mo loading wt.%
Mo/SiO <sub>2</sub>	52.5 ± 1.3	0.69 ± 0.04	27.0 ± 1.7	1.79 ± 0.23 wt%

The surface area and pore volume are determined with Hg porosimetry. The pore radius is calculated by assuming cylindrical pores. Approximately 25% of the pore volume can be attributed to macro pores.

## 2.2. HDM reaction kinetics in autoclave reactor

The kinetics experiments were carried out with VO-TPP (Rhône Poulenc) and *o*-xylene (Janssen Chimica, p.a. grade) as solvent in a 250 ml batch autoclave. Approximately 80 to 100 mg of catalyst (pellet diameter: 63 -160 μm) was weighed and introduced in the reactor. The catalyst is sulfided *in situ* for two hours with dimethyldisulfide (DMDS, Merck, >99%). DMDS is rapidly converted at elevated temperatures (623 K) in the presence of hydrogen (6.0 MPa). After introduction of VO-TPP dissolved in *o*-xylene (total reaction volume: 125 ml), the reactor was filled to 0.34 MPa with a mixture of 15 mol % H<sub>2</sub>S in H<sub>2</sub>. Next H<sub>2</sub> was added to a total pressure of 4.7 MPa. The reactor was heated to a temperature of 553 K, when the reactor contents reaches this temperature the stirrer is switched on to 2000 rpm.

The HDM reaction was carried out at industrial conditions, 553 K and 9.0 MPa H<sub>2</sub> pressure. At certain time intervals a liquid sample was taken from the autoclave and analysed *ex-situ* with UV/VIS spectroscopy to determine the porphyrin concentrations. Kinetics parameters were obtained by evaluation of concentration-time data according to a two-site Langmuir-Hinshelwood model with competitive adsorption of hydrogen (2). Details on sampling, determination of concentrations and reaction kinetics evaluation are given elsewhere (10).

## 2.3. Vanadium deposition experiments

### 2.3.1. Microflow equipment

The vanadium deposition experiments were performed in a so-called microflow reactor (10). A liquid feed, consisting of VO-TPP dissolved in an isomer mixture of xylene (Boom, 98%),

is mixed with hydrogen and fed into a fixed-bed reactor at approximately 9.0 MPa. The reactor has a length of 35 cm and an internal diameter of 15 mm. Four round trays of 5 mm high were placed in this reactor with the catalyst pellets. The top side of each tray is open and the bottom side consists of a wire gauze. These trays enable the separation of the catalyst pellets during filling and emptying of the reactor and determine the effect of the axial position in the reactor on the vanadium deposition process. At the bottom of the reactor a sieve plate was placed to avoid particles flowing out of the reactor. A detailed view of the filling of the reactor is shown in Figure 1. The catalyst pellets with a diameter of 2.1 mm were too large for microflow applications (11). For this reason the catalyst beds were diluted with fine (0.1 mm) SiC pellets. Glass wool and the SiC on top of the catalyst beds are sufficient to provide a good radial distribution of the liquid in the reactor and complete wetting of the catalyst pellets.

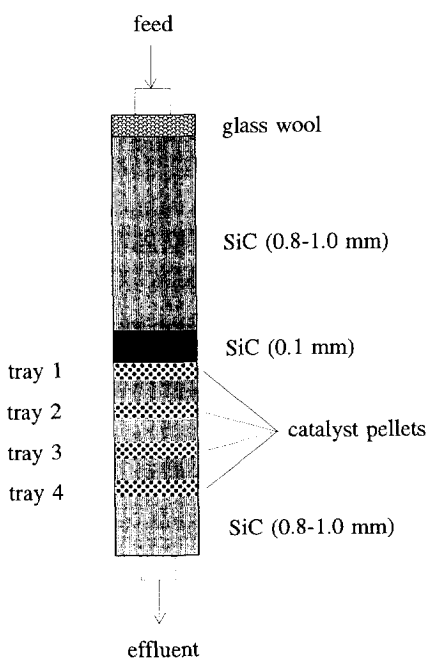


**Figure 1.** Detailed view of the filling of the microflow reactor.

### 2.3.2. Sulfiding of the catalyst

The catalyst was sulfided before starting the vanadium deposition experiment. The sulfiding has been carried out with 3 NI/h 15 mol % H<sub>2</sub>S in H<sub>2</sub> at 623 K for three hours at atmospheric pressure.

### 2.3.3. Reaction conditions

Three different long duration vanadium deposition experiments, I, II and III, have been carried out. Experiment I was a test under reference conditions. Experiment II was carried out to determine the influence of quinoline on the vanadium deposition process. Experiment III was carried out to determine the effect of a low H<sub>2</sub>S partial pressure on the vanadium deposition profiles. Each experiment was split into two parts, A and B. Experiment A is the first part of the vanadium deposition experiment. At the end of experiment A, the reactor was removed from the microflow equipment and catalyst pellets from every tray were collected and analysed. After this short stop, the reactor was mounted again in the microflow equipment, the catalyst sulfided and experiment B started. Again at the end of experiment B, catalyst pellets were collected and analysed. Details on the reaction conditions of the three experiments are summarized in Table 2.

**TABLE 2**  
Reaction conditions applied in catalyst deactivation experiments.

Experiment	I		II		III	
	A	B	A	B	A	B
Duration (h)	350	338	251	294	286	397
Temperature (K)	553	553	553	553	553	553
Pressure (MPa)	9.1	9.1	9.1	9.1	9.0	9.0
Liquid feed rate (ml/h)	12.9	12.9	28.0	28.0	12.3	12.3
Concentration VO-TPP (mol/m <sup>3</sup> )	0.39	0.39	0.39	0.39	0.039	0.039
Concentration DMDS (mol/m <sup>3</sup> )	10.6	10.6	10.6	10.6	1.06	1.06
Feed rate hydrogen (NI/h)	3.8	3.8	4.9	4.9	2.5	2.5
Concentration quinoline (mol/m <sup>3</sup> )	0	0	150	150	0	0



The major differences between experiment I and II are the liquid feed rate and the addition of quinoline. Approximately  $150 \text{ mol}_{\text{quinoline}}/\text{m}^3_{\text{solvent}}$  equivalent to 2000 wt.ppm nitrogen is added to the liquid feed in experiment 2. The liquid feed rate was 12.9 ml/h for experiment I and 28.0 ml/h for experiment II.

Dimethyldisulfide was used for the *in-situ* production of  $\text{H}_2\text{S}$ , which is a reactant in the lumped ring cleavage step of the VO-TPP hydrodemetallisation reaction. As indicated in Table 2, experiment III has a ten times lower concentration DMDS in the feed, which resulted in a lower  $\text{H}_2\text{S}$  partial pressure in the reactor.

The liquid effluent was analysed during the experiments with UV-VIS spectroscopy. The analysis procedure is analogous to the analysis of the batch reactor samples. The concentration of reactant and intermediates is used to monitor the conversion in the reactor.

#### *2.3.4. EPMA analysis*

Electronprobe microanalysis (EPMA, Jeol JXA 733) was used for radial analysis of the fresh and spent catalyst pellets, therefore, the catalyst pellets were halved first. To mount the pellet in the analysis apparatus the sample was bedded in an acrylate polymer. The problem of low conductance of the catalyst material was solved using a layer of gold.

After each vanadium deposition experiment, two pellets from every axial position in the reactor were analysed with EPMA. In thirty points of every pellet, the signals of molybdenum, silicium and vanadium were quantitatively measured in order to determine the radial profile. Together with atomic absorption spectroscopy (AAS), in which the overall weight fraction of vanadium and molybdenum were determined, a quantitative analysis of the radial distribution of metals could be obtained.

#### *2.3.5. High Resolution Electron Microscopy*

Spent catalysts were investigated with a Philips EM 30-ST HREM equipped with EDX for element identification. The spent catalyst samples were transported from the reactor in the solvent via a glove-box to the HREM facilities.

#### *2.4. Computer simulations on vanadium deposition in catalyst pellets*

The model used to describe the metal deposition process during hydrodemetallisation includes a system of nonlinear parabolic partial differential equations (PDEs) in one space variable (6, 7). These equations were solved numerically with a CONVEX 3840 workstation.

Subroutines to solve the set of PDEs are obtained from the NAG Fortran library (1988) (12).

The simulations were performed in using the reaction rate constants obtained from the autoclave experiment. The bulk diffusion coefficients for reactant and intermediates were estimated according to the Wilke-Chang correlation (13). A value of  $3.0 \cdot 10^{-8} \text{ m}^2/\text{s}$  was found, the restrictive factor for hindered diffusion determined by Satterfield (5) was used. The values characterising the porous texture of the catalyst are taken from Table 1. A cubic tessellation was used as percolation model to evaluate the change in catalyst porous texture.

### 3. RESULTS

#### 3.1. Estimation of reaction kinetics parameters of VO-TPP hydrodemetallisation

Figure 2 shows the concentration versus time profiles as obtained from autoclave experiments for VO-TPP hydrodemetallisation over the Mo/SiO<sub>2</sub> catalyst. As can be observed, the concentration of reactant VO-TPP is decreasing, the first intermediate VO-TPC is passing through a maximum and approaching zero. The concentration of the second intermediate VO-TPiB always remains very low. Kinetics parameters were obtained by evaluation of the concentration-time data according to a two-site Langmuir-Hinshelwood model with competitive adsorption of hydrogen (2). In this kinetics analysis, the hydrogenation and dehydrogenation rate constants were not taken as independent variables, but the ratios  $k_1/k_2$  and  $k_3/k_4$ , *i.e.* the equilibrium constants  $K_{12}$  and  $K_{34}$ , were kept constant. Table 3 summarizes the values of the parameters of the reaction kinetics test,  $k_1$  (first hydrogenation),  $k_3$  (second hydrogenation), and  $k_5$  (lumped ring cleavage) normalized on the total catalyst surface area. The solid line in Figure 2 represents the fitted concentrations according to the reaction kinetics model.

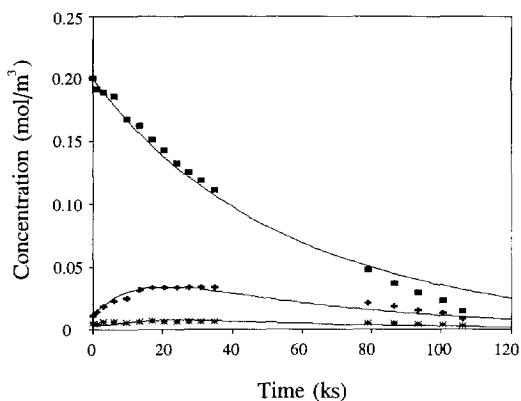


**Figure 2.** Concentration-time profiles for VO-TPP HDM over a Mo/SiO<sub>2</sub> catalyst.

(■: VO-TPP, +: VO-TPC; \*: VO-TpIB; — : fit according to two-site model (2))

**TABLE 3**

Values for the VO-TPP hydrodemetallisation reaction rate constants.

	$k_1$ $\text{m}^3/\text{m}^2_{\text{cat}} \cdot \text{s}$	$k_3$ $\text{m}^3/\text{m}^2_{\text{cat}} \cdot \text{s}$	$k_5$ $\text{m}^6/\text{m}^2_{\text{cat}} \cdot \text{mol} \cdot \text{s}$
Reaction rate constants	$(1.7 \pm 0.1) \cdot 10^{-8}$	$(6.6 \pm 1.1) \cdot 10^{-8}$	$(4.6 \pm 2.4) \cdot 10^{-7}$

The hydrogen adsorption coefficient  $K_H$  equals  $(7.5 \pm 6.2) \cdot 10^{-5} \text{ m}^3/\text{mol}$ .

### 3.2. Vanadium deposition experiments

This section is divided into the three deactivation experiments I (reference), II (addition of quinoline) and III (low H<sub>2</sub>S partial pressure). Quantitative vanadium deposition profiles in catalyst pellets are presented as a function of the axial position in the reactor.

#### *Experiment I A and B*

Figure 3 shows the vanadium deposition profiles in the Mo/SiO<sub>2</sub> catalyst pellets as a function of the axial position in the reactor for experiments I A and B. As can be observed, for all pellets the vanadium deposition maximum is observed at the centre of the pellet. An increasing amount of deposited vanadium, as determined with AAS, is found in axial direction in the reactor.

#### *Experiment II A and B*

Figure 4 shows the vanadium deposition profiles as a function of the axial position in the reactor for experiments II A and B. As can be observed much lower amounts of vanadium are deposited on the catalyst pellets. Similar to experiments I A and B, deposition maxima are observed in the centre of the pellet.

#### *Experiment III A and B*

Figure 5 shows the vanadium deposition profiles as a function of the axial position in the reactor for experiments III A and B. In this experiment, similar reaction conditions were applied as in experiments I A and B, except a lower H<sub>2</sub>S partial pressure and a lower feed concentration VO-TPP was added. A shift in the shape of the vanadium deposition profile is observed in axial direction in the reactor. The first two trays show, similar to experiment I and II, a vanadium deposition maximum in the centre of the pellet. Tray 3 and 4 show a deposition maximum in the outer shell of the pellet and very little vanadium deposition in the centre. Again the deposited amount of vanadium are low as compared to experiment I.

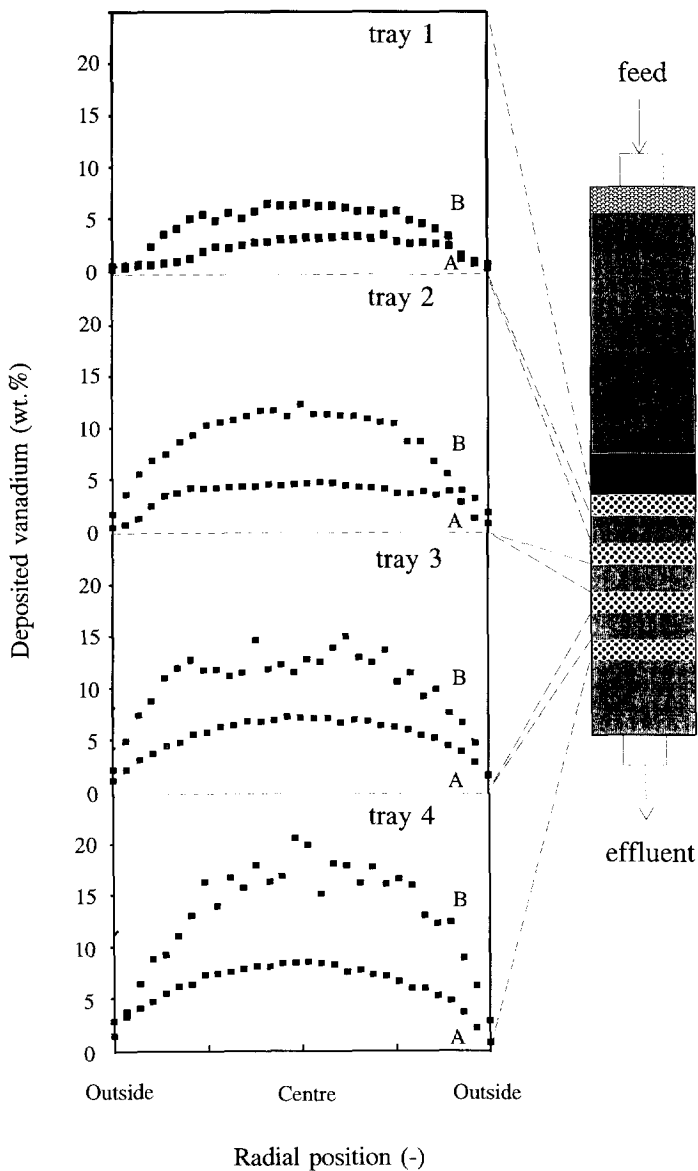


**Figure 3.** Vanadium deposition profiles in Mo/SiO<sub>2</sub> catalyst pellet as a function of the axial position for the reference experiment I A and B.

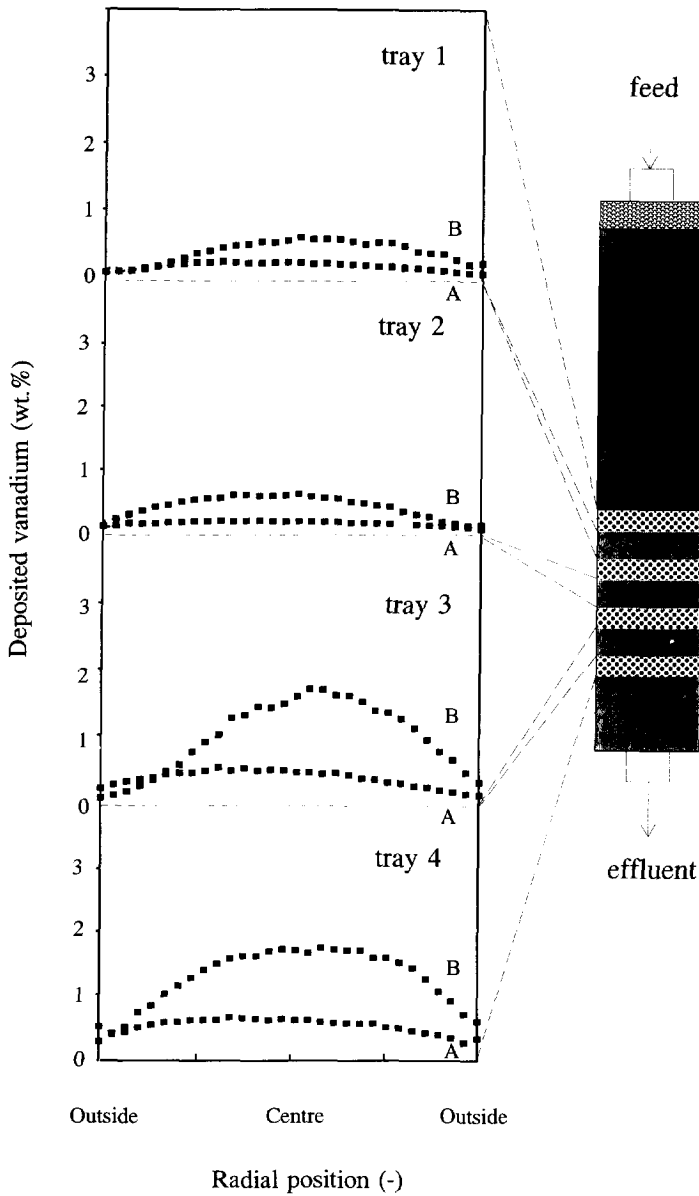


**Figure 4.** Vanadium deposition profiles in Mo/SiO<sub>2</sub> catalyst pellet as a function of the axial position for experiment II A and B with quinoline addition.

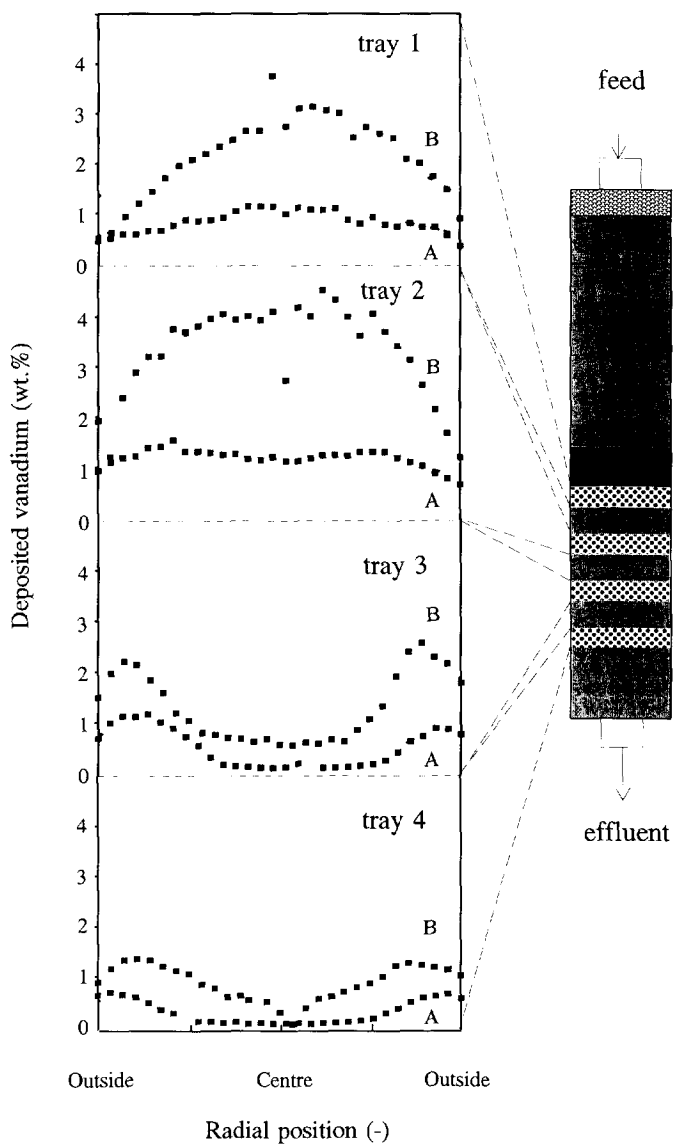


**Figure 5.** Vanadium deposition profiles in Mo/SiO<sub>2</sub> catalyst pellet as a function of the axial position for experiment III A and B with low H<sub>2</sub>S partial pressure.

UV-VIS analysis of the effluent liquid showed no significant change in conversion level of reactant and intermediates during experiment I, II and III.

### 3.3. Localisation of vanadium deposits on Mo/SiO<sub>2</sub> catalyst

Two different morphologies of vanadium deposits on the Mo/SiO<sub>2</sub> catalyst could be identified with HREM and EDX;

- i) a phase non-visible for HREM, but present according to EDX,
- ii) a crystalline phase, a layered structure of vanadium sulfide.

Figure 6 shows an image of the spent Mo/SiO<sub>2</sub> catalyst with the layered structure of vanadium sulfide. According to EDX, vanadium sulfide is present on silica. Molybdenum could only be identified in very small traces. The copper peaks in the EDX spectrum are due to the grid which supports in catalyst powder in the microscope.

HREM/EDX analysis at several positions on the spent catalyst showed that vanadium was present as isolated clusters on the bare support and in the surroundings of the active phase.

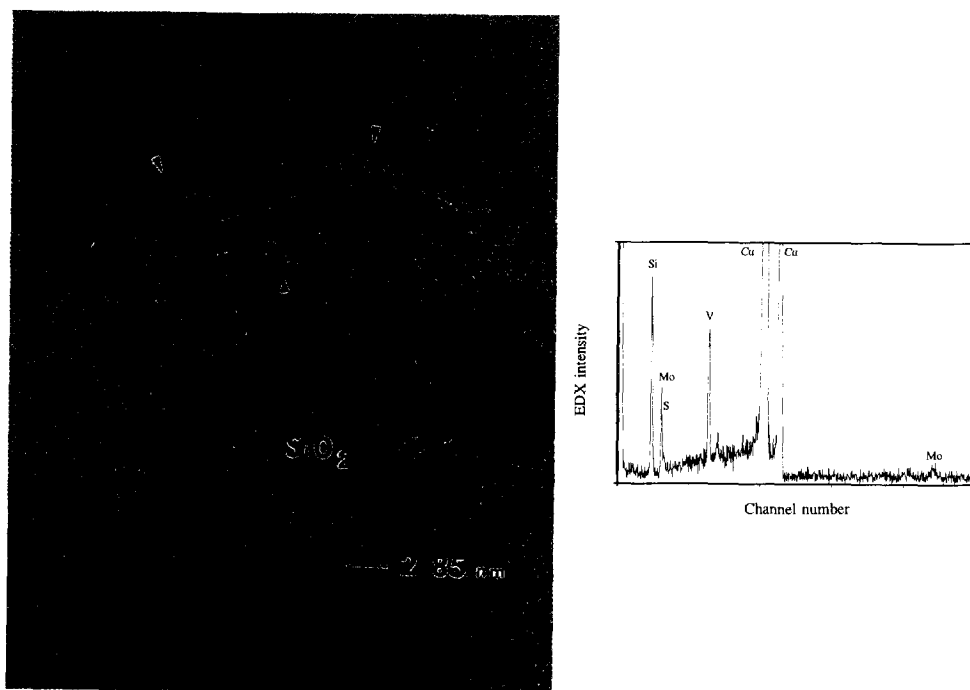


**Figure 6.** HREM image and EDX spectrum of spent catalyst.



#### 4. DISCUSSION

Vanadium deposition profiles in catalyst pellets have been determined by various researchers (14-30). For this purpose porphyrinic model compounds and industrial feedstocks are used. The used catalysts are mainly conventional hydrotreating catalysts with narrow pores. Therefore, metal deposition profiles show mainly deposition in the outer shells of the catalyst pellets (M- or U-shaped profiles), indicating that the metal deposition process is diffusion limited.

Present work shows the vanadium deposition process on a low molybdenum loaded silica catalyst with wide pores. Our results show, for the reference experiment I A and B, maximum vanadium deposition in the centre of the pellet. The diffusion rate of the reactant and intermediates into the catalyst pellet is high enough to reach the centre. The deposition maximum in the centre of the pellet can be explained by the sequential reaction mechanism of VO-TPP hydrometallisation. At the outside of the pellet the concentration of reactant VO-TPP is high, however in the first tray almost no intermediates are present. VO-TPP has to diffuse in the pellet, gradually forming the intermediates VO-TPC and VO-TPiB and finally vanadium is deposited on the catalyst surface. In the subsequent trays in axial direction in the reactor, intermediates are present at the outside of the pellet due to hydrogenation of the reactant and diffusion out of the catalyst pellet. The build-up of the last intermediate causes a higher rate in the vanadium deposition (proportional to the concentration) and therefore higher amounts of vanadium are found in the subsequent trays.

The results of experiment II A and B show an identical course in the vanadium deposition profiles as the reference experiment I. The amounts of vanadium deposited are of course lower which is due to the competitive adsorption of quinoline and the higher liquid feed rate. The decrease in the rate of metal removal caused by quinoline addition was already found in previous work (8).

Experiment III A and B, which were carried out under a low  $H_2S$  partial pressure and a lower feed concentration of VO-TPP showed a remarkable shift in the vanadium deposition profiles as a function of the axial position in the reactor. In the first two trays a similar vanadium deposition profile is found as in the reference experiment I. However, the shift towards M-shaped deposition profiles in tray 3 and 4 indicate a diffusion limited metal deposition process. This shift is due to the low  $H_2S$  partial pressure which causes a build-up in the concentration of the last intermediate VO-TPiB. Apparently, in the last two trays the concentration of VO-TPiB becomes so high, that the metal deposition rate overrules the diffusion rate into the catalyst pellet which causes metal deposition in the outer shell.

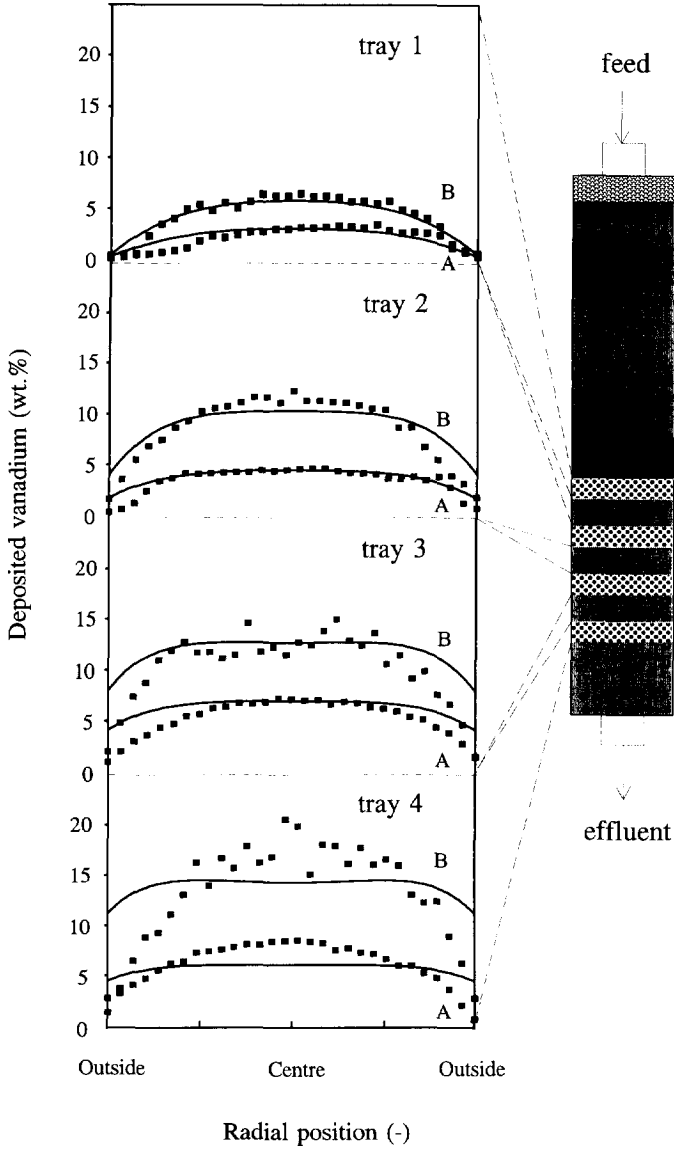


**Figure 7.** Comparison between experiment I A and B and model simulations (the solid lines represent the model simulations).

An attempt is made to model the experimental vanadium deposition profiles of the three experiments. Figure 7 shows the experimental and simulated vanadium deposition profiles as a function of the axial position in the reactor for experiment I A and B. As can be observed identically shaped vanadium deposition profiles are obtained for both experiment and simulation. However, an increasing discrepancy is observed as a function of the axial position in the reactor. Similar results are obtained for the comparison between experiment II and III and simulations, as shown in Figure 8 and 9. These discrepancies are probably caused by inaccuracies of the input parameters in the model, such as the boundary concentrations of reactant and intermediates in the subsequent trays (*i.e.* the plug flow reactor model) and variation in reaction rate constants (*i.e.* the reaction kinetics). As can be observed from Figure 2, there appears to be a relation between the deposited amount of vanadium and the reaction rates in the kinetic analysis. The reaction rates are increasing with increasing vanadium deposited. This vanadium loading dependence could justify the increasing discrepancy between the simulated and experimental vanadium deposition profiles in axial direction in the reactor.

Vanadium deposits showed to have two different morphologies, *i.e.* disperse and crystalline. Crystalline vanadium could be present as layered structures (similar as  $\text{MoS}_2$ ) and are therefore difficult to identify. The location of vanadium is either in the surrounding of the active phase or as isolated clusters on the support material.

Vanadium deposits in the surroundings of the active phase cause *active site poisoning* due to the coverage of the active phase and or the edges. *Active site generation* occurs by the formation of isolated vanadium phase on the support material which has a catalytic activity for hydrometallisation. Both phenomena could explain the UV-VIS results of the liquid effluent. Apparently the nett effect is zero catalyst deactivation up to 9 wt.% vanadium deposition.

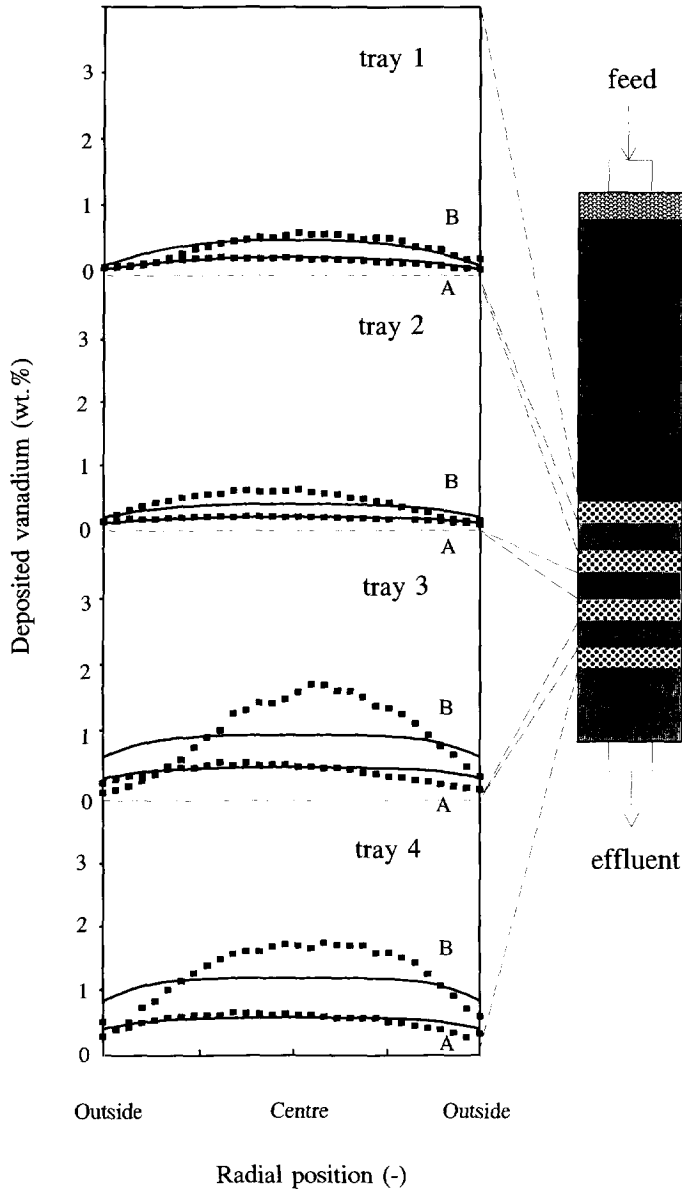


**Figure 8.** Comparison between experiment II A and B and model simulations (the solid lines represent the model simulations).

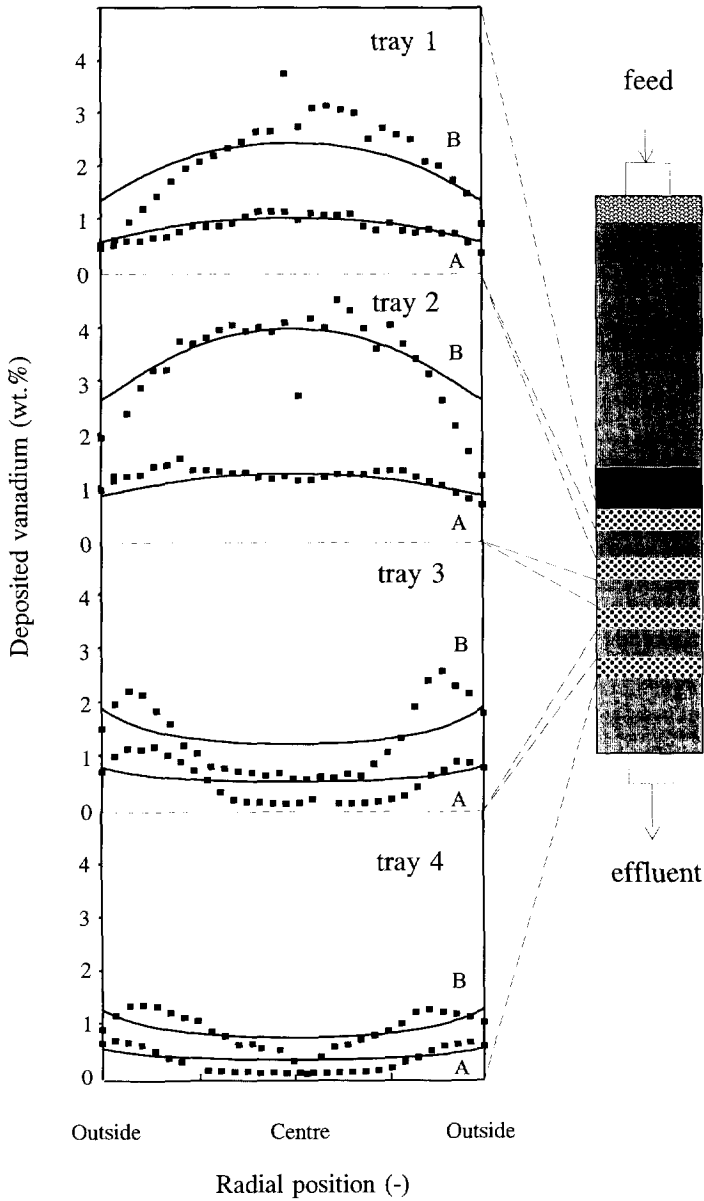


**Figure 9.** Comparison between experiment III A and B and model simulations (the solid lines represent the model simulations).

## 5. CONCLUSIONS

Present work details on a study on the metal deposition process during hydrodemetallisation of vanadyl-tetraphenylporphyrin on wide pore molybdenum on silica catalyst. The effect of quinoline and a low  $H_2S$  partial pressure on the vanadium deposition profiles in catalyst pellets are determined in comparison with a reference experiment.

The vanadium deposition process showed profiles with deposition maxima in the centre of the pellet indicating the absence of diffusion limitations and supporting a sequential reaction mechanism for VO-TPP HDM. Quinoline addition showed to have a decreasing effect on the rate of metal removal and showed similar shaped deposition profiles. The low  $H_2S$  partial pressure caused a change of the vanadium deposition profiles into M-shaped profiles due to the build-up of the last intermediate and an increasing metal deposition rate.

Simulations of the vanadium deposition process based on intrinsic kinetic data and percolation theory showed reasonable agreement, at least at reactor inlet conditions. However, improvements should be made since increasing discrepancies are observed in axial direction in the reactor. The accuracy of the input parameters of the proposed model, such as the boundary concentrations of the reactant and intermediates at the downstream catalyst pellets, should be improved.

The location of vanadium deposits are both in the surrounding of the active phase, causing active site poisoning, and as isolated vanadium sulfide clusters, causing active site generation. In our vanadium deposition experiments (up to 9 wt.% vanadium) no significant catalyst deactivation occurred, indicating that both effects are compensating each other.

## ACKNOWLEDGMENTS

Dr. P. Kooyman, Dr. H. Zandbergen, P. Colijn and E. Fakkeldij of the Materials Science Department of Delft University of Technology are gratefully acknowledged for carrying out the HREM and EPMA measurements. The European Community (contract number JOUF 0049) and Shell Research and Technology Centre, Amsterdam (SRTCA) are thanked for the financial support.

## REFERENCES

1. Sie, S.T., in 'Catalyst deactivation', Delmon, B. and Froment, G.F. (Eds.), Elsevier Scientific Publishing Company, Amsterdam (1980) 545.
2. Bonn , R.L.C., Steenderen, P. van, and Moulijn, J.A., *Bull. Soc. Chim. Belg.*, **100** (11-12) (1992) 877.
3. Chapter 7 of this thesis.
4. Janssens, J.P., Elst, G., Schrikkema, E.G., Langeveld, A.D. van, Sie, S.T. and Moulijn, J.A., accepted for publication in *Recueil*.
5. Satterfield, C.N., Colton, C.K., and Pitcher, W.H., *AIChE J.*, **19** (3) (1973) 628.
6. Chapter 5 of this thesis.
7. Janssens, J.P., Langeveld, A.D. van, Sie, S.T., and Moulijn, J.A., *ACS Symposium Series*, **634**, O'Connor, P., Takatsuka, T., and Woolery, G.L. (Eds.), June 1996.
8. Chapter 4 of this thesis, submitted for publication in *FUEL*.
9. Bosch, H., Ph.D thesis Twente University of Technology (1987).
10. Chapter 2 of this thesis.
11. Sie, S.T., *Rev. Inst. Fr. P trol.*, **46** (4) (1991) 501.
12. NAG Fortran library (1988).
13. Tsai, C.H., Massoth, F.E., Lee, S.Y., and Seader, J.D., *Ind. Eng. Chem. Res.*, **30** (1991) 22.
14. Sato, M., Takayama, N., Kurita, S., and Kwan, T., *Nippon Kagaku Zasshi*, **92** (1971) 834.
15. Oxenreiter, M.F., Frye, C.G., Hoekstra, G.B., and Sroka, J.M., *Jpn. Petrol. Inst.*, Nov. (1972) 30.
16. Dautzenberg, F.M., Klinken, J. van, Pronk, K.M.A., Sie, S.T., and Wijffels, J-B, *ACS Symp. Ser.*, **65** (1978) 254.
17. Tamm, P.W., Harnsberger, H.F., and Bridge, A.G., *Ind. Eng. Chem. Process Des. Dev.*, **20** (2) (1981) 262.
18. Galiasso, R., Blanco, R., Gonzalez, C., and Quinteros, N., *FUEL*, **62** (1983) 817.
19. Pazos, J.M., Gonzalez, J.C., and Salazar-Guillen, A.J., *Ind. Eng. Chem. Process Des. Dev.*, **22** (1983) 653.
20. Agrawal, R., and Wei, J., *Ind. Eng. Chem. Process Des. Dev.*, **23** (1984) 505, 515.
21. Takeuchi, C., Asaoka, S., Nakata, S., and Shiroto, Y., *Prepr. ACS Div. Petrol. Chem.*, **30** (1985) 96.
22. Ware, R.A., and Wei, J., *J. Catal.*, **93** (1985) 122, 135.
23. Khang, S-J, and Mosby, J.F., *Ind. Eng. Chem. Process Des. Dev.*, **25** (2) (1986) 437.
24. Aldag, A.W., *Prepr. ACS Div. Petrol. Chem.*, Denver Meeting, (1987) 443.
25. Sie, S.T., *I<sup>2</sup>-Procestechologie*, **5** (1987) 37.
26. Pereira, C.J., Beeckman, J.W., Cheng, W-C, and Suarez, W., *Ind. Eng. Chem. Res.*, **29** (1990) 520.
27. Toulhoat, H., Szymanski, R., and Plumail, J.C., *Cat. Tod.*, **7** (1990) 531.
28. Simpson, H.D., in 'Catalyst deactivation', Bartholomew, C.H. and Butt, J.B. (Eds.), Elsevier

## Chapter 6

Science Publishers, Amsterdam (1991) 265.

29. Hubaut, R., Dejonghe, S., Grimblot, J., and Bonnelle, J.P., *React. Kinet. Catal. Lett.*, **51** (1) (1993) 9.
30. Fozard, P.R., McMillan, J.W., and Zeuthen, P., *J. Catal.*, **152** (1995) 103.



# Chapter 7

## Development of a Mechanistic Picture of the Hydrodemetallisation Reaction of Metallo-Tetraphenylporphyrin on a Molecular Level

### ABSTRACT

---

Heavy oil residua contain a large amount of hetero-atoms, such as sulfur, nitrogen, oxygen and metals. A significant proportion of the metal compounds in heavy oil residua is complexed in porphyrins. The use of porphyrinic model compounds in reaction kinetics research eliminates many of the complicated and competing reactions encountered with heavy oil residua, thus enabling a clearer picture of the reactions to be ascertained. A detailed knowledge of the reaction mechanism of porphyrinic compounds is necessary and the present research is focused on the hydrodemetallisation (HDM) reaction mechanism of vanadyl- and nickel-tetraphenylporphyrins (VO-TPP and Ni-TPP), chosen as model compounds for the metallo-porphyrin (-like) fraction in heavy oil residua.

Goal of this study was to validate and to extend the present known reaction mechanism for the hydrodemetallisation of metallo-tetraphenylporphyrin (M-TPP). Based on molecular modelling calculations and GC-MS analysis new reaction intermediates could be identified and an extended reaction mechanism for the HDM of M-TPP is proposed.

The mechanism proceeds via three hydrogenation steps on  $\beta$ -pyrrole positions of the porphyrinic structure to a meso-bridge hydrogenated structure. After an acid attack, ring opening and a possible elimination of a tolyl group, the final product before metal removal is an open chain molecule. Metal removal and further conversion leads to mono-pyrrole containing molecules and metal deposition on the catalyst surface.

---

## 1. INTRODUCTION

Heavy oil residua contain organically bound metals, primarily vanadium and nickel. Depending on the origin of the oil, the concentrations range from 1 wt.ppm (Sumatran Light, Indonesia) to 1553 wt.ppm (Boscan, Venezuela) for vanadium and from 6 wt.ppm (Arabian Light, Saudi Arabia) to 156 wt.ppm (Beta, California USA) for nickel. The organo-metal compounds are found in heavy oil residua in the form of relatively small petroporphyrins and as large asphaltene-like structures (1). Removal of metals by hydrotreating is called hydrodemetallisation (HDM) which prevents fast catalyst deactivation of downstream catalysts (hydrocracking-, hydrodesulfurisation-, fluid catalytic cracking catalysts) by active site poisoning and pore plugging (2). Typical process conditions for the HDM process are temperatures between 623 K and 673 K and hydrogen pressures between 10 MPa and 15 MPa.

Porphyrins always exist in residual oil as metallo-porphyrins. Metallo-porphyrins are reported to account for as much as 5-70 % of the metal compounds in crude oils, the remaining part are non-porphyrins. Of the total vanadium and nickel content, 6-34 wt% is complexed in porphyrins (1). Vanadium has been shown to appear exclusively in the vanadyl state ( $V=O^{2+}$ , vanadium present as  $V^{4+}$ ) whereas nickel is found to appear as  $Ni^{2+}$  in porphyrins. Typical porphyrins found in petroleum are the  $Ni^{2+}$  and  $VO^{2+}$  forms of etioporphyrins (Etio) and deoxophylloerythroetioporphyrins (DPEP) series (Figure 1 a and b).

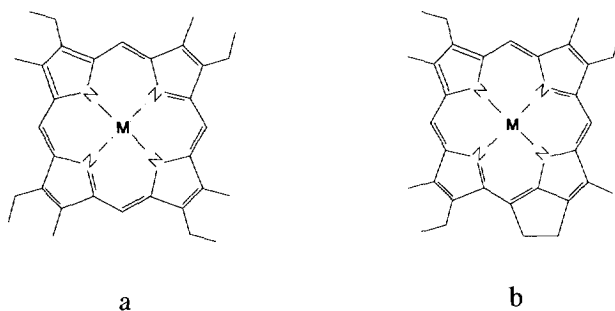


**Figure 1.** Typical porphyrines occurring in crude oil, a- metallo-etio porphyrin (M-Etio) and b- metallo-deoxophylloerythroetioporphyrin (M-DPEP).

Because of the high content of metallo-porphyrins in residual oil, porphyrins are used as model compounds for research on reaction mechanism and kinetics. Especially metallo-tetraphenylporphyrins (Figure 2 a and b), although not naturally occurring in oil residua, are favourite because of the strong aromatic character of the tetraphenylporphyrin which gives the metal ion a similar surrounding as in the structure of asphaltenes.

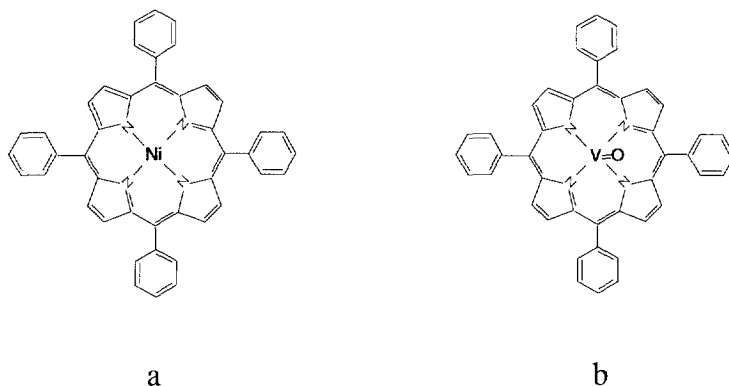


**Figure 2.** Metallo-porphyrins used in this study, a- nickel-tetraphenylporphyrin (Ni-TPP) and b- vanadyl-tetraphenylporphyrin (VO-TPP).

Metallo-tetraphenylporphyrin (M-TPP) reacts via a sequential mechanism, which is depicted in Figure 3. M-TPP is reversibly hydrogenated to metallo-tetraphenylchlorin (M-TPC), which is subsequently reversibly hydrogenated to metallo-tetraphenylisobacteriochlorin (M-TPiB). M-TPiB is assumed to react via a series of hydrogenation and hydrogenolysis reactions, resulting in fragmentation of the porphyrin macrocycle and deposition of the metal on the catalyst surface. This last reaction step is called the lumped ring cleavage step.

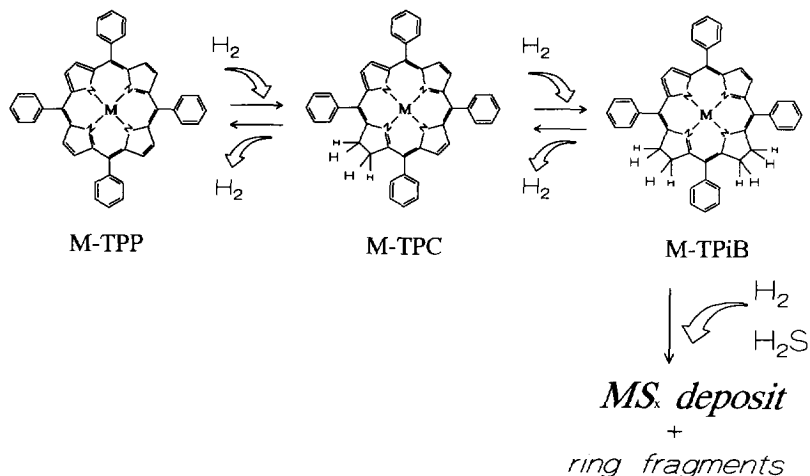


**Figure 3.** Reaction mechanism of metallo-tetraphenylporphyrin (M-TPP) with lumped ring cleavage step.

It is of interest to clarify the elementary reaction steps in this ring cleavage step of the reaction mechanism, which can give information on the position of ring opening and the chemical structures of the molecules before metal removal. Clarification of the reaction mechanism is a necessity from catalyst design and development point of view and can be a tool for determining the correct reaction kinetics model. Present work describes research on the reaction mechanism of metallo-tetraphenylporphyrin on a molecular level. Molecular modelling is used to calculate the geometry and heat of formation of new reaction intermediates. Gas Chromatography-Mass Spectrometry (GC-MS) is applied for providing information about the formed products after demetallisation.

## 2. EXPERIMENTAL AND COMPUTATIONAL TECHNIQUES

### 2.1. Catalyst

Table 1 summarizes the properties of the used catalyst. A V/ $\gamma$ -Al<sub>2</sub>O<sub>3</sub> catalyst was prepared by multi-step wet impregnation. Details on preparation are given elsewhere (3). This catalyst was used since vanadium is the most abundant metal in oil residua and deposits on the internal catalyst surface during hydrodemetallisation.

**TABLE 1**  
Properties of catalyst used in present work.

Catalyst	Active phase loading (wt.% V)	Surface area (m <sup>2</sup> /g)	Pore volume (cm <sup>3</sup> /g)
V/ $\gamma$ -Al <sub>2</sub> O <sub>3</sub>	3.4	180	0.73

surface area and pore volume determined with N<sub>2</sub> adsorption.

### 2.2. Batch autoclave experiments

The batch autoclave experiments were carried out with the reactant tetraphenylporphyrin in *o*-xylene as solvent in 250 ml reactor. The catalyst was introduced in the reactor and *in-situ* sulfided with dimethyldisulfide (DMDS) at 623 K and 6.0 MPa hydrogen pressure for 3 hours. After the introduction of tetraphenylporphyrin dissolved in *o*-xylene (total reaction volume: 125 ml), the reactor was filled to 0.4 MPa with a mixture of 15 mol% H<sub>2</sub>S in H<sub>2</sub>, next H<sub>2</sub> was added to a total pressure of 5.0 MPa. The reactor was heated to a temperature of 578 K; at this point the stirrer was switched on and the liquid sampling started.

### 2.3. Gas Chromatography-Mass Spectrometry

Analyses of the reaction products is possible with the use of the combined technique GC-MS. Unfortunately, the experiments could not be performed with Ni-TPP or VO-TPP due to the poisoning of the available GC-column by nickel or vanadium deposits. Instead of a M-

TPP the free base form, H<sub>2</sub>-TPP, was used. The hydrogenation and hydrogenolysis reactions of the free base form are believed to occur according to a similar pathway as the metallo-porphyrins. Direct metal abstraction is not occurring during HDM of M-TPP.

Two batch autoclave experiments were performed with a sulfided V/ $\gamma$ -Al<sub>2</sub>O<sub>3</sub> catalyst, one with H<sub>2</sub>-TPP and one without H<sub>2</sub>-TPP (blank test). Three samples were analysed with GC-MS; one taken in the beginning, one in the middle and one after completion of the experiment. A quadrupole mass spectrometer with electron impact (EI) as ionisation method was used. The chromatograph is equipped with a 6 meter CP-Sil-5 column.

#### 2.4. Molecular Modelling

Molecular modelling calculations were performed with BioSym software on a Silicon Graphics workstation with 32 MB internal memory and a 4 Gigabyte harddisc. Semi-empirical methods were used in the molecular modelling calculations which are combined in MOPAC (Molecular Orbital PACKage) of BioSym (4). The Modified Neglect of Diatomic Overlap (MNDO) semi-empirical methods were used to optimize molecular structures.

Molecular optimizations were performed for all compounds mentioned. Besides the structures already known in literature, a few new possible intermediates were proposed and optimized. Unfortunately, parameters for both metals, Ni<sup>2+</sup> and VO<sup>2+</sup>, are not available in the MOPAC program. Therefore another chemically and physically corresponding metal ion has been used. Based on charge, metal coordination and ion radius, Zn<sup>2+</sup> showed to be the best alternative (5). Optimizing the molecular structures of the HDM model compounds and their reaction intermediates on hydrogenation provides the following information about the molecules and the reaction path: heats of formation and reaction (298 K, 1 atm.), (inter)-molecular distances and the molecular 3D-geometry.

The resulting geometrical structures of the intermediates in the HDM reaction mechanism of M-TPP are displayed in two manners:

- i*) a stick image, which is an image of the geometry of the porphyrin macrocycle (the phenyl groups have been omitted for clarity);
- ii*) an image, in which the type of bonds ( $\sigma$ - or  $\pi$ -) between the different atoms in the molecule are displayed.

### 3. RESULTS

#### 3.1. Analyses of the ring fragments with GC-MS

The products of the ring cleavage of the free base porphyrin H<sub>2</sub>-TPP and the blank test are summarised in Table 2. The GC-MS analyses of different samples at various reaction times gave identical spectra.

**TABLE 2**  
Reaction products of the ring cleavage of H<sub>2</sub>-TPP.

experiment	molecule peak (g/mol)	fragment peak intensity order (g/mol)
H <sub>2</sub> -TPP	247	156, 247, 170, 91
H <sub>2</sub> -TPP	157	157, 80, 91, 128
H <sub>2</sub> -TPP and blank test	210	105, 210, 77, 91
H <sub>2</sub> -TPP and blank test	224	106, 119, 224, 91

With the results presented in Table 2 it is clear that only the spectra of the molecules with molecular masses 247 (g/mol) and 157 (g/mol) are of interest. The other two found products with the molecular masses 224 (g/mol) and 210 (g/mol) were also present in the blank experiment and are most likely formed out of the solvent *o*-xylene or are a pollution in this solvent.

The structures found for the ring fragments with molecular mass 247 (g/mol) are depicted in Figure 4. The molecules consist of two phenyl groups bonded via methine bridges to a pyrrole group. Discrimination between these components is unfortunately not possible with GC-MS. The structures found for the ring fragments with molecular mass 157 (g/mol) have one phenyl group linked to a pyrrole ring via a methine bridge (Figure 5).

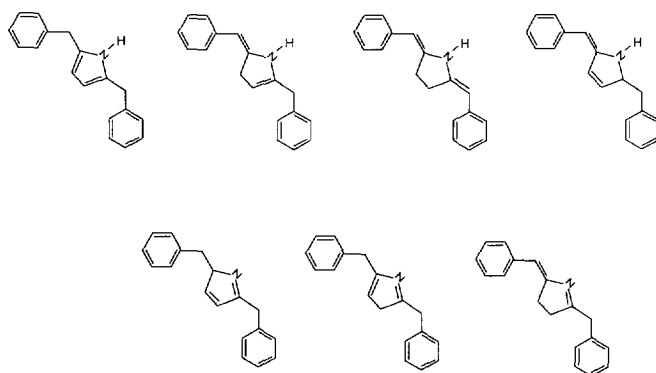


**Figure 4.** Reaction products of ring cleavage of  $H_2$ -TPP with molecular mass 247 g/mol.

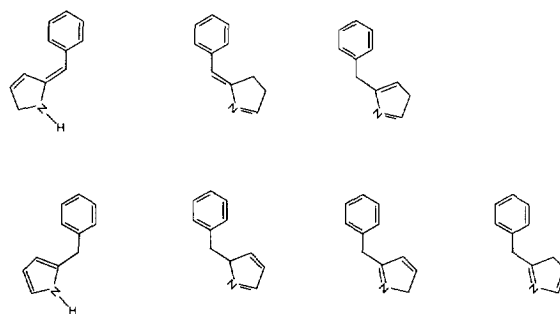


**Figure 5.** Reaction products of ring cleavage of  $H_2$ -TPP with molecular mass 157 g/mol.

### 3.2. Molecular modelling of reactant and intermediates

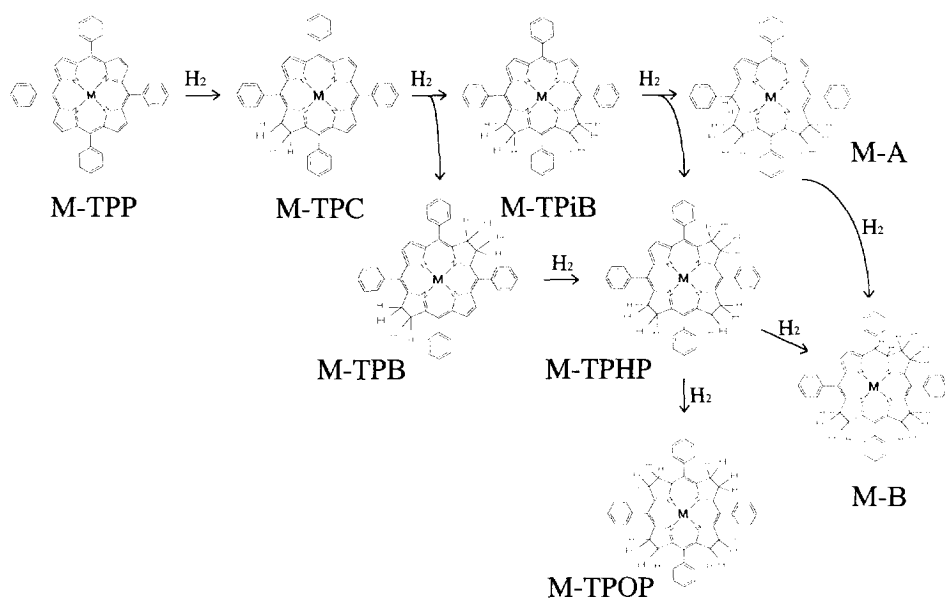
The investigated intermediates formed by subsequent hydrogenation reactions of M-TPP preceding the ring cleavage are given in Figure 6. The reactant M-TPP can first be hydrogenated to M-TPC (chlorin or dihydroporphyrin) on one of the  $\beta$ -pyrrole positions. M-



TPC can be hydrogenated into two possible intermediates, M-TPiB (isobacteriochlorin or tetrahydroporphyrin) and M-TPB (bacteriochlorin or tetrahydroporphyrin). M-TPiB is hydrogenated on two opposite  $\beta$ -pyrrole positions, whereas TPB is hydrogenated at two adjacent positions.

M-TPiB and M-TPB can both be hydrogenated to M-TPHP (hexahydroporphyrin) (6). The other possibility is the formation of M-A, which is hydrogenated on a meso bridge position. M-TPHP can be hydrogenated to two intermediates, M-TPOP (octahydroporphyrin) hydrogenated on the fourth  $\beta$ -pyrrole position and M-B hydrogenated on a meso bridge position. M-B can also be formed out of M-A by hydrogenation on a  $\beta$ -pyrrole position.

The optimized structures of the above mentioned compounds have been evaluated using MOPAC and are given Figure 7. Heat of formation, intermolecular distances and molecular diameter are given in Table 3.

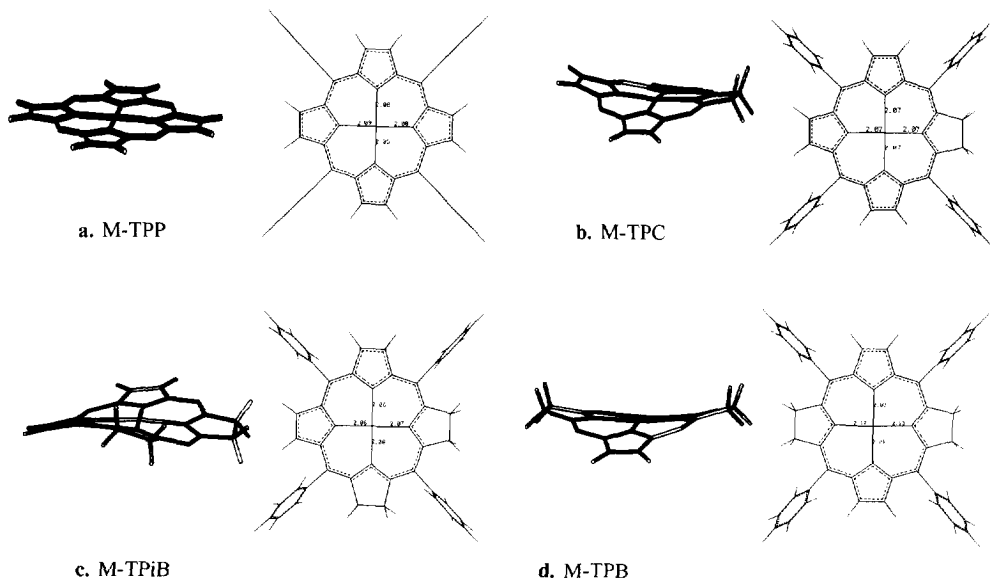


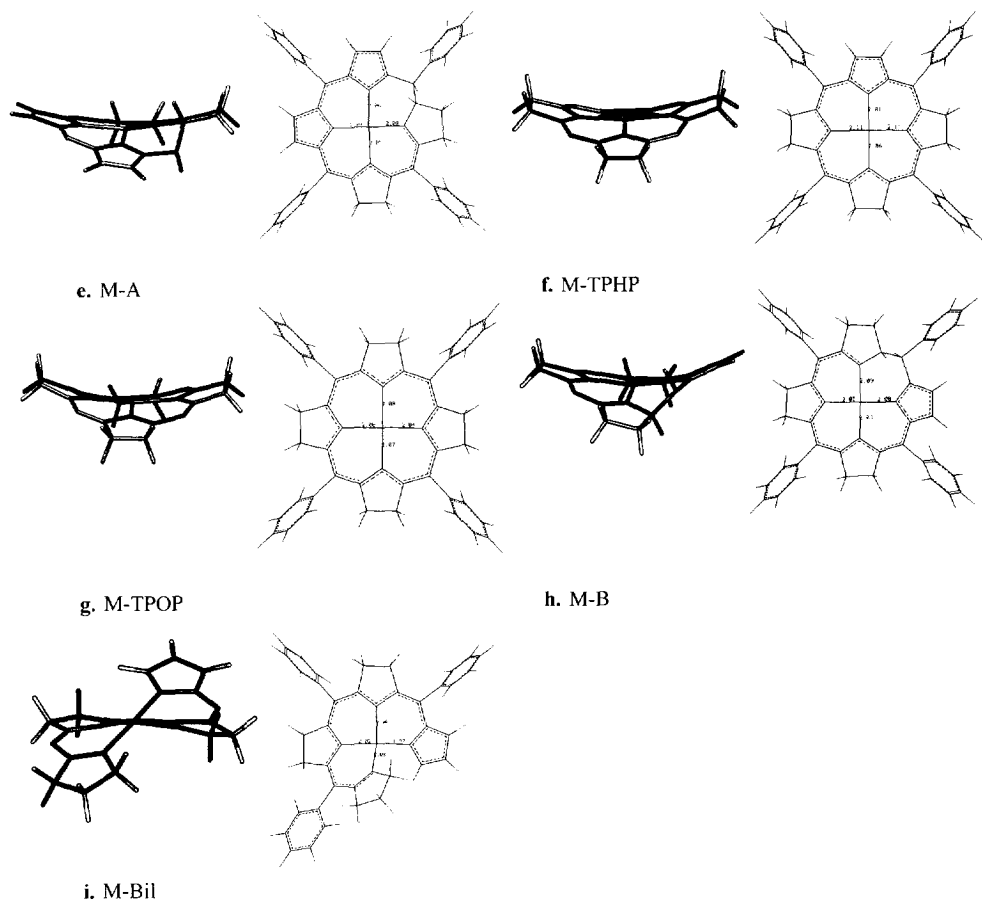
**Figure 6.** Intermediates in the hydrodemetallisation of metallo-tetraphenylporphyrin.

TABLE 3

Heat of formation, intermolecular distances and molecule diameter of reactant and intermediates.

	(M-N) <sub>average</sub> (nm)	D <sub>max</sub> (nm)	ΔH <sub>f</sub> (298 K, 1 atm) (kJ/mol)
M-TPP	0.208	1.784	- 1311.45
M-TPC	0.207	1.780	- 1188.32
M-TPiB	0.207	1.745	- 1072.67
M-TPB	0.207	1.778	- 1097.17
M-TPHP	0.208	1.777	- 971.73
M-A	0.206	1.774	- 1042.02
M-TPOP	0.207	1.773	- 936.29
M-B	0.205	1.770	- 937.65
M-Bil	0.203	1.728	- 761.99





**Figure 7.** Optimized structures of reactant and the intermediates of Figure 6.  
 (left: 'stick' image of porphyrin macrocycle; right:  $\sigma$ - (—) and  $\pi$ - (- -) bonds of intermediates)

## 4. DISCUSSION

Different reaction mechanisms have been proposed in recent years both for thermal and catalytic hydrodemetallisation of tetraphenylporphyrins (6, 7, 8, 9). Based on the previous work and molecular modelling results of the proposed reaction intermediates (see Figure 6) combined with the GC-MS results an extended reaction mechanism is proposed.

### 4.1. Molecular modelling of reactants and intermediates in HDM reaction mechanism of M-TPP

#### 4.1.1. First hydrogenation step: formation of M-TPC out of M-TPP

The optimized structure of M-TPP (tetraphenylporphyrin) and M-TPC (tetraphenylchlorin) is depicted in Figure 7 a and b respectively. The porphyrin macrocycle in M-TPP is flat with the phenyl groups perpendicular bonded to it. The maximum diameter of the M-TPP molecule is 1.784 nm (Table 3). This planar structure is the result of the strong  $\pi$ -electron interaction over the entire macrocycle and of the particular favourable structure of the coordination centre, consisting of the four nitrogen atoms and the metal ion (10). A bent structure would decrease the overlap of the  $\pi$ -orbitals of the different atoms in the delocalised pathway and thus lower the stability of the molecule. The phenyl groups are positioned perpendicular towards the macrocycle to minimize the sterical hindrance.

The molecular modelling results shown in Table 3 for M-TPP are in fair agreement with literature. The flat structure of the macroring is also reported by Scheidt (11). The calculated average M-N distance is 0.208 nm. The value for the metal-nitrogen distance is in good agreement with the values reported in literature. Scheidt (12) reports a distance of 0.2036 nm. In contrast with the calculations, Buchler (13) reports that the zinc ion is a little too large to fit in the hole of the macrocycle and is located 0.019 nm outside the plane of the macrocycle. This is not supported by our results.

As shown in Table 3 the maximum diameter of M-TPC is 1.780 nm which is a little smaller than M-TPP. Its heat of formation is, as expected, lower than that of M-TPP. M-TPC has one of the four  $\beta$ -pyrrole positions hydrogenated giving rise to a bent structure, a so-called saddle or  $S_4$ -ruffled conformation. This is due to the sterical hindrance between the hydrogen atoms on  $\beta$ -pyrrole position and the phenyl groups. As a consequence the hydrogenated site is lifted a little out of the macrocycle plane and the phenyl groups are rotated. This type of conformation is reported for other  $\beta$ -position hydrogenated porphyrins like Ni-TMC (nickel-tetramethylchlorin) (14). Due to the bent structure the aromatic character of the molecule is

reduced and the molecule will be more vulnerable to further hydrogenation.

As reported in literature for similar  $\beta$ -position hydrogenated porphyrins like Ni-TMC (14), the length of bond between metal and the nitrogen in the hydrogenated pyrrole group should be a little shorter due to the lower aromaticity of the hydrogenated pyrrole group of the porphyrin. This is not found in our calculations, the small differences in the M-N distances are probably caused by inaccuracies in the MOPAC program and are not statistically significant.

#### *4.1.2. Second hydrogenation step: formation of M-TPB and M-TPiB out of M-TPC*

The optimized structure for M-TPiB (tetraphenylisobacteriochlorin) and M-TPB (tetraphenylbacteriochlorin) are depicted in Figure 7 c and d respectively. M-TPiB has two of the four neighbour  $\beta$ -pyrrole hydrogenated resulting into the structure presented. The structure of M-TPiB has not only a saddle conformation but the hydrogenated sites are also twisted. The phenyl groups are rotated further to the porphyrin macrocycle. Like in the structure of M-TPC the bent structure is due to the sterical hindrance between the hydrogen atoms on the hydrogenated sites and the phenyl groups. Due to the fact that the hydrogenated sites are neighbours to each other the only way to lower the hindrance between the hydrogenated sites and the phenyl group between them is a twisted structure. The phenyl group is lowered in relation to the macroring and the two hydrogenated sites are both twisted. The interactions between the phenyl group and the hydrogenated sites are so kept to a minimum.

M-TPB is the other possible product of the hydrogenation of M-TPC. Like M-TPiB, M-TPB has also two of the four  $\beta$ -pyrrole positions hydrogenated but now the opposite positions are hydrogenated. Compared to the structure of M-TPiB the structure is more bent (a so-called saddle or  $S_4$ -ruffled conformation). Like in the structure of M-TPiB the bent structure is due to the sterical hindrance between the hydrogen atoms on the hydrogenated sites and the phenyl groups.

The formation of M-TPiB out of M-TPC is favourable compared to the formation of M-TPB, based on the heat of reaction. It should be kept in mind that this is not a decisive criterium for the prediction of the most favoured reaction path, the factors determining the real reaction pathway are the activation energy and the frequency factor of a reaction step. However, it is self-evident that, in general, activation energy and heat of reaction are coupled in series of elementary steps with comparable intermediates.

Using the heat of reaction together with the fact that M-TPiB has a flatter structure and therefore a more aromatic character due to a larger overlap of  $\pi$ -orbitals than M-TPB, M-TPiB is concluded to be the favoured intermediate. Both intermediates have been detected.

However, M-TPB was found only under special reaction conditions, that is, at very low  $H_2$  and  $H_2S$  partial pressures. M-TPiB is predominately present in reaction mixtures (8), supporting the above mentioned conclusion.

#### 4.1.3. Third hydrogenation step: formation of M-TPHP and M-A out of M-TPiB or M-TPB

The optimized structure for M-TPHP (tetraphenylhexahydroporphyrin or corphin type of porphyrin) and M-A are depicted in Figure 7 e and f respectively.

M-TPHP has three of the four  $\beta$ -pyrrole positions hydrogenated giving rise to a bent structure, a so-called saddle or  $S_4$ -ruffled conformation. The structure is even more bent than the structures of M-TPC or M-TPiB due to the stronger sterical hindrance between the hydrogen atoms on the hydrogenated sites and the phenyl groups.

The second possible product of the third hydrogenation step is M-A. This product is related to the compound Ni-Corr (corrin type of porphyrin) proposed by Ware & Wei (9) as an intermediate in the conversion of Ni-T3MPiB. As shown, the structure is strongly twisted due to the hydrogenation of the meso-bridge position. The resulting type of structure is not very commonly reported in literature (15) and is probably an unstable and short living intermediate.

As we take the values for the heat of formation as an indication, the formation of M-TPHP out of M-TPiB is favourite compared to the formation of M-A. This is in agreement with literature (16) which reports that M-TPHP is detected in case of VO-TPP hydrodemetallisation. The formation of M-B out of M-A is therefore not considered to be of importance.

#### 4.1.4. Fourth hydrogenation step: formation of M-TPOP and M-B out of M-TPHP

For the fourth hydrogenation step two reaction pathways are possible. First, one based on a  $\beta$ -pyrrole position hydrogenation giving M-TPOP (tetraphenylloctahydroporphyrin). The other possible product, M-B, has a M-A like structure and is a product of a meso-bridge position hydrogenation of M-TPHP. Both intermediates are hypothetical and have never been detected experimentally.

The optimized structures for M-TPOP and M-B are depicted in Figure 7 g and h respectively. M-TPOP has all four  $\beta$ -pyrrole positions hydrogenated giving a highly bent structure. The structure is even more bent than the structures of M-TPHP due to the very strong sterical hindrance between the hydrogen atoms on the hydrogenated sites and the phenyl groups. The other possible intermediate M-B is a little bent but less than M-TPOP, indicating that a meso-bridge position hydrogenation is the most probable step in the fourth

hydrogenation step.

As we take the value for the heat of formation as an indication, both intermediate structures are equally probable. Looking at the geometry M-B is the more likely intermediate of the fourth hydrogenation step.

#### 4.1.5. Formation of a corrin-type of porphyrin M-Corr out of M-A

Ware & Wei (9) proposed a new reaction intermediate in the hydrodemetallisation of Ni-T3MPP (nickel-tetra-(3-methyl-phenyl)porphyrin). They suggested that a so-called corrin type of porphyrin Ni-Corr is formed out of Ni-A. Corrins have the same chemical structure as porphyrins but one of the four carbon atoms at the meso positions is removed and a direct bond is formed between the two pyrrole groups (17, 18). The formation of Ni-Corr out of Ni-A, as proposed by Ware & Wei, is depicted in Figure 8. The possible existence of Ni-Corr was supported with UV-VIS spectroscopy and GC-MS analysis.

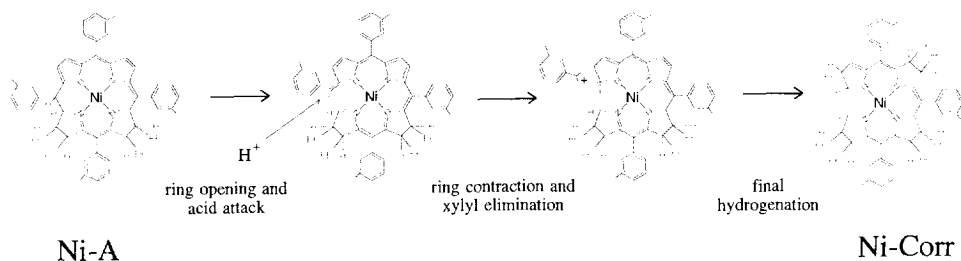


**Figure 8.** Detailed reaction mechanism for the formation of Ni-Corr out of Ni-A as proposed by Ware & Wei (9).

However, to our opinion this reaction step can not be correct. The conversion of Ni-A into Ni-Corr has some steps, which are not probable, in particular the 'spontaneous' opening of the porphyrinic ring. In acid catalysed reactions this takes place after an acid attack. The final hydrogenation step on the  $\beta$ -pyrrole position has a large effect on the aromatic structure of the molecule and seems therefore not plausible. In the compound Ni-Corr, the aromatic structure is very uncommon and the existence of related compounds could not be confirmed in literature. No optimized geometry could be obtained for Ni-Corr with molecular modelling. In order to give an explanation for the UV-VIS and GC-MS results of Ware & Wei (9), an alternative intermediate structure, a bilane-type of porphyrin M-Bil, is presented.

#### 4.1.6. Formation of a bilane-type porphyrin M-Bil out of M-B

In order to explain the results found by Ware & Wei in the hydrodemetallisation of Ni-T3MPP, a new type of reaction intermediate is proposed. After the hydrogenation at the meso-bridge position of the porphyrin, the macrocyclic conjugation is disrupted. The meso position becomes susceptible to an acid attack. This acid attack causes an opening of the macrocycle and formation of a carbonium ion. In analogy with the reaction mechanism proposed by Ware & Wei, a tolyl group can be eliminated forming a bilane type porphyrin (M-Bil). The formation of M-Bil is depicted in Figure 9.

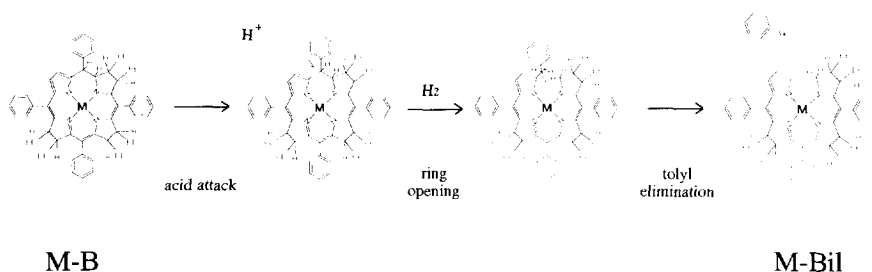


**Figure 9.** Detailed reaction mechanism for the formation of M-Bil out of M-B.



The optimized structure of M-Bil is depicted in Figure 7 i. The structure is strongly twisted due to sterical hindrance between the hydrogens of the two pyrrole groups near the opening in the porphyrinic ring. The nitrogen and metal atoms are no longer in one plane which makes the M-N bonds weaker and the molecule is likely to become more susceptible to metal removal. The calculations performed with MOPAC gave results for M-Bil as shown in Table 3.

M-Bil type of structures are known in literature, for example octaethylformylbiliverdinate (bilane type porphyrins) (16, 18). The open structure of M-Bil can probably be formed due to some stabilising influence of the central metal in the macrocycle in terms of  $\pi$ -d interactions. Donation of metal ion d-electrons to the macrocycle contributes to the aromatic character (10).

Ware & Wei (9) detected with GC-MS and UV-VIS spectroscopy an intermediate, which was assumed to be a corrin type of an intermediate called Ni-Corr. As mentioned earlier, this structure and the accompanying reaction mechanism are associated with a lot of uncertainties. Based on the molecule mass from GC-MS (converted to the case of M-TPP), the most plausible structure is an open chain porphyrin, in present work called M-Bil. Also, the absorption spectra for these types of components are quite similar to the spectrum recorded of the component found by Ware & Wei (19).

M-Bil is believed to be an intermediate before metal removal due to the unstable non-planar metal coordination in the molecule.

#### *4.1.7. Ring cleavage: formation of ring fragments*

The results of the GC-MS analysis on the reaction products of tetraphenylporphyrins show a clear picture. The reaction products of the ring cleavage of tetraphenylporphyrins consist of molecules with one pyrrole bonded to one or two phenyl rings via methine bridges. This type of structures can only be formed when the porphyrin macrocycle opens on a meso-bridge position. So, probably after the meso-bridge hydrogenation step, the porphyrin is cleaved into ring fragments. Furthermore, the pyrrole and phenyl rings in the porphyrinic structure stay intact until the porphyrin macrocycle opens.

#### *4.2. Proposal for an extended reaction mechanism*

Based on the molecular modelling results, the hydrodemetallisation of metallo-tetraphenylporphyrin proceeds via a series of hydrogenation steps; (1) M-TPC is formed from the reactant M-TPP, (2) M-TPiB is formed from M-TPC, (3) M-TPHP is formed from M-TPiB

and (4) M-B is formed from M-TPHP.

A complete description of the hydrodemetallisation reaction mechanism for VO-TPP and Ni-TPP is now possible and depicted in Figure 10. The little differences between the two model components Ni-TPP and VO-TPP are believed to be not of great influence on the reaction mechanism. The first two hydrogenation steps are the same as in the reaction mechanism proposed by Bonn e (8) leading from M-TPP via M-TPC to M-TPiB. M-TPiB is converted into M-TPHP. A meso-bridge position hydrogenation converts the M-TPHP into M-B. In the M-B intermediate the macrocyclic conjugation is disrupted. The meso position becomes susceptible to an acid attack, which causes an opening of the macrocycle. This could lead to either an immediate ring cleavage and metal removal or to a tolyl elimination and the new proposed structure M-Bil.

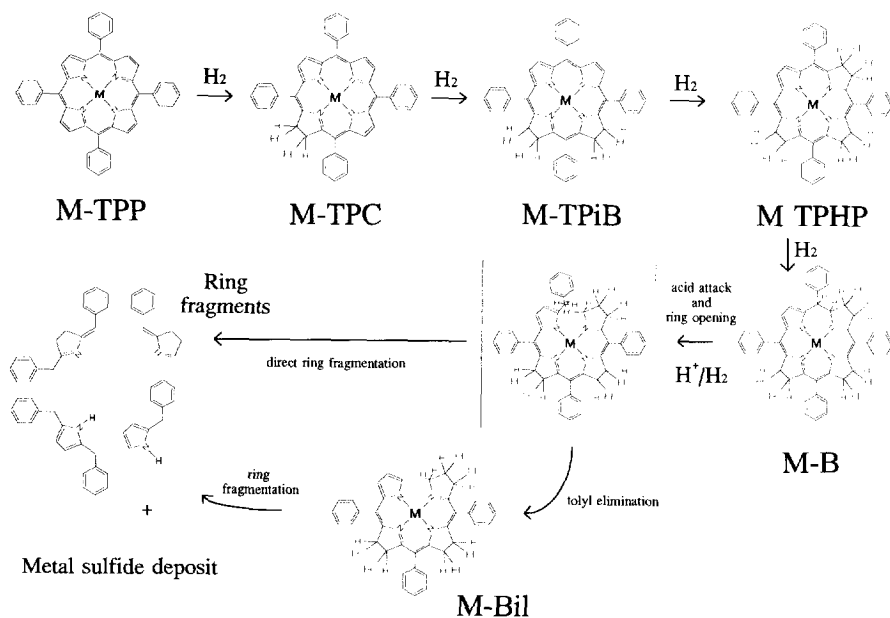


**Figure 10.** Proposal for a complete reaction mechanism for the hydrodemetallisation of metallo-tetraphenylporphyrin.

The heats of formation with respect to the reactant M-TPP are depicted in Figure 11. The path of the extended reaction mechanism is also shown in this Figure.

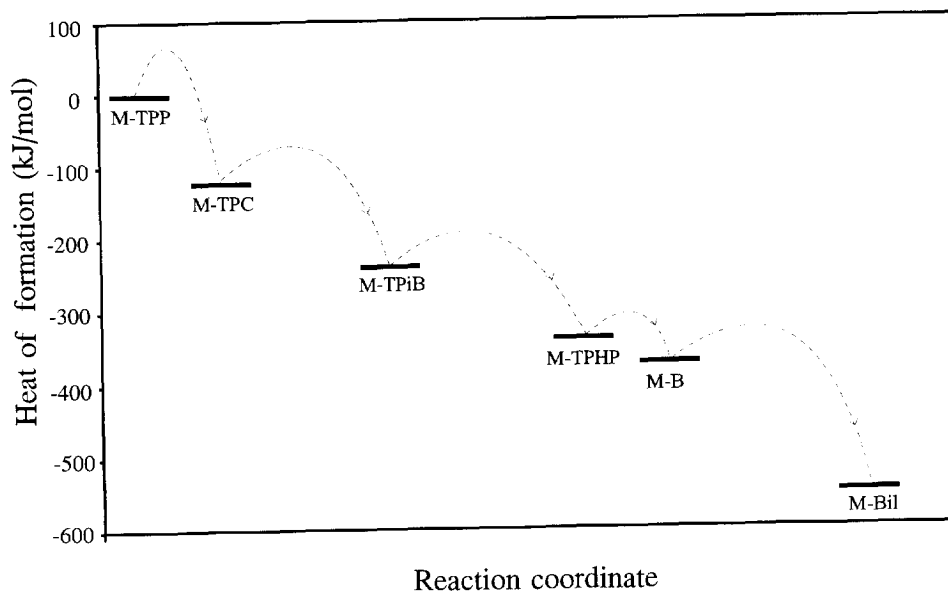


**Figure 11.** Heats of formation with respect to the reactant M-TPP of the optimized structures (dotted line is the path of the extended reaction mechanism, activation energies are arbitrary chosen).

Because of the quite unstable metal coordination in the M-Bil molecule the most likely next step in the reaction mechanism is metal removal. Eliminations of pyrrole groups before metal removal are not unlikely due to the minimum coordination number of four of the metal atom. The metal atom is removed under influence of  $H_2S$  forming a metal-sulfide deposition on the catalyst surface and a multiple-pyrrole ring containing molecule. Further hydrogenations leads to the products detected with GC-MS, mono-pyrrole and phenyl group containing molecules.

The details on the metal removal step are not clear but is believed to proceed via a  $H_2S$  ligand coordination on the central metal atom (20, 21). Hydrogen atoms replace the metal ion in the porphyrin macrocycle to maintain the neutral charge, and the sulfur atom reacts with the metal ion itself, forming either nickelsulfide or vanadium(oxy)sulfide.

The central metal group influences the reactivity of tetraphenylporphyrins as follows,  $H_2$ -TPP > VO-TPP > Ni-TPP, dependent on the stabilising effect of the metal group on the porphyrin macroring. However, the reaction mechanism is not influenced by the type of central metal group and the type of catalyst, it is unique for the type of porphyrin (8).

## 5. CONCLUSIONS

Present work elucidates the elementary steps in the reaction mechanism of metallo-tetra-phenylporphyrin (M-TPP). In order to extend and to investigate the reaction mechanism of M-TPP, GC-MS analyses and molecular modelling techniques have been used.

The modelling of the first two hydrogenation steps known in literature for Ni-TPP as well as for VO-TPP seems to confirm the present understandings of these reactions. The judging criteria used were the heat of formation and the geometry, in particular the degree in flatness of the porphyrinic ring. The heat of reaction predicts a reaction path via M-TPC (chlorin) and M-TPiB (isobacteriochlorin). The geometry of these intermediates is in each step a little more bent, due to the lowering of the aromaticity of the macrocycle of the porphyrinic compound.

The third hydrogenation step is likely to result in M-TPHP (corphin type).

An extended reaction mechanism is proposed leading via a meso-bridge position hydrogenation of M-TPHP to a new intermediate called M-B. An acid attack followed by opening of the porphyrin macrocycle can lead to either an immediate ring cleavage and metal removal or to a tolyl elimination and a new proposed intermediate M-Bil (bilane type). This component is believed to be a final product before metal removal. After metal removal, the components found with GC-MS are the resulting products of the break down of the porphyrinic ring with simultaneous metal deposition on the catalyst surface.

Conclusions on the ring cleavage step in the reaction mechanism of the model components Ni-TPP and VO-TPP can be drawn; the pyrrole and phenyl rings in the porphyrin are still intact after opening of the porphyrinic ring and the porphyrinic ring itself opens on a meso-bridge position. The GC-MS analyses indicated the formation of two different pyrrole ring containing molecules. The first component appeared to be a mono-pyrrole ring containing molecule connected via a methine bridge to a phenyl group. The second component consisted of one pyrrole and (connected via methine bridges) two phenyl rings.

## REFERENCES

1. Quann, R.J., Ware, R.A., Hung, C.W., and Wei J., *Adv. Chem. Eng.*, **14** (1988) 95.
2. Sie, S.T., in 'Catalyst Deactivation' (Delmon, B. and Froment G.F., Ed.), 545, Elsevier Scientific Publishing Company, Amsterdam (1980).
3. Chapter 3 of this thesis.
4. Insight II User and Reference Guide, Version 2.3.0., December 1993, BioSym Technologies, San Diego, USA.

5. Weast, R.C., 'CRC Handbook of Chemistry and Physics', CRC Press, Florida, 64th Edition (1983-1984)
6. Kameyama, H., Sugishima, M., Yamada, M., and Amano, A., *J. Japan. Petrol. Inst.*, **24**(5) (1981) 317.
7. Tsai, C.H., Massoth, F.E., Lee, S.Y., and Seader, J.D., *Fuel Proc. Techn.*, **29** (1991) 153.
8. Bonn e, R.L.C., 'Hydrodemetallisation of Ni-TPP and VO-TPP over Sulfided Molybdenum and Vanadium Catalysts', Ph.D thesis, University of Amsterdam (1992).
9. Ware, R.A., and Wei, J., *J. Catal.*, **93** (1985) 100.
10. Hambricht, P., in 'Porphyrins and Metalloporphyrins' (Smith, K.M., Ed.), Elsevier, Amsterdam (1975).
11. Scheidt, W.R., in 'Porphyrin Chemistry Advances'(Longo, F.R., Ed.), Ann Arbor Science, Michigan (1979).
12. Scheidt, W.R., in 'The Porphyrins' (Dolphin, D., Ed.), Vol. 3, Chapt. 10, Academic Press, New York (1978).
13. Buchler, J.W., in 'The Porphyrins' (Dolphin, D., Ed.), Vol.1, Chapt. 10, Academic Press, New York (1978).
14. Galluci, J.C., Swepton, P.N., Ibers, J.A., *Acta Cryst.*, **B38** (1982) 2134.
15. Furrhop, J.-H., in 'The Porphyrins' (Dolphin, D., Ed.), Vol. 2, Chapt. 5, Academic Press, New York (1978).
16. Subramanian, J., and Furrhop, J.-H., in 'The Porphyrins' (Dolphin, D., Ed.), Vol. 2, Chapt. 8, Academic Press, New York (1978).
17. Katada, M., Tyagi, S., Rajoria, D.S., and Nath, A., in 'Porphyrin Chemistry Advances'(Longo, F.R., Ed.), Ann Arbor Science, Michigan (1979).
18. Cavaleiro, J.A.S., Evans, B., and Smith, K., in 'Porphyrin Chemistry Advances'(Longo, F.R., Ed.), Ann Arbor Science, Michigan (1979).
19. Gossauer, A., and Engel, J., in 'The Porphyrins' (Dolphin, D., Ed.), Vol. 2, Chapt. 7, Academic Press, New York (1978).
20. Dautzenberg, F.M., and Deken, J.C. de, *ACS Prepr. Div. Petr. Chem.*, **30** (1985) 8.
21. Kn zinger, H., Cordischi, D., and Vielhaber, B., *Catal. Tod.*, **7** (1990) 447.



# Chapter 8

## Summary and Evaluation

### Characterisation, Testing and Deactivation of Sulfided Catalysts in the Hydrodemetallisation of Vanadyl-tetraphenylporphyrin

The oil demand of the Western World has undergone major changes in the last decades due to overcapacity of primary crude, fluctuating crude prices, oil crises and the development of other energy sources, like coal and nuclear fission. In general, the oil market shows an increasing demand for light and middle distillates, such as naphtha, gasoline, jet fuels and diesel and a decreasing demand for heavy products, such as heavy fuel oil and coke. To cope with this change in the oil market, the refining industry has to convert heavy feedstocks such as residual oils into lighter and more employable products, the so-called '*whitening of the barrel*'.

The heavy feedstocks can be defined in terms of a high carbon to hydrogen (C/H) ratio, high viscosity, large amounts of asphaltenes and high contents of hetero-atoms, such as sulfur, nitrogen, oxygen and metals, such as vanadium and nickel. Therefore, the main objectives of upgrading and conversion of these heavy feedstocks are the lowering of the C/H ratio, the viscosity and the hetero-atom content for further conversion downstream.

Governments put an additional constraint on refineries by more stringent environmental demands on the products and processes. The presence of sulfur and nitrogen in crudes poses serious environmental hazards in the form of  $\text{SO}_x$  and  $\text{NO}_x$  emissions in combustion processes. Since these emission contribute to the greenhouse effect, acid rain and the destruction of the ozone layer, the society will be put more and more stringent regulations on these emissions.

The available catalytic and thermal heavy oil upgrading processes can be divided into the following classes:

- i) hydrogen addition: - catalytic hydroprocesses (hydrotreating, hydrocracking)  
- non-catalytic hydroprocesses (hydrovisbreaking, donor-solvent-processes, hydropyrolysis)
- ii) carbon rejection: - catalytic cracking (Fluid Catalytic Cracking)  
- thermal processes (visbreaking, coking)
- iii) other processes: - partial oxidation, steam reforming, production of syngas

Thermal processes are, in general, less selective for the desired product and require higher temperatures than catalytic processes, therefore, catalytic processes are the most promising for the future.

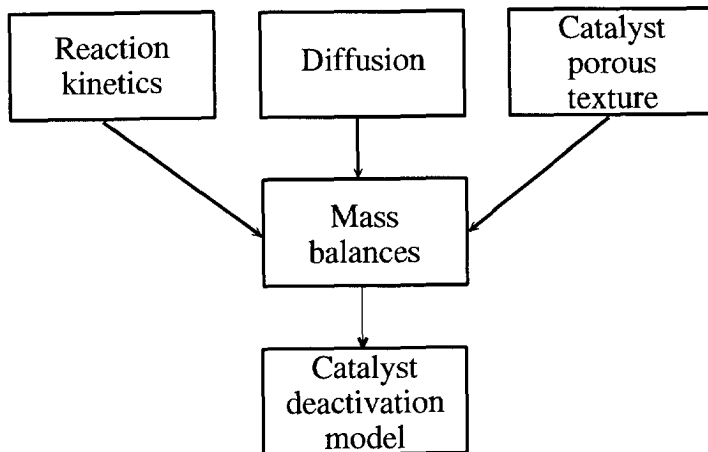
Catalytic hydrotreating is a well established process for the removal of impurities or hetero-atoms, such as sulfur (HydroDeSulfurisation, HDS), nitrogen (HydroDeNitrogenation, HDN), oxygen (HydroDeOxygenation, HDO) and metals (HydroDeMetallisation, HDM). These hetero-atoms are hydrogenated and removed as hydrogen sulfide, ammonia, water and metal sulfides, respectively. Hydrogen sulfide, ammonia and water leave the reactor in the gas phase, whereas the metals, mainly vanadium and nickel, are deposited as sulfide on the internal catalyst surface and remain in the reactor.

Vanadium and nickel are present in heavy oil as soluble organo-metallic complexes and fall into two categories; metallo-porphyrins and non-porphyrin complexes. Metallo-porphyrins are well defined structures. The basic skeleton of porphyrin is a closed ring of four pyrrole groups linked by methine bridges. Porphyrins may have various substituents replacing the hydrogens at the eight  $\beta$ -pyrrolic carbon positions and the four methine bridge positions. Non-porphyrins are all other metal complexes in crude oil and are, in general, poorly characterized with respect to their properties and structure. Therefore, metallo-porphyrins are extremely suitable as model compounds for fundamental research on hydrodemetallisation.

The type of catalyst used in the HDM and/or HDS process determines the catalyst deactivation process. CoMo or NiMo catalysts deactivate due to the interaction of the deposited metals with the original active sites (*'active site poisoning'*) and the loss of pore volume due to the obstruction of catalyst pores (*'pore plugging'*). Metal deposition on bare support material or low loaded catalysts with high metal tolerance cause an increase in activity for HDM due to the auto-catalytic effect of the deposited nickel and vanadium (*'active site generation'*). Eventually, at high metal loadings *'pore plugging'* becomes the dominant deactivation phenomenon.



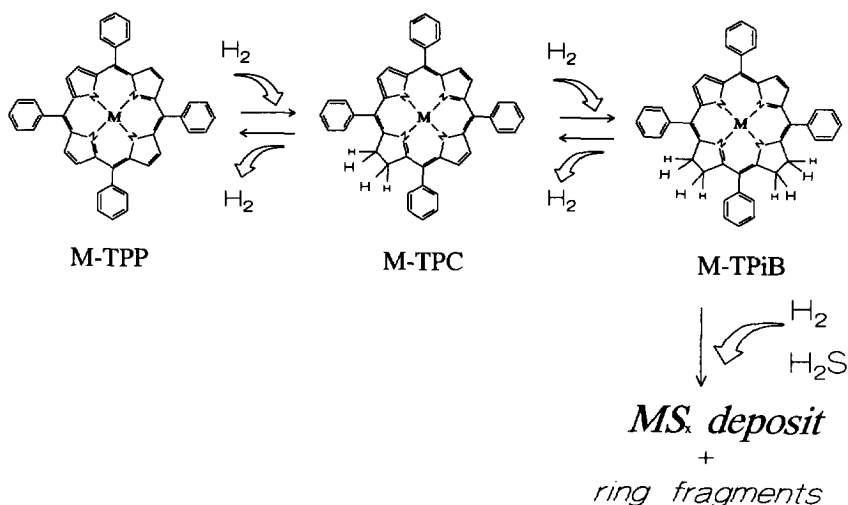
The development of catalyst deactivation models, which give reliable predictions of catalyst life-time and activity, is a key-issue in HDM process design and operation and provides a tool for designing optimized catalysts. This thesis proposes a general approach for describing the catalysts deactivation process, as depicted in Figure 1. Consequently, reaction kinetics, diffusion and the changing catalyst porous texture during hydrodemetallisation are the important phenomena and are the main focus points in this thesis.



**Figure 1.** General approach to HDM catalyst deactivation modelling.

HDM reaction kinetics and mechanistic literature studies are limited to porphyrinic metal containing model compounds. As argued above, HDM studies with model compounds can provide insight into fundamental rate processes. The reason is that the use of porphyrinic model compounds eliminates many of the complicated and competing reactions encountered with oil residua, thus enabling a clearer picture of the reactions to be ascertained.

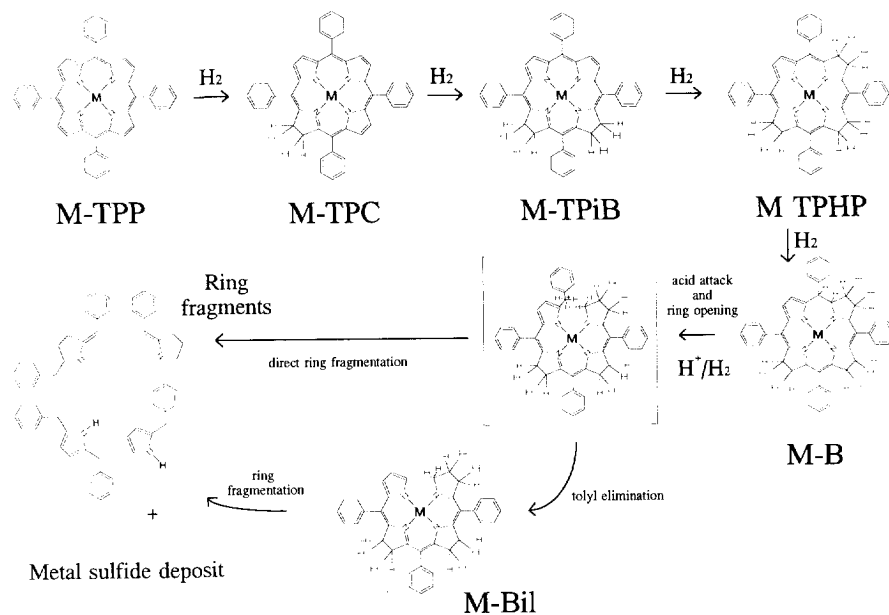
The reaction mechanism for the hydrodemetallisation of metallo-tetraphenylporphyrin (M-TPP), which is used as model compound in present work, is depicted in Figure 2. M-TPP is reversibly hydrogenated to metallo-tetraphenylchlorin (M-TPC), which is also reversibly hydrogenated to metallo-tetraphenylisobacteriochlorin (M-TPiB). In the last ring cleavage reaction M-TPiB is demetallised and forms metal sulfide deposits on the internal catalyst surface and ring fragments. This last reaction is a lumped step which consists of several hydrogenation and hydrogenolysis reactions.



**Figure 2.** Hydrodemetallisation reaction mechanism of metallo-tetraphenylporphyrin (M-TPP). (M-TPC: metallo-tetraphenylchlorin, M-TPiB: metallo-tetraphenylisobacteriochlorin)

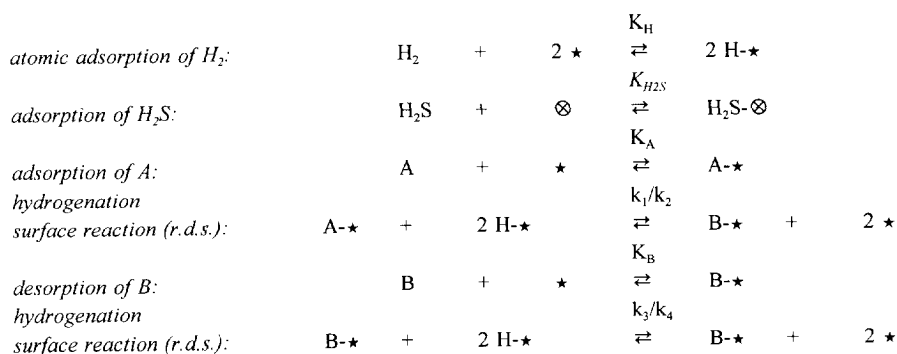
Based on molecular modelling calculations and GC-MS analysis new reaction intermediates are identified in the last lumped ring cleavage step and an extended reaction mechanism for the HDM of M-TPP is proposed, as depicted in Figure 3. The mechanism proceeds via three hydrogenation steps on the  $\beta$ -pyrrole positions of the porphyrinic structure to a meso-bridge hydrogenated structure. After an acid attack, ring opening and a possible elimination of a tolyl group, the final product before metal removal is an open chain molecule. Metal removal and further conversion leads to mono-pyrrole containing molecules and metal deposition on the catalyst surface.

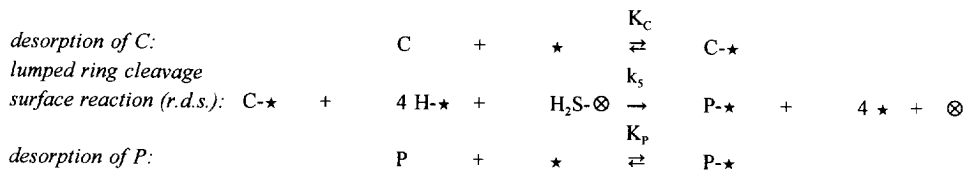
A two-site reaction kinetics model, in which hydrogenation and hydrogenolysis occur on two different sites, is found to apply for the hydrodemetallisation of M-TPP. Hydrogenation reactions occur on sites which are thought to consist of sulfur vacancies or coordinatively unsaturated (Lewis acid) sites, whereas hydrogenolysis occurs on Brønsted acid sites. As shown in the extended reaction mechanism for M-TPP, a  $H^+$  acid attack is necessary to open the porphyrinic ring.



**Figure 3.** Extended hydrodemetallisation reaction mechanism of M-TPP.

The following set of elementary reactions has been used for the hydrodemetallisation reaction kinetics of M-TPP. The ring cleavage reaction is lumped, since it is often fast compared to the first two hydrogenation steps (A = M-TPP, B = M-TPC, C = M-TPiB, P = products; ★ = hydrogenation site, ⊗ = hydrogenolysis site) (1):





A Langmuir-Hinshelwood type of kinetics with competitive adsorption of hydrogen applies for the M-TPP hydrodemetallisation:

$$-r_A = \frac{k_1 K_H C_A C_{H_2} - k_2 C_B}{(1 + \sqrt{K_H C_{H_2}})^3} \quad (1)$$

$$-r_B = \frac{-k_1 K_H C_A C_{H_2} + k_2 C_B + k_3 K_H C_B C_{H_2} - k_4 C_C}{(1 + \sqrt{K_H C_{H_2}})^3} \quad (2)$$

$$-r_C = \frac{-k_3 K_H C_B C_{H_2} + k_4 C_C}{(1 + \sqrt{K_H C_{H_2}})^3} + \frac{k_5 K_H^2 C_C C_{H_2}^2 C_{H_2S}}{(1 + \sqrt{K_H C_{H_2}})^5} \quad (3)$$

where  $k_1$  and  $k_3$  are the first and second hydrogenation reaction rate constants,  $s^{-1}$ ,  $k_2$  and  $k_4$  the first and second dehydrogenation reaction rate constants,  $s^{-1}$ ,  $k_5$  is the lumped ring cleavage reaction rate constant,  $m^3/mol \cdot s$ ,  $K_H$  is the hydrogen adsorption constant,  $m^3/mol$ ,  $r$  is the reaction rate,  $mol/m^3 \cdot s$  and  $C$  is the liquid phase concentration,  $mol/m^3$ .

Values for the  $H_2$  adsorption constant were found to be small but statistically significant:

$$K_H = (7.5 \pm 6.2) \cdot 10^{-5} \text{ m}^3/\text{mol}$$

The values for the equilibrium constants  $K_{12}$  and  $K_{34}$  were found to be (for VO-TPP):

$$K_{12} (= k_1/k_2) = 42 \pm 16$$

$$K_{34} (= k_3/k_4) = 46 \pm 24$$

Figure 4 shows the values of the reaction rate constants for several different types of catalysts and supports. The values for the first and second hydrogenation reaction rate constants ( $k_1$  and  $k_2$ ) and the lumped ring cleavage step ( $k_3$ ) are given.

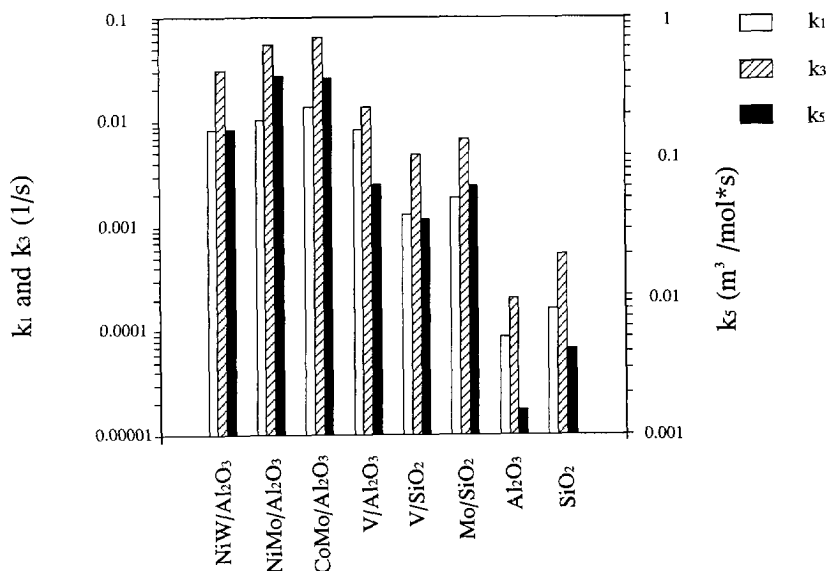


**Figure 4.** Reaction rate constants for the hydrodemetallisation of VO-TPP of several types of catalysts at approximately 10 MPa H<sub>2</sub> pressure and 578 K.

(catalysts: NiW/Al<sub>2</sub>O<sub>3</sub>: 2.4 wt.% Ni, 18.8 wt.% W; NiMo/Al<sub>2</sub>O<sub>3</sub>: 4.5 wt.% Ni, 12.7 wt.% Mo; CoMo/Al<sub>2</sub>O<sub>3</sub>: 4.2 wt.% Co, 12.1 wt.% Mo; V/Al<sub>2</sub>O<sub>3</sub>: 3.4 wt.% V; V/SiO<sub>2</sub>: 1.0 wt.% V, Mo/SiO<sub>2</sub>: 1.8 wt.% Mo)

The presence of sulfur, nitrogen and oxygen containing compounds in heavy oil residua can influence the rate at which the metals are removed since they can adsorb competitively on the active site of the catalyst and decrease the rate of the hydrogenation and ring cleavage reactions of organo-metallic compounds. The competition by the hetero-atom containing compounds, *i.e.*, quinoline, ammonia, benzofuran, water, dibenzothiophene, and anthracene on the hydrodemetallisation of vanadyl-tetraphenylporphyrin is investigated. The spiked amount of hetero-atoms is chosen near to that occurring in oil residua. Quinoline, benzofuran, dibenzothiophene and anthracene showed to have a decreasing effect on the rate of metal

removal due to competitive adsorption with vanadyl-tetraphenylporphyrin. Reaction rate constants are decreased by a factor of 2 to 5 due to the presence of these hetero-atoms.

Water and ammonia proved to coordinate with the vanadyl-group via hydrogen bonding which stabilizes the porphyrin for metal removal. It is found that hetero-atom containing compounds can influence the rate of metal removal in heavy feedstocks. However, competitive adsorption of reaction products from the ring cleavage of VO-TPP is negligible due to the low concentrations.

Vanadium deposits formed during hydrodemetallisation can act as catalysts for the HDM reaction. Therefore, it is of importance to determine the structure and catalytic activity of vanadium on silica and alumina support. Vanadium showed to be more disperse on alumina than on silica. This dispersion effect is clearly noticeable in catalyst activities, vanadium on silica shows a much lower activity for thiophene HDS and a lower hydrogenation rate in VO-TPP HDM than vanadium on alumina. Large differences in hydrogenation-ring cleavage selectivity for VO-TPP HDM are observed. For vanadium on alumina a much higher selectivity is found than for vanadium on silica. It is suggested that hydrogenation reactions in VO-TPP HDM take place on structure or dispersion sensitive sites, whereas ring cleavage is associated with large clusters of active phase and the type of support material. Again this result supports the two-site reaction kinetics model for the hydrodemetallisation of M-TPP.

These hydrogenation-ring cleavage selectivity differences can be used for optimisation of the HDM process. A two-stage process, in which the hydrogenation reactions take place in the first reactor (with for instance a  $V/Al_2O_3$  catalyst) and the ring cleavage reactions take place in the second reactor which is loaded with a catalyst with a high ring cleavage activity and a high metal storage capacity (for instance a  $V/SiO_2$  catalyst), is a possibility of an optimised HDM process. A catalyst containing Brønsted acid sites is of major importance for a high ring cleavage activity.

Hydrodemetallisation reactions require the diffusion of polyaromatic molecules into the pore structure of the catalyst pellet prior to the reaction. When the pore diameter approaches the effective molecular diameter of the diffusing species, the diffusion rate drops dramatically due to a reduced solute mobility. This results from geometric exclusion near the pore wall and increased viscous drag in the pore and is termed restrictive or configurational diffusion. Literature correlations for (restrictive) diffusion coefficients are used in this work to estimate rates of diffusion of porphyrins in catalyst porous textures. A Wilke-Chang type of correlation is used for calculating the bulk diffusion coefficient,  $D_b$ , of M-TPP in its solvent (2, 3):

$$D_b = 18.7 \cdot 10^{-12} \frac{M_b^{0.30} T}{\mu_b^{0.84} V_a^{0.55}} \quad (4)$$

where  $M_b$  is the solvent molecular weight, g/mol,  $V_a$  is the molar volume of the solute at its boiling point,  $\text{cm}^3/\text{mol}$ ,  $T$  is the temperature in K and  $\mu_b$  is the solvent viscosity, cP.

The effective diffusion coefficient,  $D_{\text{eff}}$ , for the diffusion of large molecules in relatively small catalyst pores results in:

$$D_{\text{eff}} = \frac{\epsilon}{\tau} D_b F(\lambda) \quad \text{with} \quad F(\lambda) = e^{-4.6 \cdot \lambda}, \quad \lambda = \frac{r_s}{r_p} \quad (5)$$

where  $\epsilon$  is the catalyst pellet porosity,  $\tau$  is the catalyst pellet tortuosity and  $F(\lambda)$  is the restrictive factor, which is a function of  $\lambda$ , the ratio of the diffusing solute molecular size,  $r_s$ , and the pore radius,  $r_p$  (4).

In the present work, the simple Fick formulation is used to describe intraparticle diffusion. A more consistent manner would be the Maxwell-Stefan formulation, which uses a more realistic mechanistic picture of diffusion (5).

Reaction kinetics and diffusion are the important phenomena determining the rate of metal deposition and, possibly, the rate of catalyst deactivation. However, an important phenomenon is the description of the catalyst porous texture. Variables characterising the catalyst porous texture, such as the porosity, tortuosity and interconnectivity of pores, are changing during the metal deposition process and have to be described. Percolation concepts showed to be suitable for this purpose and showed to behave more realistic than conventional cylindrical pore models.

An HDM catalyst deactivation model based on percolation concepts is developed in the present work. This model is based on the reaction kinetics as determined in this thesis, diffusion according to literature correlations and a topologically-disordered network (cubic tessellation) to model the changing catalyst porous texture. A comparison of simulated results for model compound VO-TPP and experimental catalyst deactivation results of an industrial feedstock showed qualitative agreement, as depicted in Figure 5. Vanadium deposition profiles in catalyst pellets can be reproduced. The remarkable similarity in results derived from the model compound and the industrial feedstock implies that these model compounds are a

convenient tool in deactivation studies, since research on hydrotreating catalyst testing and deactivation, using industrial feedstocks, is very time consuming and expensive.

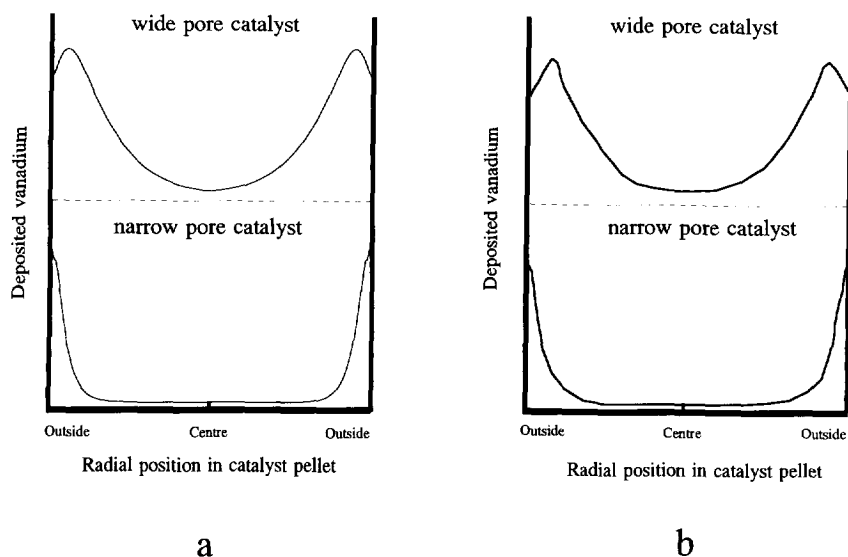


**Figure 5.** Simulated and experimental vanadium deposition profiles in a wide- and narrow pore silica catalyst at an average axial position in the reactor, a- model simulations for model compound VO-TPP and b- experimental deposition profiles for industrial feedstock.

The Thiele modulus determines the shape of the metal deposition profiles, which is apparently equal in the case of model compound VO-TPP and an industrial feedstock. Since the bulk diffusion coefficient of an industrial feedstock is about two orders of magnitude lower than porphyrinic model compounds (6), the reaction rate of model compounds should be two orders of magnitude higher than industrial feedstocks in order to preserve equal Thiele moduli (7). The lower reaction rates of industrial feedstocks are due to *i*) the intrinsic lower reactivity of metal containing structures in real feeds and *ii*) the limited accessibility of metal containing structures within asphaltenes to catalytic active sites. The effect of competitive adsorption of hetero-atom species present in heavy oil is in this case relatively small, reaction rates are decreased by a factor 2 to 5.



## Summary and Evaluation

This thesis investigates on the vanadium deposition process with model compound VO-TPP under industrial conditions. Catalyst pellets of a wide pore molybdenum on silica catalyst are used to determine the deposition process with ElectronProbe MicroAnalysis and High Resolution Electron Microscopy. Vanadium deposition profiles show a deposition maximum in the centre of the pellet, indicating the absence of diffusion limitations into the catalyst pellet and a sequential reaction mechanism for VO-TPP hydrodemetallisation. Comparison of simulations and experimental data of vanadium deposition profiles as a function of the axial position in the reactor showed reasonable agreement, at least at reactor inlet conditions (see Figure 6).

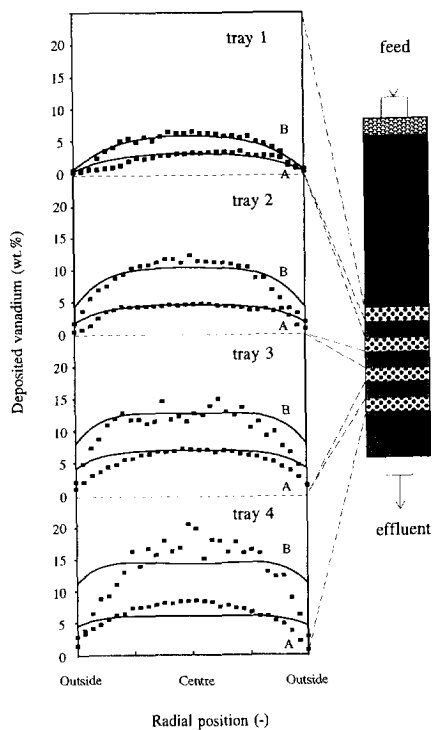


**Figure 6.** Comparison between experiment and model as a function of the axial position in the reactor. (solid lines represent the model, A and B are different, increasing times on stream)

However, increasing discrepancies between model and experiment are observed in axial direction in the reactor. These deviations are probably caused by inaccuracies in the input parameters, that is the boundary concentrations of reactant and intermediates and variation in the reaction rate constants.

Two different morphologies of vanadium sulfide deposits have been identified on low loaded molybdenum on silica catalysts, *i*) a disperse, non-crystalline phase and *ii*) a crystalline phase, *e.g.* consisting of a layered structure. Vanadium deposits either in the surroundings of the active phase, causing active site poisoning, or as isolated vanadium sulfide clusters, causing active site generation. The nett result is that no significant deactivation is observed starting from low loaded or bare support materials up to 9 wt.% vanadium deposited.

The results presented in this thesis provide fundamental insight in the (rate) processes which are responsible for hydrodemetallisation of model compounds. Reaction kinetics, diffusion, catalyst porous texture and morphology of metal deposits form the main focus points. A state-of-the-art catalyst deactivation model is presented, which gives predictions on metal deposition profiles in catalyst pellets and catalyst life-time.

## REFERENCES

1. Bonné, R.L.C., Steenderen, P. van, and Moulijn, J.A., *Bull. Soc. Chim. Belg.*, **100**(11-12) (1991) 877.
2. Tsai, C.H., Massoth, F.E., Lee, S.Y., and Seader, J.D., *Ind. Eng. Chem. Res.*, **30** (1991) 22.
3. Wilke, C.R., and Chang, P., *AIChE J*, **1** (1955) 264.
4. Satterfield, C.N., Colton, C.K., and Pitcher, W.H., *AIChE J*, **19** (1973) 628.
5. Wesselingh, J.A., and Krishna, R., 'Mass Transfer', Ellis Horwood, New York (1990).
6. Chantong, A., and Massoth, F.E., *AIChE J*, **29** (1985) 100.
7. Dongen, R.H. van, Bode, D., Eijk, H. van der, and Klinken, J. van, *Ind. Eng. Chem. Process Des. Dev.*, **19** (1980) 630.

## Samenvatting

De laatste decennia is de vraag naar aardolie in de westerse wereld sterk veranderd door de overproductie van ruwe aardolie, fluctuerende prijzen, olie crises en het gebruik van alternatieve energie bronnen zoals kolen en kernsplijting. In het algemeen neemt de vraag naar lichte en middel destillaten (transport brandstoffen), zoals benzine, diesel en kerosine, toe, terwijl er een afnemende vraag is naar zware produkten, zoals zware stookolie en coke. Om deze verandering in vraag naar aardolie produkten aan te kunnen, zullen aardolie (-verwerkende) maatschappijen de zware olieresiduen om moeten zetten naar de meer bruikbare en lichtere produkten.

De zware aardolieresiduen worden gekarakteriseerd door een hoge koolstof tot waterstof (C/H) verhouding, hoge viscositeit, grote hoeveelheden asfaltenen en verontreinigingen in de vorm van zwavel, stikstof, zuurstof en metalen (nikkel en vanadium). Om die reden is de belangrijkste doelstelling van de opwerking van olieresiduen het verlagen van de C/H verhouding, de viscositeit en de hoeveelheid verontreinigingen.

Overheden leggen een extra beperking op aan aardolie raffinaderijen in de vorm van meer stringente milieu-eisen aan zowel de produkten als de processen. De aanwezigheid van zwavel en stikstof in olieprodukten brengt het milieu ernstige schade toe in de vorm van zwavel- en stikstofoxides, die vrijkomen bij verbrandingsprocessen. Deze zwavel- en stikstofoxide emissies dragen bij aan het broeikaseffect, zure regen en de afbraak van de ozonlaag.

Katalytische waterstofbehandeling ('hydrotreatment') is een bewezen technologie voor de verwijdering van de verontreinigingen, zoals zwavel ('HydroDeSulfurisation' of HDS), stikstof ('HydroDeNitrogenation' of HDN), zuurstof ('HydroDeOxygenation', HDO), metalen ('HydroDeMetallisation' of HDM), en voor de verlaging van de C/H verhouding uit olie-residuen. De verontreinigingen worden gehydrogeneerd tot respectievelijk waterstofdisulfide, ammoniak, water en metaalsulfides. Waterstofdisulfide, ammoniak en water verlaten de reaktor in de gasfase, terwijl de metalen in de reaktor achterblijven door neer te slaan op het katalysator oppervlak. De neerslag van deze metalen zal de activiteit van de katalysator beïnvloeden.

Het type katalysator dat gebruikt wordt voor hydrodemetallisatie bepaalt tevens het deactiveringsgedrag. Katalysatoren met als actieve fase cobalt-molybdeen of nikkel-molybdeen deactiveren door de interactie tussen de oorspronkelijke actieve fase en de neergeslagen

## Samenvatting

vanadium en nikkel, en door het verlies aan porie volume dat ontstaat doordat de neergeslagen vanadium en nikkel die poriën blokkeren. Vanadium en nikkel neerslagen op een kale drager of dragers met een lage belading van de actieve fase kunnen een verhoging van de HDM activiteit veroorzaken doordat vanadium en nikkel een auto-katalytische werking hebben op de HDM reactie (vorming van actieve fase). Bij hoge vanadium en nikkel afzettingen wordt porie blokkering wederom het dominerende deactiveringsverschijnsel.

De ontwikkeling van katalysator deactiveringsmodellen, welke betrouwbare voorspellingen geven voor de levensduur en activiteit van de katalysator, neemt een sleutel positie in bij het hydrodemetallisatie procesontwerp en is een gereedschap voor het ontwerp van geoptimaliseerde katalysatoren. In dit proefschrift wordt een algemene aanpak voor de beschrijving van het katalysator deactiveringsproces ontwikkeld. Reactie kinetiek, diffusie, de beschrijving van de veranderende katalysator poreuze textuur evenals de morfologie van de metaal afzetting tijdens hydrodemetallisatie zijn de belangrijkste elementen in het model en vormen om deze reden de zwaartepunten van dit proefschrift.

Hydrodemetallisatie reactie kinetiek en mechanistische literatuur studies zijn beperkt tot porphyrische metaalverbindingen. Het gebruik van porphyrische modelverbindingen voor hydrodemetallisatie studies geven fundamenteel inzicht in dit proces. De reden voor het gebruik van deze modelverbindingen is dat veel gecompliceerde en competitieve reacties, die in olieresiduen voorkomen, kunnen worden uitgesloten. Hierdoor ontstaat een helder beeld van de hydrodemetallisatie reacties. In dit proefschrift is metallo-tetraphenylporphyrine (M-TPP) gebruikt als organo-metaal modelverbinding.

Vanadium afzettingen kunnen als katalysator fungeren voor de HDM reactie. Het is daarom van belang om de structuur en reactiviteit van vanadium, neergeslagen op alumina en silica, te bepalen. Vanadium is meer dispers aanwezig op alumina dan op silica. Dit dispersie effect is duidelijk zichtbaar in de katalytische activiteit. Vanadium op silica laat een veel lagere thiofeen hydrodesulfurisatie activiteit en hydrogeneringsactiviteit in vanadyl-tetraphenylporphyrine (VO-TPP) HDM zien dan vanadium gedragen op alumina. Grote verschillen in hydrogenering-hydrogenolyse selectiviteit voor VO-TPP HDM zijn waargenomen. Voor vanadium op alumina wordt een veel hogere selectiviteit gevonden dan vanadium op silica. Voorgesteld is dat hydrogeneringsreacties voor VO-TPP HDM plaatsvinden structuur en dispersie gevoelige actieve plaatsen, terwijl de hydrogenolyse reactie wordt geassocieerd met grotere clusters actieve fase en de invloed van het type dragermateriaal. Dit resultaat ondersteunt het 'two-site' reactie kinetiek model voor de hydrodemetallisatie van VO-TPP. Deze resultaten zijn in hoofdstuk 3 beschreven.

De aanwezigheid van zwavel, stikstof en zuurstof bevattende verbindingen in olieresiduen kan de snelheid waarmee metalen worden verwijderd beïnvloeden. Deze verbindingen kunnen

## Samenvatting

competitief adsorberen op de actieve plaatsen van de katalysator en de hydrogenering en hydrogenolyse van organo-metaalverbindingen remmen. Deze remming door hetero-atoom bevattende verbindingen, chinoline, ammoniak, benzofuraan, water, dibenzothiofeen en anthraceen op de hydrodemetallisatie van vanadyl-tetraphenylporphyrine is onderzocht. De hoeveelheid toegevoegde hetero-atomen is gekozen dichtbij die in olieresiduen. Chinoline, benzofuraan, dibenzothiofeen en anthraceen laten een remmende werking zien op de snelheid van metaalverwijdering door competitieve adsorptie met vanadyl-tetraphenylporphyrine. De reactie snelheid wordt met een factor 2 tot 5 verlaagd door de aanwezigheid van deze hetero-atomen. Water en ammoniak, welke de sterkste remmers zijn, coördineren met de vanadyl-groep via een waterstofbrug welke de porphyrine stabiliseert voor metaalverwijdering. Hetero-atoom bevattende verbindingen blijken de metaalverwijdering in olieresiduen te kunnen vertragen. Een remmende werking op de metaalverwijdering door de ontledingsprodukten van VO-TPP is verwaarloosbaar door de lage concentraties. De invloed van hetero-atoom bevattende componenten op de hydrodemetallisatie reacties is beschreven in hoofdstuk 4.

Reactie kinetiek en diffusie zijn de belangrijke verschijnselen die de metaalverwijderings-snelheid en -depositie en mogelijk de snelheid van katalysator deactivering bepalen. Echter, een ander belangrijk verschijnsel is de beschrijving van de katalysator-textuur. De variabelen die de poreuze textuur van de katalysator karakteriseren, zoals de porositeit, tortuositeit en interconnectie van poriën, veranderen tijdens het metaal depositie proces en dienen te worden beschreven. Percolatie concepten blijken geschikt te zijn voor dit doel en gedragen zich fysisch realistisch (beter dan conventionele cilindrische poriën modellen).

Een HDM katalysator deactiveringsmodel gebaseerd op percolatie concepten is ontwikkeld in hoofdstuk 5. Dit model is gebaseerd op reactie kinetiek (zoals bepaald in dit proefschrift), diffusie (volgens literatuur correlaties) en een topologisch onregelmatig netwerk (de kubische tessellatie) om de veranderende poreuze textuur van de katalysator te beschrijven. Een vergelijking tussen gesimuleerde resultaten voor de modelverbinding VO-TPP en experimentele deactiveringsresultaten van een industriële voeding laten een kwalitatieve overeenkomst zien. Experimentele vanadium depositie profielen in katalysatordeeltjes kunnen worden gereproduceerd. De opvallende overeenkomst tussen de modelverbinding en de industriële voeding houdt in dat modelverbindingen geschikt zijn in deactiveringsstudies, aangezien research aan hydrotreating katalysatoren gebruik makende van industriële voedingsmiddelen tijdrovend en duur is. Het gebruik van modelverbindingen is interessant zowel vanuit het oogpunt van 'screening' als het testen van katalysatoren.

In hoofdstuk 6 is het vanadium depositie proces met modelverbinding VO-TPP onderzocht onder industriële condities. Een molybdeen katalysator, gedragen op silica met grote poriën, is gebruikt om het depositie proces te volgen. Vanadium depositie profielen laten een

## Samenvatting

maximum metaalafzetting zien in de kern van het katalysatordeeltje, hetgeen er op duidt dat diffusie limitaties niet aanwezig zijn voor transport het deeltje in en dat een sequentieel reactie mechanisme geldig is voor de hydrodemetallisatie van VO-TPP. Een vergelijking tussen modellering en experimentele resultaten van vanadium depositie profielen als functie van de axiale positie in de reaktor laat een redelijke overeenstemming zien, zeker bij de reaktor inlaat condities. Discrepancies tussen het model en experiment worden bepaald door onnauwkeurigheden in de invoerparameters, met name de concentraties reaktant en intermediären aan de rand van het katalysator deeltje en de variatie in de lokale reactie snelheidsconstanten.

Twee verschillende typen morfologie van het neergeslagen vanadiumsulfide zijn geïdentificeerd op de laag beladen molybdeen-silica katalysator, *i)* een disperse, niet-kristallijne fase en *ii)* een kristallijne fase, o.a. bestaande uit een gelaagde structuur. Vanadium depositie vindt plaats in de omgeving van de actieve plaatsen op de katalysator, daarmee de actieve plaats vergiftigend, en als geïsoleerde clusters, hetgeen actieve plaatsen vormt. Het netto resultaat is dat er geen significante deactivering plaatsvindt uitgaande van laag beladen katalysatoren en/of kale dragers tot 9 gew.% vanadium.

Met behulp van 'molecular modelling' en Gas Chromatografie-Massa Spectrometrie (GC-MS) kunnen reactie intermediären in de laatste gelumpde reactie stap worden geïdentificeerd, waarmee het bestaande reactie mechanisme voor de hydrodemetallisatie van metallo-tetra-phenylporphryine kan worden uitgebreid. Het mechanisme verloopt via drie hydrogeneringsstappen op de  $\beta$ -pyrrol posities van de porfyrinische structuur naar een structuur die op de meso-brug positie is gehydrogeneerd. Na een protonaanval, welke noodzakelijk is voor het openen van de ring, is een eliminatie van een tolyl groep mogelijk. Het uiteindelijke product voor metaalverwijdering is een open-keten molecule. Metaalverwijdering uit, en verdere omzetting van het laatste intermediair leidt tot mono-pyrrol bevattende moleculen en de metaal neerslag op het katalysator oppervlak. Dit mechanisme is uitgebreid beschreven in hoofdstuk 7.

In hoofdstuk 8 worden de belangrijkste resultaten uit dit proefschrift op een rij gezet en geëvalueerd.

## List of Symbols

A	: absorption at its specific wavelength $\lambda$	-
C	: liquid phase concentration	mol/m <sup>3</sup>
D <sub>b</sub>	: bulk diffusion coefficient in liquid phase	m <sup>2</sup> /s
D <sub>eff</sub>	: effective or restrictive diffusion coefficient	m <sup>2</sup> /s
D <sub>max</sub>	: maximum molecule diameter	nm
E <sub>a</sub>	: activation energy	kJ/mol
F( $\lambda$ )	: restrictive factor for diffusion	-
H <sub>f</sub>	: heat of formation	kJ/mol
k <sub>1</sub> , k <sub>3</sub>	: hydrogenation reaction rate constants	s <sup>-1</sup>
k <sub>2</sub> , k <sub>4</sub>	: dehydrogenation reaction rate constants	s <sup>-1</sup>
k <sub>5</sub>	: lumped ring cleavage reaction rate constant	m <sup>3</sup> /mol·s
k <sub>HDS</sub>	: first order thiophene hydrodesulfurisation rate constant	m <sup>3</sup> /mol V·s
K <sub>ij</sub>	: equilibrium constant of reaction i and j	-
K <sub>H</sub>	: hydrogen adsorption coefficient	m <sup>3</sup> /mol
K <sub>H<sub>2</sub>S</sub>	: hydrogensulfide adsorption coefficient	m <sup>3</sup> /mol
K <sub>A</sub> , K <sub>B</sub> , K <sub>C</sub> , K <sub>P</sub>	: adsorption coefficient for component A, B, C, P	m <sup>3</sup> /mol
L	: radiation path-length in the liquid (or cuvette length)	m
M <sub>b</sub>	: molecular weight of solvent	g/mol
M <sub>M</sub>	: molecular weight of metal deposit	kg/mol
n	: number	-
r	: reaction rate	mol/m <sup>3</sup> ·s
r	: radial length coordinate from centre of catalyst pellet	m
r <sub>s</sub>	: diffusing solute molecular radius	m
r <sub>p</sub>	: catalyst pore radius	m
R	: universal gas constant	kJ/mol·K
R <sub>c</sub>	: radius of catalyst pellet	m
S <sub>v</sub>	: surface area per unit volume of catalyst pellet	m <sup>2</sup> /m <sup>3</sup>
SSR, SSR <sub>0</sub>	: sum of squares of residuals in local and global minimum	-
t	: time	s
T	: temperature	K
T <sub>max</sub>	: temperature with maximum reduction rate	K
V <sub>a</sub>	: molar volume of the solute at its boiling point	cm <sup>3</sup> /mol
W	: wetting number	-
W <sub>M</sub>	: mass concentration of metal deposit	kg/m <sup>3</sup>
z	: coordination number	-

### Greek

$\alpha$	: ratio of number of metal atoms in deposit to number of metal atoms in porphyrin precursor	-
$\Delta$	: difference, differential	-
$\epsilon$	: molar extinction coefficient	m <sup>2</sup> /mol
$\epsilon$	: total void space or total porosity	-
$\epsilon^A$	: fraction of accessible void space or accessible porosity	-
$\epsilon_c$	: percolation threshold	-
$\epsilon^E$	: effective transport coefficient	-
$\epsilon^I$	: fraction of isolated void space or isolated porosity	-
$\lambda$	: ratio of diffusing solute molecular radius and catalyst pore radius	-
$\lambda$	: wavelength	nm
$\mu_b$	: solvent viscosity	cP
$\mathcal{R}$	: reaction rate	mol/m <sup>2</sup> ·s
$\rho_M$	: density of metal deposit	kg/m <sup>3</sup>
$\sigma$	: dimensionless deposited vanadium, $W_M/\rho_M \cdot \epsilon^A$	-
$\tau$	: catalyst pellet tortuosity	-

### Subscripts

-	: vector
CALC	: calculated
EXP	: experimental or measured
eq	: equilibrium
A,B,C,P	: M-TPP, M-TPC, M-TPiB, Products
H <sub>2</sub> , H <sub>2</sub> S	: hydrogen, hydrogensulfide
i	: compound, number
j	: number
ref	: reference

### Abbreviations

AAS	: Atomic Absorption Spectroscopy
BET	: Brunauer, Emmet and Teller
Bil	: Bilane type of porphyrin
Corr	: Corrin type of porphyrin
C/H	: Carbon-Hydrogen ratio
DCR	: Demetallisation Catalyst Rejuvenation
DEA	: DiEthanolamine
DMDS	: DiMethylDiSulfide
DPEP	: DeoxoPhylloErythroetioPorphyrin



EDX	: Energy Dispersive analysis of X-ray
EPMA	: ElectronProbe MicroAnalysis
FCC	: Fluid Catalytic Cracking
GC-MS	: Gas Chromatography - Mass Spectrometry
HCON	: HydroCONversion
HDM	: HydroDeMetallisation
HDN	: HydroDeNitrogenation
HDO	: HydroDeOxygenation
HDS	: HydroDeSulfurisation
HP	: High Pressure
HREM	: High Resolution Electron Microscopy
HTBA	: High Temperature Batch Adsorption
IFP	: Institut Français de Pétrole
IUPAC	: International Union of Pure and Applied Chemistry
LP	: Low Pressure
M	: Metal or Metallo
MNDO	: Modified Neglect of Diatomic Overlap
MOPAC	: Molecular Orbital PACKage
Ni	: Nickel
NLS	: Non-Linear Systems
ODE	: Ordinary Differential Equations
OEP	: OctaEthylPorphyrin
PDE	: Partial Differential Equation
r.d.s.	: rate determining step
rpm	: rotations per minute
SRTCA	: Shell Research and Technology Centre, Amsterdam
T3MPP	: Tetra(-3-Methyl-Phenyl)Porphyrin
T3MPiB	: Tetra(-3-Methyl-Phenyl)isoBacteriochlorin
TCD	: Thermal Conductivity Detector
TPB	: TetraPhenylBacteriochlorin
TPC	: TetraPhenylChlorin
TPHP	: TetraPhenylHexahydroPorphyrin
TPiB	: TetraPhenylisoBacteriochlorin
TPOP	: TetraPhenylOctahydroPorphyrin
TPP	: TetraPhenylPorphyrin
TPR	: Temperature Programmed Reduction
TPS	: Temperature Programmed Sulfiding
UV	: Ultra-Violet
VIS	: Visible
VO	: Vanadyl



## List of Publications and Orals

### Publications:

- » J.P. Janssens, B.J. Bezemer, A.D. van Langeveld, S.T. Sie, and J.A. Moulijn, *Catalyst Deactivation 1994, Studies in Surface Science and Catalysis* (B. Delmon and G.F. Froment, Eds.), **88**, Elsevier Science BV, (1994) 335.
- » J.P. Janssens, A.D. van Langeveld, R.L.C. Bonn , C.M. Lok, and J.A. Moulijn, *ACS Prepr. Div. Petrol. Chem.*, **39** (4) (1994) 571.
- » J.P. Janssens, A.D. van Langeveld, S.T. Sie, and J.A. Moulijn, *ACS Prepr. Div. Petrol. Chem.*, **40** (3) (1995) 534.
- » J.P. Janssens, G. Elst, E.G. Schrikkema, A.D. van Langeveld, S.T. Sie and J.A. Moulijn, 'Development of the hydrodemetallisation reaction mechanism of metallo-tetraphenylporphyrin on a molecular level', accepted for publication in *Recueil*.
- » J.P. Janssens, A.D. van Langeveld, S.T. Sie, and J.A. Moulijn, *ACS Symposium Series*, **134**, (P. O'Connor, T. Takatsuka, G.L. Woolery, Eds.), June 1996.

### Publications in preparation:

- » J.P. Janssens, Y. Xu, A.D. van Langeveld, S.T. Sie and J.A. Moulijn, 'Influence of hetero-atom containing compounds on the hydrodemetallisation of vanadyl-tetraphenylporphyrin', submitted for publication in *FUEL*.
- » J.P. Janssens, A. Effendi, C. Zoetekouw, J. Liu, A.D. van Langeveld, and J.A. Moulijn, 'Influence of the support material on the hydrotreating activity and selectivity of vanadium' to be published in *Appl. Catal.*
- » J.P. Janssens, R.M. de Deugd, A.D. van Langeveld, S.T. Sie, and J.A. Moulijn, 'On the Metal Deposition Process during the Hydrodemetallisation of Vanadyl-tetraphenylporphyrin', to be published in *Ind. Eng. Chem.*
- » J.P. Janssens, R. Chandoesing, A.D. van Langeveld, R.L.C. Bonn , C.M. Lok, and J.A. Moulijn, 'Characterisation and sulfiding behaviour of nickel catalyst precursors for hydrogenation processes', to be published in *J. Catal. or Appl. Catal.*

### Orals at international conferences

- » J.P. Janssens, A.D. van Langeveld, R.L.C. Bonn , C.M. Lok, and J.A. Moulijn, 'Role of sulfiding procedure on activity and dispersion of nickel hydrotreating catalysts', *ACS second Symposium on Advances in Hydrotreating Catalysts*, Division of Petroleum Chemistry, Washington DC, USA, 21-26 August 1994.
- » J.P. Janssens, B.J. Bezemer, A.D. van Langeveld, S.T. Sie, and J.A. Moulijn, 'Catalyst deactivation in hydrodemetallisation of model compound vanadyl-tetraphenylporphyrin', *6th International Symposium on Catalyst Deactivation*, Oostend, Belgium, 3-5 October 1994.
- » J.P. Janssens, A.D. van Langeveld, R.L.C. Bonn , C.M. Lok, and J.A. Moulijn, 'Activity and dispersion effects in nickel hydrotreating catalysts; Effect of sulfiding procedure', *1995 Spring AIChE National Meeting*, Houston, USA, 19-23 March 1995.
- » J.P. Janssens, A.D. van Langeveld, S.T. Sie, and J.A. Moulijn, 'Catalyst deactivation in hydrodemetallisation', *ACS Symposium on Deactivation and Testing of Hydrocarbon Conversion Catalysts*, Division of Petroleum Chemistry, Chicago, USA, 20-25 August 1995.
- » J.P. Janssens, R. Chandoesing, A.D. van Langeveld, R.L.C. Bonn , C.M. Lok, and J.A. Moulijn, 'Activity and dispersion effects in nickel hydrotreating catalysts; Effect of sulfiding routine', *EUROPACAT II Conference*, Maastricht, The Netherlands, 3-8 September 1995.
- » A.D. van Langeveld, J.P. Janssens, B. Vogelaar, R.L.C. Bonn , C.M. Lok, and J.A. Moulijn, 'Hydrogenation activity of nickel catalysts', *ACS Symposium on Removal of Aromatics, Sulfur and Olefins from Gasoline and Diesel*, Division of Petroleum Chemistry, Orlando, Florida, USA, 18-22 August 1996.



## Dankwoord

'Wanneer is je proefschrift af?' en 'Heb je al een promotie datum?', gelukkig zijn dit vragen die ik niet meer hoeft te beantwoorden. Na 4 jaar 'wetenschappelijk' onderzoek ben ik blij dat het proefschrift af is. De mogelijkheid is nu aangebroken om alle mensen te bedanken die, in wat voor vorm dan ook, hebben bijgedragen tot de totstandkoming van dit proefschrift.

Allereerst wil mijn (toegevoegd) promotoren (*ook wel* inspiratoren) bedanken. Jacob Moulijn, het is moeilijk om jouw bijdrage in een paar zinnen op te schrijven. Ik zal met genoegen terugdenken aan de prettige (wetenschappelijke) discussies, jouw brede kennis (helikopter view), ervaring en de motiverende werking die van jouw persoon uitgaat. Bedankt voor de vrijheid die je mij hebt gegeven tijdens dit onderzoek en de begeleiding die precies goed was. Dick van Langeveld (*ook wel* de spellingschecker en oppervlakte-ingenieur), bedankt voor alle adviezen, tips en discussies. Het feit dat jouw kamer een lage drempel heeft, komt de begeleiding van je AIO's erg ten goede. Tiong Sie, jouw ervaring is onontbeerlijk voor de werkgroep Industriële Katalyse. Het is een waar genoegen om naar je te luisteren!

Goed onderzoek is alleen mogelijk als de apparatuur goed blijft draaien. De technici, die in de werkgroep Moulijn werken (hebben gewerkt), blijken hier altijd uitstekend voor te zorgen. Saeed Tajik, Gerard Ruigrok, Bart Boshuizen en Bas Vogelaar bedankt voor alle hulp tijdens het ontwerp, bouw en onderhouden van de apparatuur. Voor de betere soldeerboutklus moet je bij Joop Wolvekamp zijn. Joop bedankt voor alle klusjes aan de TPS, batch en microflow apparatuur.

Voor de afstudeerders zal het een aardige speurtocht zijn om hun werk terug te vinden in dit boekje. Echt, het staat er allemaal in! Astrid Effendi, Bas Bezemer, Arjan Ambachtsheer, Corrie Zoetekouw, Gerald Witte, Gerald Elst, Koen Homburg, Edo Schrikkema en Ronald de Deugd bedankt voor de grote hoeveelheden werk die jullie hebben verricht in het HDM (Ha-Die-Moulijn) project. The (foreign) guests Albena Bossilkova, Youming Xu ('smells like hell'), Boyke Chandoesing, Liu Jingli and Prof. Gu are thanked for their multicultural input in this project.

Het Koninklijke/Shell Laboratorium, Amsterdam (later Shell Research and Technology Centre, Amsterdam) voor de financiële steun en samenwerking. De discussies tijdens de diverse KSLA/TUD- meetings en lunches hebben zeker een grote stimulans en invloed gehad hebben op dit werk. Jos den Ouden en Bob Scheffer, die het project begeleiden, wil ik in het bijzonder bedanken.

Van Unilever Research Port Sunlight wil ik Martin Lok en Raimond Bonné bedanken voor de samenwerking in het Nikkel project. Helaas is er geen Ni-hoofdstuk in dit proefschrift verschenen, maar de aparte publikaties op stapel en de diverse congresbijdragen geven de vruchten van deze samenwerking weer! Bovendien is het een luxe om met je voorganger bijna dagelijks contact te kunnen hebben!

Van Materiaalkunde (TU-Delft) wil ik Patricia Kooyman en Henny Zandbergen bedanken voor de 'atomaire blik' op katalysatoren. Elke Fakkeldij en Pieter Colijn bedankt voor de vele XPS en EPMA metingen. San de Beer, Wim Welters en Marcel Vissenberg (TU-Eindhoven) wil ik bedanken voor de vele thiofeen HDS metingen.

Bij de werkplaats, de instrumentmakerij, het analyse lab, de glasblazerij, de gasfles-verwisselploeg en de firma Jan Smit kwam ik altijd met haast-klusjes. Jullie verstaan de kunst om de 'klant' de indruk te geven dat het werk met spoed af is (en dat was ook zo!). Bedankt voor alles !

Alle collega \*IO's (de rij is te groot om op te noemen) bedankt voor de gezelligheid tijdens mijn promotie-onderzoek. De vele evenementen, zoals het Ardennen weekend, zeilen, skiën, borrels, BBQ's, 'stappen in Nighttown', squashmiddag, oliebollenfestijn, bierexcursie, fiets-weekends en voetbalwedstrijden, maakten de werksfeer altijd erg prettig ! Houden zo ! In het bijzonder wil ik mijn collega's Mark (Helmut) Helmsing, Guido M(e)ul, Wridzer Bakker, Hank Reinhoudt, Robert Stockmann, Jan Remmert Pels en Michiel Makkee bedanken voor de steun in (voor mij persoonlijk) zware tijden.

Last but certainly not least, wil ik mijn familie en vrienden bedanken. Jullie moeten vaak gedacht hebben *waar is ie nog eigenlijk mee bezig* (het resultaat heb je nu in handen). Ik hoop dat het enige duidelijkheid verschaft ! Mijn ouders wil ik bedanken voor de onuitputtelijke steun (in de breedste zin) tijdens mijn studie en promotie-onderzoek. Vrienden voor alle opvang, discussies en gezelligheid naast het werk. Ingrid voor het besef dat er naast hard werken en promoveren nog meer bestaat. Ik hoop dat we in de toekomst veel tijd samen kunnen doorbrengen !

## CURRICULUM VITAE

Jean Paul Janssens werd op 27 juli 1966 te Haarlem geboren. De middelbare school werd doorlopen op het Coornhert Scholengemeenschap te Haarlem. Op 30 mei 1984 behaalde hij het Atheneum B diploma. De opleiding werd vervolgd aan de Hogere Technische School te Amsterdam waar hij op 7 juli 1988 afstudeerde in de richting Chemisch Techniek.

Na de H.T.S. werd de studie vervolgd aan de Technische Universiteit Delft. De opleiding Scheikundige Technologie met als afstudeerrichting Chemisch Proces Technologie werd afgerond op 19 december 1991. Het afstudeeronderzoek 'Radiale dispersie in trickle-bed reactoren' werd uitgevoerd bij het Koninklijke/Shell Laboratorium te Amsterdam, sectie Equipment Engineering en de werkgroep Reactorkunde o.l.v. Prof. ir. C.M. van den Bleek.

In de periode 1 februari 1992 t/m 1 februari 1996 is hij als Assistent in Opleiding in dienst geweest van de TU-Delft. Gedurende deze periode is het onderzoek uitgevoerd naar de karakterisering, het testen en de deactivering van hydrotreating katalysatoren waarvan een deel is beschreven in dit proefschrift. Dit onderzoek is uitgevoerd o.l.v. Prof. dr. J.A. Moulijn, Prof. dr. ir. S.T. Sie en Dr. A.D. van Langeveld en werd financieel mogelijk gemaakt door de Europese Gemeenschap en het Shell Research and Technology Centre, Amsterdam.

In de periode 1 september 1993 t/m 1 september 1995 was hij lid van de Faculteitsraad der Scheikundige Technologie en Materiaalkunde voor het tijdelijk wetenschappelijk personeel.

## Notities